

TECHNISCHE UNIVERSITÄT MÜNCHEN

Institut für Wasserchemie und Chemische Balneologie

Lehrstuhl für Analytische Chemie

Magnetic Bead-Based Immunoassays for Aflatoxin B1 Using Biofunctionalized Gold Nanoparticles

Xu Wang

Vollständiger Abdruck der von der Fakultät für Chemie der Technischen Universität München zur Erlangung des akademischen Grades eines

Doktors der Naturwissenschaften (Dr. rer. nat.)

genehmigten Dissertation.

Vorsitzender: Univ.-Prof. Dr. Th. Brück

Prüfer der Dissertation: 1. Univ.-Prof. Dr. R. Nießner
2. apl. Prof. Dr. D. Knopp

Die Dissertation wurde am 02.09.2015 bei der Technischen Universität München eingereicht und durch die Fakultät für Chemie am 21.10.2015 angenommen

ACKNOWLEDGEMENTS

This work was carried out from October 2012 to September 2015 at the Institute of Hydrochemistry, Chair for Analytical Chemistry, Technische Universität München. The thesis would not be completed without the help from following people.

First and foremost, I would like to thank Prof. Dr. Reinhard Nießner for giving me the opportunity to do my PhD under his guidance and for his kind help and support in my research work. I am impressed by his rigorous scientific attitude and profound knowledge.

I would also express my sincerest gratitude to Prof. Dr. Dietmar Knopp, who gives me a lot of enthusiastic help, invaluable encouragements and excellent guidance throughout my work. I really enjoy working under his friendly supervision and appreciate the freedom he gives to me for exploring chemistry. It is a precious experience for me and I learned a lot from him.

Many thanks to Matthias Jakob and Ryan Karongo, who directly took part in my work. I would also thank Dr. Jutta Pauli and Dr. Ute Resch-Genger from Bundesanstalt für Materialforschung und -prüfung, Berlin, for experimental help and useful suggestions. Dr. Marcus Knopp from Max Planck Institute of Neurobiology, Munich, is thanked for the cooperation at the beginning of my work. I also thank Dr. Clemens Helmbrecht from Particle Metrix GmbH, Diessen, for providing the DLS instrument.

Furthermore, I would like to thank Maria Hübner and Anna-Cathrine Neumann for their consistent help and support in the lab. I really enjoy the pleasant working atmosphere.

All other colleagues at the institute are also sincerely thanked for their kind help all the time, especially Dr. Susanna Oswald, Dr. Michael Pschenitza, Lu Pei, Dr. Elisangela M. Linares, Dr. Haibo Zhou, Dr. Danting Yang, Klemens Thaler, Anika Wunderlich, Andreas Kunze and Dr. Dongyang Li.

The financial support of the China Scholarship Council is gratefully acknowledged. With the scholarship, I spent a memorable time in Germany. In addition, special thanks to my

ACKNOWLEDGEMENTS

Master supervisor, Prof. Dr. Xiaojun Peng at Dalian University of Technology, China, who taught me how to become a researcher.

At the end, I want to thank my family for their consistent love and unconditional support all the time.

PUBLICATIONS

Parts of this thesis have been published in following scientific journals:

Xu Wang, Jutta Pauli, Reinhard Niessner, Ute Resch-Genger and Dietmar Knopp*. Gold Nanoparticle-Catalyzed Uranine Reduction for Signal Amplification in Fluorescent Assays for Melamine and Aflatoxin B1. *Analyst*, accepted.

Xu Wang, Reinhard Niessner, and Dietmar Knopp*. Controlled Growth of Immunogold for Amplified Optical Detection of Aflatoxin B1. *Analyst*, 2015, 140, 1453-1458.

Xu Wang, Reinhard Niessner, and Dietmar Knopp*. Magnetic Bead-Based Colorimetric Immunoassay for Aflatoxin B1 Using Gold Nanoparticles. *Sensors*, 2014, 14, 21535-21548.

PUBLICATIONS

ABSTRACT

Aflatoxins are highly toxic secondary metabolites produced mainly by *Aspergillus flavus* and *A. parasiticus*, present in a wide range of food products. More than 20 aflatoxins (e.g., B1, B2, G1, G2 and M1) have been identified. Among them aflatoxin B1 (AFB1) is usually predominant in amount and constitutes the most hazardous, which is listed as Group I carcinogen by the International Agency for Research in Cancer. In this thesis, a series of highly sensitive and selective methods have been developed for the detection of AFB1 in food samples.

In the first part, a competitive colorimetric immunoassay for AFB1 was established using biofunctionalized magnetic beads (MBs) and gold nanoparticles (AuNPs). AFB1-bovine serum albumin conjugates (AFB1-BSA) modified MBs were employed as immunosensing probe, which could specifically bind with AuNP-labeled *anti*-AFB1 antibodies through immunoreaction, while such specific binding was competitively inhibited by the addition of AFB1. After magnetic separation, the supernatant solution containing unbound AuNPs was directly tested by UV-Vis spectroscopy. The absorption intensity was directly proportional to the AFB1 concentration. The influence of AuNP size, incubation time and pH was investigated in detail. After optimization, the developed method could detect AFB1 in a linear range from 20 to 800 pg/mL, with the limit of detection at 12 pg/mL. The recoveries for spiked maize samples ranged from 92.8% to 122.0%.

In the second part, a sensitive and cost-effective method for the analysis of AFB1 was developed based on controlled growth of immunogold. AFB1-BSA conjugate modified MBs were employed as capture probe and *anti*-AFB1 antibody-coated gold colloids were used as detection probe for the immunological recognition of AFB1, as well as for signal transduction. The immune recognition event was converted into the gold enlargement signal which can be quantitatively measured by UV-vis spectroscopy. The autocatalytic enlargement of immunogold was conducted in aqueous solution containing chloroauric

ABSTRACT

acid, hexadecyltrimethylammonium bromide and ascorbic acid. The reaction could be stopped by the addition of sodium thiosulfate. The final absorbance and resonance light scattering intensity were highly dependent on immunogold concentration. After gold enhancement, the sensitivity of the immunoassay was improved and total assay time was about 1 h. Under optimized conditions, the linear range and lower detection limit were 0.01-1 ng/mL and 7 pg/mL, respectively.

In the third part, a multifunctional fluorescence platform was constructed based on AuNP-catalyzed uranine reduction. The catalytic reduction of uranine was conducted in aqueous solution using AuNPs as catalyst and sodium borohydride as reducing reagent, which was monitored by fluorescence and UV-vis spectroscopy. The reaction rate was related to the concentration, size and dispersion state of AuNPs. When AuNPs aggregated, their catalytic ability decreased, and thereby a label-free fluorescent assay was developed for the detection of melamine, which can be used for melamine determination in milk. In addition, a fluorescent immunoassay for AFB1 was established using the catalytic reaction for signal amplification based on target-induced concentration change of AuNPs, where AFB1-BSA-coated MBs and *anti*-AFB1 antibody-conjugated AuNPs were employed as capture and signal probe, respectively. The detection can be accomplished in 1 h and acceptable recoveries in spiked maize samples were achieved. The established immunoassays are simple, time-saving, highly sensitive and selective, which offer great promise for sensitive detection of other toxins in the field of food safety.

Contents

ACKNOWLEDGEMENTS	i
PUBLICATIONS	iii
ABSTRACT	v
1 Theoretical Background	1
1.1 Introduction	3
1.2 Detection methods for aflatoxins	8
1.2.1 Chromatographic methods	8
1.2.1.1 TLC	8
1.2.2.2 HPLC	9
1.2.1.3 LC-MS	11
1.2.2 Immunological methods	12
1.2.2.1 Radioimmunoassay	12
1.2.2.2 ELISA	13
1.2.2.3 Immunochromatographic assay (Dipstick technology)	14
1.2.2.4 Biosensor	16
1.3 Magnetic particles	17
1.3.1 Synthesis of magnetic particles	17
1.3.1.1 Chemical coprecipitation	18
1.3.1.2 Thermal decomposition	19
1.3.1.3 Solvothermal synthesis	20
1.3.2 Surface modification	21
1.3.3 Applications of magnetic particles	23
1.3.3.1 Serving as carrier	23
1.3.3.2 Serving as signal tag	24
1.4 Gold nanoparticles	27
1.4.1 Preparation of AuNPs	28
1.4.1.1 Citrate reduction	28
1.4.1.2 Seeded growth synthesis	29
1.4.2 Optical properties of AuNPs	30
1.4.3 Applications of AuNPs	31
1.4.3.1 Serving as carrier	32
1.4.3.2 Colorimetric assays based on aggregation of AuNPs	32
1.4.2.3 Fluorescence assays based on FRET	34
1.4.3.4 Silver/Gold staining	35
1.4.3.5 Enzyme-like activity of AuNPs	37
1.5 Nanoparticle-based immunoassays for aflatoxins	39
1.5.1 Colorimetric detection	39
1.5.2 Fluorescent detection	40
1.5.3 Light scattering detection	41
1.5.4 Electrochemical detection	42

1.5.5 Other methods.....	43
1.6 Outline of this thesis.....	44
2 Experimental Section.....	47
2.1 Materials and instrumentation	49
2.1.1 Chemicals.....	49
2.1.2 Instrumentation.....	51
2.2 Colorimetric immunoassay for AFB1	51
2.2.1 Preparation of AFB1-BSA-Fe ₃ O ₄	51
2.2.2 Preparation of Ab-AuNPs	52
2.2.3 Optimization and detection procedures.....	54
2.2.4 Preparation of maize samples	54
2.3 Controlled growth of immunogold for signal amplification	55
2.3.1 Preparation of gold growth solution	55
2.3.2 Growth of AuNPs in aqueous phase.....	55
2.3.3 Analysis of maize samples	55
2.3.4 Assay procedure	56
2.4 AuNP-catalyzed uranine reduction for signal amplification	56
2.4.1 Catalytic reduction of uranine.....	57
2.4.2 Detection of melamine	57
2.4.3 Detection of AFB1	58
3 Results and Discussion.....	61
3.1 Colorimetric immunoassay for AFB1	63
3.1.1 Characteristics of AuNPs	65
3.1.2 Characteristics of MBs	67
3.1.3 Optimization of experimental conditions.....	69
3.1.4 Influence of AuNP size on the immunoassay.....	71
3.1.5 Measurement of AFB1.....	72
3.1.6 Analysis of AFB1 spiked maize samples	74
3.1.7 Summary.....	75
3.2 Homogeneous gold staining for signal amplification	75
3.2.1 Proposed mechanism of gold enlargement	77
3.2.2 Controlled growth of immunogold in aqueous solution	80
3.2.3 Monitoring the gold enlargement by RLS spectra.....	84
3.2.4 Amplified optical detection of AFB1	85
3.2.5 Summary.....	88
3.3 AuNP-catalyzed uranine reduction for signal amplification	89
3.3.1 AuNP-catalyzed uranine reduction.....	91
3.3.2 The role of NaBH ₄	94
3.3.3 The effect of AuNPs	96
3.3.4 Detection of melamine	98
3.3.5 Detection of AFB1	103
3.3.6 Summary.....	108

3.4 Comparison between three methods	108
4 Summary and Outlook	111
4.1 Research summary	113
4.2 Outlook	114
5 Abbreviations	117
6 References	121

1 Theoretical Background

1 Theoretical Background

1.1 Introduction

Aflatoxins are highly toxic secondary metabolites produced mainly by *Aspergillus flavus* and *A. parasiticus*, present in a wide range of agricultural products such as maize, rice, pistachio, cereals and peanuts (Figure 1.1).¹ Moreover, aflatoxins can be spread and accumulated in the environment like surface water and agricultural field.²

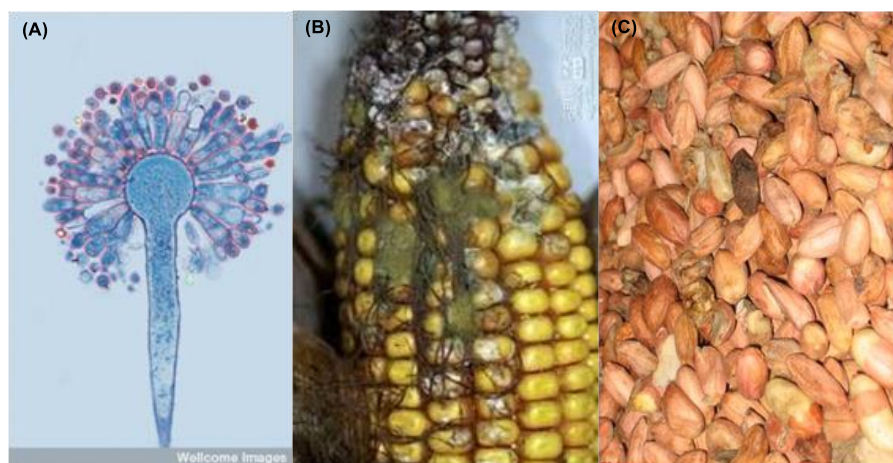


Figure 1.1 (A) *Aspergillus flavus* seen under an electron microscope and photos of moldy maize (B) and peanuts (C).²

Until now, more than 20 aflatoxins (e.g., B1, B2, G1, G2 and M1) have been identified.³ Chemically, aflatoxins are a group of difuranocoumarin derivatives, consisted of a coumarin and a double-furan-ring moiety, as shown in Figure 1.2.

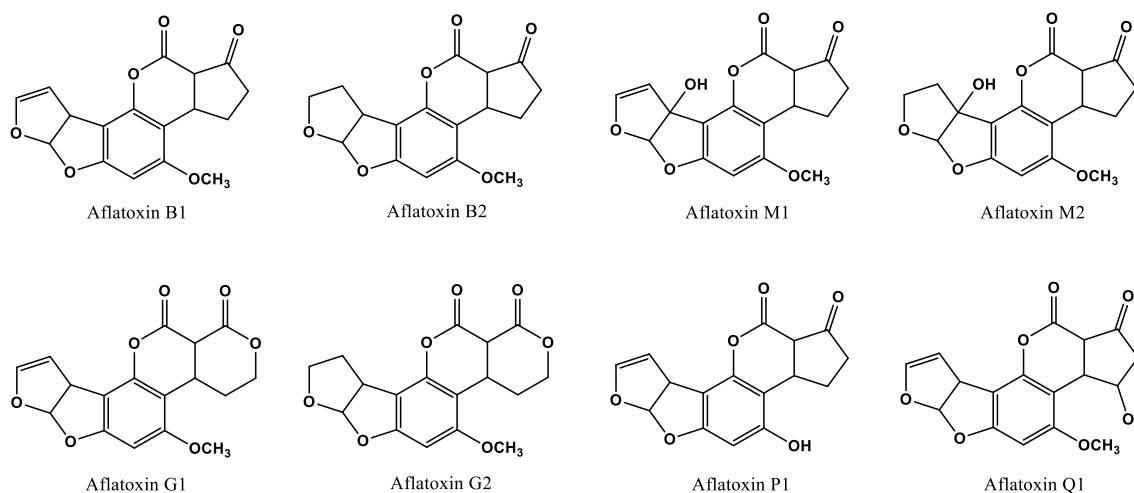


Figure 1.2 Chemical structures of some aflatoxins.

1 Theoretical Background

Aflatoxins were discovered in early 1960s when a mysterious new disease 'Turkey X' swept through the UK which caused mass deaths of more than 100,000 turkeys and ducklings.⁴ After detailed investigation into the deaths, a clue was found that the feed had come from the same batch of peanut from Brazil. Further investigations demonstrated that the peanut feed was heavily contaminated with the organism *Aspergillus flavus*, which produced extremely toxic compounds designated as aflatoxins. The aflatoxins were capable of inducing acute liver disease in ducklings and liver cancer in rats. From then on, much attention has been paid to aflatoxins. Figure 1.3 illustrates the time line for key events about aflatoxins including the discovery, toxicological characterization, molecular epidemiology, and regulation.

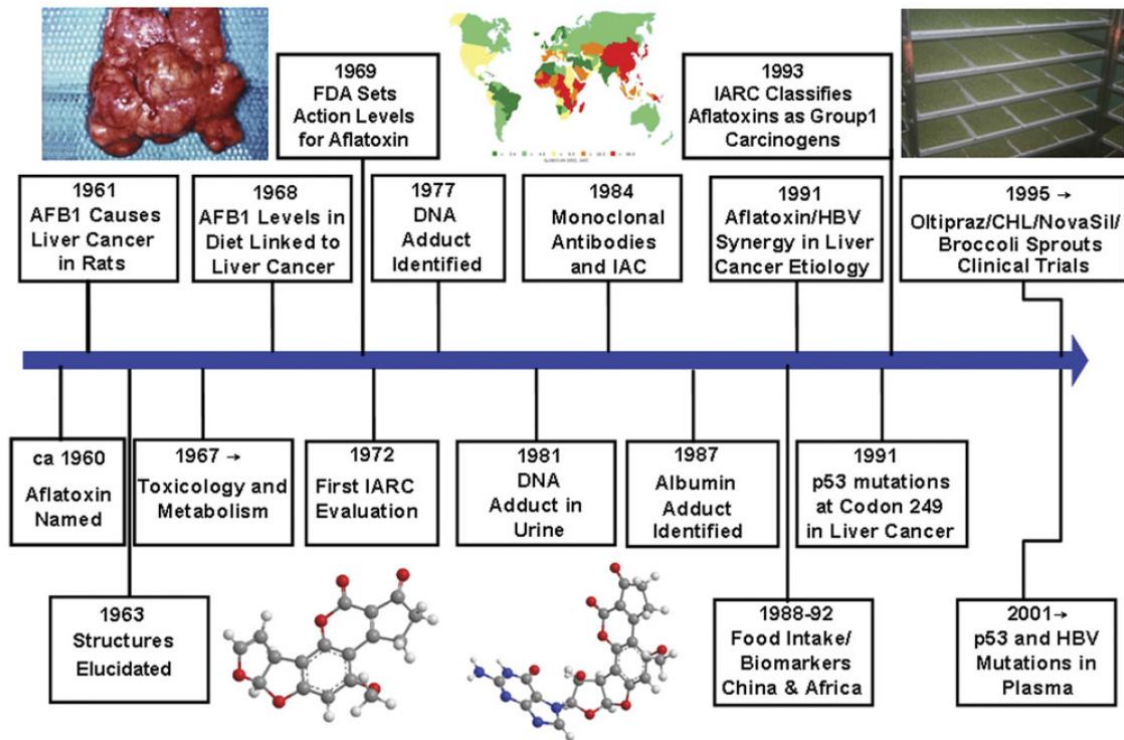


Figure 1.3 Time line for key events about aflatoxins. Reprinted from ref.⁴

Among this group of toxins, aflatoxin B1 (AFB1) is usually predominant in amount and constitutes the most hazardous. The acute toxicity of AFB1 is 10 times of potassium cyanide, 68 times of arsenic and 416 times of melamine. Moreover, its carcinogenicity is 70 times higher than that of dimethylnitrosamine and 10000 times higher than that of

benzene hexachloride.⁵ So it is listed as Group I carcinogen by the International Agency for Research in Cancer.

The main way that people are exposed to aflatoxins is through diet. Moldy foods like maize and peanuts usually contain a high amount of aflatoxins. In addition, milk products might also contain aflatoxins (AFM1 and M2) if the cows were fed on moldy foods containing AFB1 and B2. The intake of a large amount of aflatoxins in short time can cause vomiting, abdominal pain, edema, jaundice, acute liver damage or even death.⁶ In addition, people may suffer liver cancer after exposure to small amounts of aflatoxins over a long period. This is because the metabolism of aflatoxins takes place in the liver. The formation of AFB1-DNA adducts causes gene mutation. As shown in Figure 1.4, AFB1 is converted into different reactive metabolites and adducts.⁴ The formed derivatives such as AFM1, P1 and Q1 are also very toxic. In addition, reactive AFB1-8,9-*exo*-epoxide is generated, which can covalently react with nucleophilic sites of either DNA or RNA, resulting in gene mutations that may change the normal function of cells. Typically, AFB1-8,9-*exo*-epoxide reacts with DNA (alkylation), inducing G→T transversion mutation (Figure 1.5).⁷ Such a mutation is associated with hepatocellular carcinoma, a kind of cancer whereby AFB1 promotes AGG→AGT (Arg→Ser) transversion point mutation of p53 gene at codon 249 that alters p53 gene, which is responsible for DNA repair.⁸

1 Theoretical Background

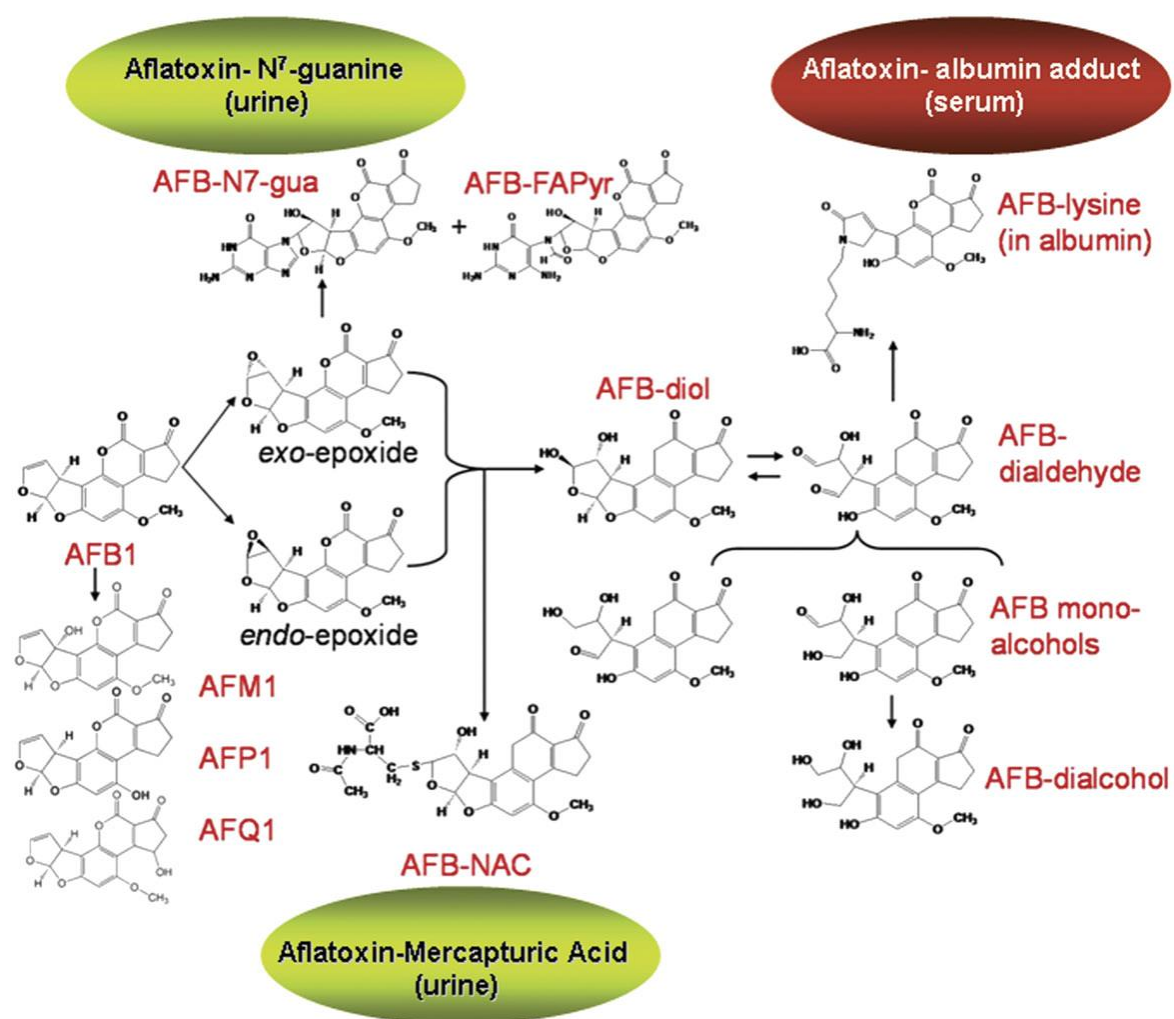


Figure 1.4 Biotransformation pathways for AFB₁. Reprinted from ref.⁴

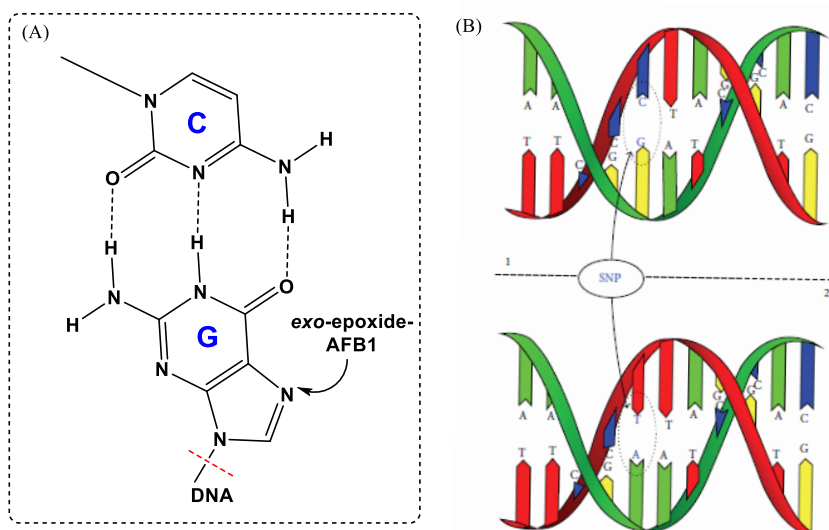


Figure 1.5 Schematic illustration of (A) alkylation of G-base through the reaction with active *exo*-epoxide-AFB₁ and (B) point mutation of G → T at codon 249 in the p53 gene. Reprinted from ref.⁸

Due to the extremely high toxicity and carcinogenicity of aflatoxins, it is important to remove aflatoxins in foods. However, aflatoxins are chemically stable compounds. They are not destroyed under traditional cooking conditions such as microwave or oven heating. On the other hand, natural agricultural products might be easily contaminated with aflatoxins due to the growth of *Aspergillus*. Since optimum temperature for *Aspergillus flavus* is around room temperature (30°C) and the chance of mildew contamination increases if the crops are exposed to a high humidity environment. As a result, strict control of maximum residue level of aflatoxins in foodstuff is set by many countries in the world. Table 1.1 shows the regulation set by European Community.⁹

Table 1.1 The legal limits for aflatoxins in food according to Regulation EC No. 1881/2006

Foods	Aflatoxins	Maximum Levels (µg/kg)		
		B1	B1+B2+G1+G2	M1
Peanuts	for direct consumption	2	4	-
	raw products	8	15	-
Dried Fruit	for direct consumption	2	4	-
	raw products	5	10	-
Maize	for direct consumption	2	10	-
	raw products	5	10	-
Cereals	for direct consumption	2	4	-
	raw products	2	4	-
Raw Milk	heat-treated	-	-	0.05
	infant milk	-	-	0.025

1.2 Detection methods for aflatoxins

Because of the high toxicity and carcinogenicity of aflatoxins, various methods have been developed for the detection of aflatoxins,¹ including chromatographic methods like thin-layer chromatography (TLC), high-performance liquid chromatography (HPLC), liquid chromatography coupled to mass spectrometry (LC-MS), and immunological methods such as enzyme-linked immunosorbent assay (ELISA), immunochromatographic test and electrochemical immunoanalysis. A detailed account of each method is described in the following section.

1.2.1 Chromatographic methods

1.2.1.1 TLC

TLC is one of the most traditional methods for determination of aflatoxins.¹⁰ It consists of two phases, i.e., stationary phase and mobile phase. The stationary phase is made of either silica or cellulose or alumina, which is immobilized on an inert matrix material like glass or plastic slide. The mobile phase is composed of methanol/acetonitrile/water mixture, which carries the sample along as it moves through the solid stationary phase. Different analytes, depending on their chemical structure and interaction with the mobile and stationary phases, either adhere to the solid phase more or remain in the mobile phase, thereby achieving fast and effective separation. Because aflatoxins emit fluorescence, they can be directly observed on TLC plate under the irradiation of UV-light. TLC has been widely utilized for aflatoxins analysis in various food products.¹¹⁻¹² The main advantages of TLC are that it is cheap and fast and it can detect several mycotoxins in one sample. But its drawbacks are also apparent. For example, it requires pretreatment of sample and trained personnel. In addition, lack of automatization and high possibility to be harmful to operators and environment also limit its practical application. This method is gradually replaced by other new approaches with occurring of so many modern equipments and protocols.⁵

1.2.2.2 HPLC

HPLC has been developed since the late 1960s. By far it is the most widely used chromatographic method for separation and determination of polar organic compounds. It provides an accurate, quick and reproducible platform to evaluate the levels of aflatoxins in agricultural products, which is considered as one of the standard methods for aflatoxins analysis. So a detailed introduction about this method is presented below.

Similar to TLC, the HPLC technique also makes use of a solid stationary phase (column) and a mobile phase comprising aqueous/organic solvent mixtures. Reversed-phase C-18 chromatography columns with water/acetonitrile or water/methanol mobile phases are commonly utilized for aflatoxins determination. When the sample is injected into the column, the components to be separated are distributed between the solid and mobile phases. Because the compounds have different affinities for the two phases, they flow through the column at different rates. Thus, different components in the sample display different retention time, which can be detected and recorded by the detector. Several programmable detectors like fluorescence detector,¹³ UV-vis absorption detector¹⁴ and diode array detector¹⁵ are used in HPLC depending on the nature of analytes.

For the analysis of aflatoxins using HPLC, sample pretreatment is usually required. Aflatoxins in samples are first extracted by polar solvents like acetonitrile or methanol mixed with water, followed by a cleanup step. Immunoaffinity columns are often employed for sample purification and enrichment in the aflatoxin analysis.¹⁶⁻¹⁷ As shown in Figure 1.6, specific antibodies are immobilized on a solid phase such as magnetic particles, agarose gels or glass wool, which can capture the target analytes, while the sample matrix can be removed by a washing step. After washing completely, the immunoaffinity column is dried by nitrogen stream. The captured aflatoxins are then eluted by acetonitrile or other elution solutions. The bond between antibody and aflatoxin is broken, thus the captured analytes are removed from the antibodies and then eluted from the column.

1 Theoretical Background

In addition, solid phase extraction columns are also frequently used for the purification of aflatoxins.¹⁸⁻²⁰ Different packing materials like silica gel, C-18 (octadecylsilane) and molecular imprinted polymers are filled into the columns. The general procedure is similar to that of using immunoaffinity columns, i.e., first loading the sample into the column, then washing away impurities while retaining the analytes and finally eluting the analytes.

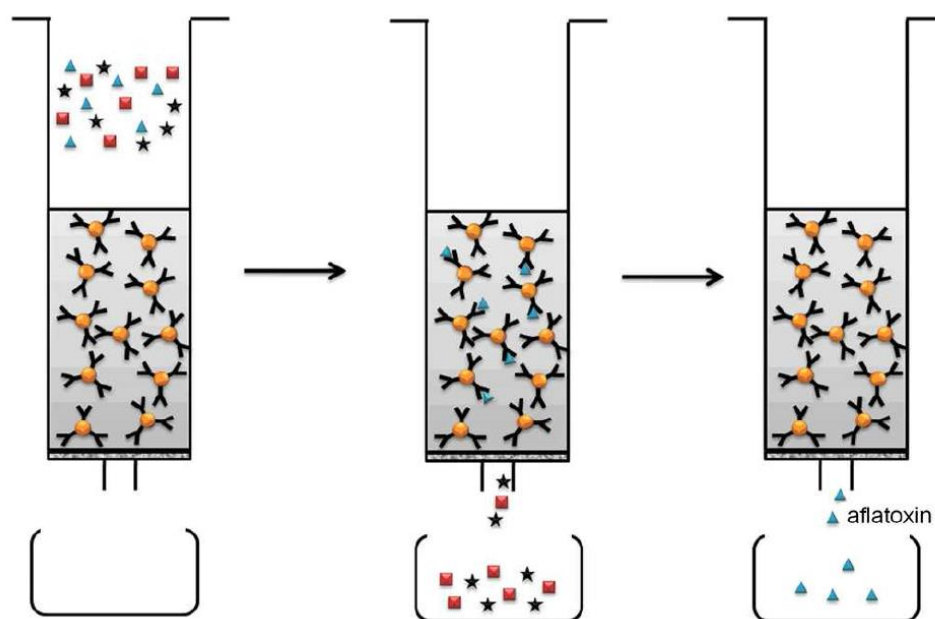


Figure 1.6 Sample cleanup and enrichment using aflatoxin immunoaffinity column. Reprinted from ref.⁵

After sample cleanup using immunoaffinity columns or solid phase extraction columns, the sample is submitted for HPLC analysis. For aflatoxins detection, fluorescence detector (FLD) is frequently utilized. This is because aflatoxins have natural fluorescence, and more importantly, fluorescence detection generally exhibits high sensitivity and specificity. Under the irradiation of laser at wavelength of ~ 360 nm, aflatoxins emit blue or green fluorescence, which can be directly detected by HPLC-FLD. But because of their low fluorescence quantum yield, the signal is low and can be easily quenched. To achieve high sensitivity, several fluorescence-enhancement reactions are used, like with trifluoroacetic acid (TFA) or halogens (Br_2 and I_2).²¹⁻²² The enhancement mechanisms vary with different kinds of enhancers (Figure 1.7). For example, under acidic conditions

(TFA), the second furan ring of AFB1 is hydrolyzed, and AFB1 is converted into B2a, which produces a high fluorescence. In addition, highly fluorescent AFB1 derivatives are formed when AFB1 reacts with halogens. Besides these enhancers, some other reagents like Hg^{2+} , cyclodextrine and its derivatives can be also used for the fluorescence enhancement.^{5, 23} After chemical derivatization, as low as 0.1 $\mu\text{g}/\text{kg}$ of aflatoxins can be detected using HPLC-FLD.¹⁴

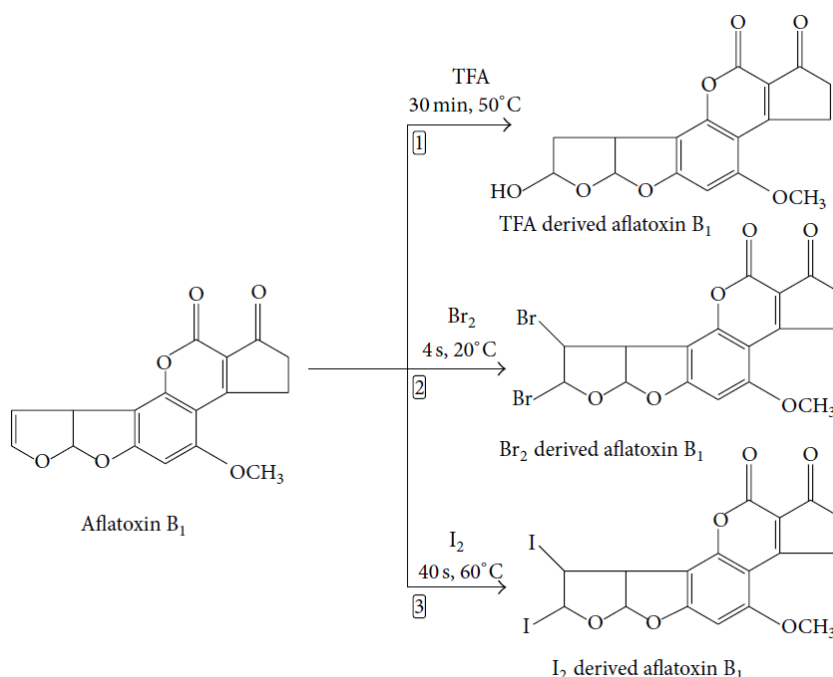


Figure 1.7 Derivatization of AFB1 with trifluoroacetic acid, bromine and iodine. Reprinted from ref.¹

1.2.1.3 LC-MS

Although HPLC combined with fluorescence detection provides fast and accurate detection for aflatoxins, a tedious derivatization process for fluorescence enhancement must be done in traditional HPLC methods.⁵ This problem has been successfully solved by coupling HPLC to mass spectrometry (LC-MS).²⁴⁻²⁶ Ionization source is used as interface between liquid chromatography and mass spectrometer. Because the structural information of target analytes can be directly analyzed by mass spectrometer, the chemical derivatization of aflatoxins is eliminated. Furthermore, LC-MS methods exhibit high sensitivity. However, the instrument is usually bulky and expensive, which limits its practical applications.¹

1 Theoretical Background

Although high sensitivity and good reproducibility are achieved using chromatographic methods (e.g., TLC, HPLC and LC-MS), the sample pretreatment for chromatographic analysis is very tedious, expensive and time consuming. In addition, it usually needs a well equipped laboratory and skilled technician, limiting the application to only laboratory environment but not field conditions.

1.2.2 Immunological methods

Aside from chromatographic methods, immunoassays have also been extensively used for the determination of aflatoxins. Compared with instrumental analysis, immunological methods have advantages such as high sensitivity and specificity, simple operation and short time consumption.³ In addition, immunological methods do not require bulky and expensive equipments, and it is possible to analyze complicated matrices without extensive pretreatment. Thus, much attention has been paid to immunological methods for the determination of aflatoxins.¹ Specifically, immunological techniques rely on the immunoreaction between antibodies and antigens. Antibody, a type of immunoglobulin specifically reacting with corresponding target, is the most important reagent for immunoassay. The affinity and specificity of antibodies determine the sensitivity and selectivity of immunoassays. By the mode of production, antibodies are divided into three kinds: polyclonal (pAb), monoclonal (mAb) and recombinant (rAb). At present, mAbs are the most frequently used antibodies for aflatoxins. A number of mAbs against aflatoxins have been developed during the past decades.²⁷⁻²⁹ Meanwhile, almost all immunoassays involve the use of label materials for signal recognition, including radioactive isotopes,³⁰ enzymes,³¹⁻³² nanoparticles,³³ fluorescent materials³⁴ and sensitive electronic or optical components (biosensor).³⁵⁻³⁶ A brief description about different types of immunoassays for aflatoxins is presented in the following section.

1.2.2.1 Radioimmunoassay

Radioimmunoassay was the first immunoassay technique developed, where the antigen or antibody was labeled by radioactive isotopes. Several radioimmunoassays for aflatoxins

were reported. For example, using ^{125}I -labeled AFB1 as competitor, Korde et al. developed a radioimmunoassay for AFB1 with an assay range of 0.2-5 ng/mL.³⁰ Langone et al. reported a radioimmunoassay for the determination of AFB1 in peanut with a detection limit of 1 $\mu\text{g}/\text{kg}$.³⁷ In addition, radioimmunoassay was used for the detection of AFM1 in milk by Qian et al. with a limit of detection (LOD) below 3 ng/mL.³⁸

Although radioimmunoassay technique shows high specificity and sensitivity, the radioactive isotopes utilized are harmful to operators. The storage and disposal of radioactive waste is also a big problem. Thus, radiolabelling for immunoassays has been replaced by other tags like enzymes and fluorescent reagents.

1.2.2.2 ELISA

As an alternative to radioimmunoassay, ELISA has been extensively utilized for the detection of various analytes like small molecules, polypeptides, bacteria and proteins.³⁹ Depending on the structure of targets, different assay formats are chosen, e.g., sandwich and competitive formats. Because aflatoxins are small molecular analytes, competitive assay format is usually selected, including direct and indirect approaches (Figure 1.8).

In a competitive indirect assay, aflatoxin-protein (e.g. ovalbumin, casein and BSA) conjugates are first immobilized on the well of microtiter plate. The immobilized aflatoxins and free analytes competitively react with *anti*-aflatoxin antibodies (primary antibody). After removing the unbound antibodies by washing, enzyme-labeled secondary antibodies are introduced to react with the primary antibodies. Finally enzyme substrates are added for signal development.

In a competitive direct assay, either the aflatoxin-protein conjugates or primary antibodies are adsorbed on the solid phase. Then free analytes and labeled primary antibodies or labeled aflatoxins are added. After incubation and removing unbound molecules, enzyme substrates are introduced for signal development. Compared with indirect format, direct assay does not need secondary antibodies.

1 Theoretical Background

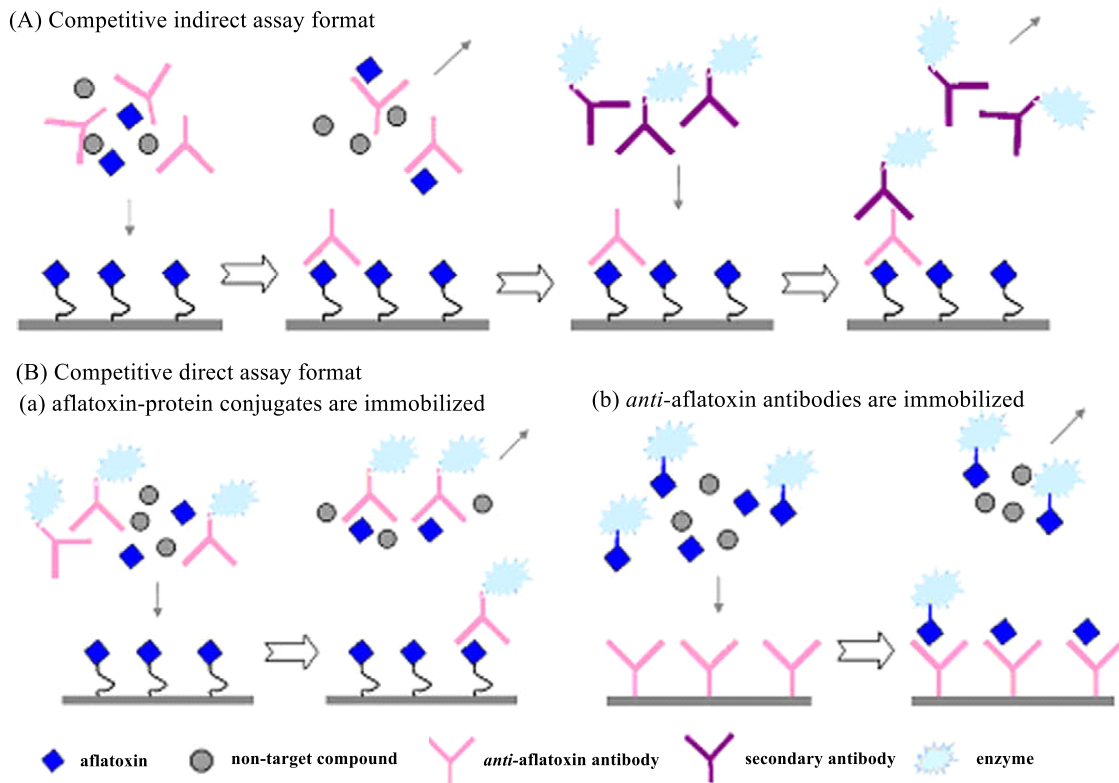


Figure 1.8 Main immunoassay formats for aflatoxins. Reprinted from ref.³

Nowadays, the ELISA method is widely applied in the detection of aflatoxins in food products⁴⁰⁻⁴² and numerous commercially available ELISA kits have been developed based on a competitive assay format.⁴³⁻⁴⁴ Alkaline phosphatase (ALP) and horseradish peroxidase (HRP) are utilized as labels in most of the kits. The ELISA method is very attractive because of the following important features: (1) a large number of samples can be analyzed simultaneously owing to the use of 96/384-well microtiter plate; (2) tedious sample cleanup steps are eliminated and (3) avoiding the use of isotopes, the ELISA kits are safe and user-friendly. But multiple separation and washing steps make the test laborious and time consuming.¹

1.2.2.3 Immunochromatographic assay (Dipstick technology)

Compared with ELISA method, detection using lateral flow devices is very easy and time-saving. Figure 1.9 shows the structure and detection principle of lateral flow strip. It consists of four pads: the sample pad which ensures the contact between the liquid sample and the immunodipstick, the release pad containing gold colloid-labeled antibodies, the

nitrocellulose membrane and the absorbent pad. With capillary action, the liquid sample moves from the sample pad to the absorbent pad. The gold colloid-labeled antibodies are transferred to the nitrocellulose membrane by the flow. In the absence of analytes, the labeled antibodies react with the immobilized antigen (aflatoxins) on the test line and secondary antibody on the control line, so two red lines are observed. If there are analytes in the sample, the binding sites of gold colloid-labeled antibodies will be occupied, so they only react with the secondary antibody. Only one red line (control line) is observed.

Lateral flow strip is the simplest, non-instrumental and user-friendly device which allows qualitative determination of aflatoxins in a very short time.⁴⁵⁻⁴⁶ A number of lateral flow devices using different signal reporters, including colloidal gold,⁴⁷⁻⁴⁸ enzymes,⁴⁹ fluorescent dyes⁵⁰ and quantum dots,⁵¹ have been developed for detecting aflatoxins in agricultural products. They are cost-effective devices which are suitable for determination of aflatoxins on-site.

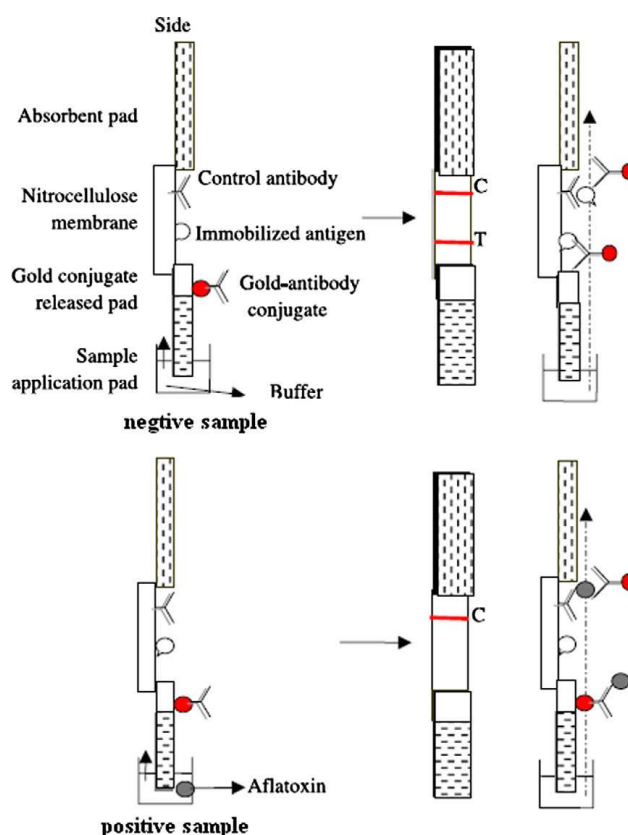


Figure 1.9 Schematic illustration of the structure and principle of lateral flow strip for the detection of aflatoxins. Reprinted from ref.³

1 Theoretical Background

1.2.2.4 Biosensor

To improve the sensitivity and simplify the detection, biosensors have been developed for the determination of aflatoxins, mainly including electrochemical and optical immunosensors.⁵²

In an electrochemical assay system, usually specific antibodies are immobilized on the electrode while the aflatoxin-enzyme conjugate is free. After competitive reaction, a different density of enzyme will bind to the electrode, which catalyzes the reaction of corresponding enzyme substrates, producing measurable electroactive signals.⁵³⁻⁵⁴ Non-enzymatic labels such as Fe₃O₄ /Au core-shell nanomaterials were also used for aflatoxins analysis.⁵⁵ In addition, enzyme-antibody conjugates were also immobilized onto the surface of electrode, the formation of antibody-aflatoxin complexes introduced a barrier of direct electrical communication between the enzyme and electrode surface, resulting in variations in the local current. Such immunosensors for AFB1 have been developed by Liu et al.⁵⁶ and Sun et al.⁵⁷ with dynamic ranges of 0.5-10 ng/mL and 0.1-12 ng/mL, respectively.

Various optical immunosensors were developed for aflatoxins based on different transduction approaches. Figure 1.10 shows the working principle of a surface plasmon resonance immunosensor. In general, antibodies are immobilized on the thin metal film (i.e., layer of Au on a glass slide). The binding of analytes to immobilized antibodies produces a change in refractive index at the sensor surface, which will be detected as a shift in the resonance angle. Daly et al.⁵⁸ and Koopal et al.⁵⁹ developed such immunosensors for AFB1 with detection limits of 3 ng/mL and 0.2 ng/g, respectively.

Microarray sensors have also been developed for aflatoxins. Recently, our group developed a microarray sensor for the detection of multiple mycotoxins using chemiluminescence as the readout. A dynamic range of 2.4-11.4 µg/kg was obtained for AFB1 using an indirect competitive procedure.⁶⁰

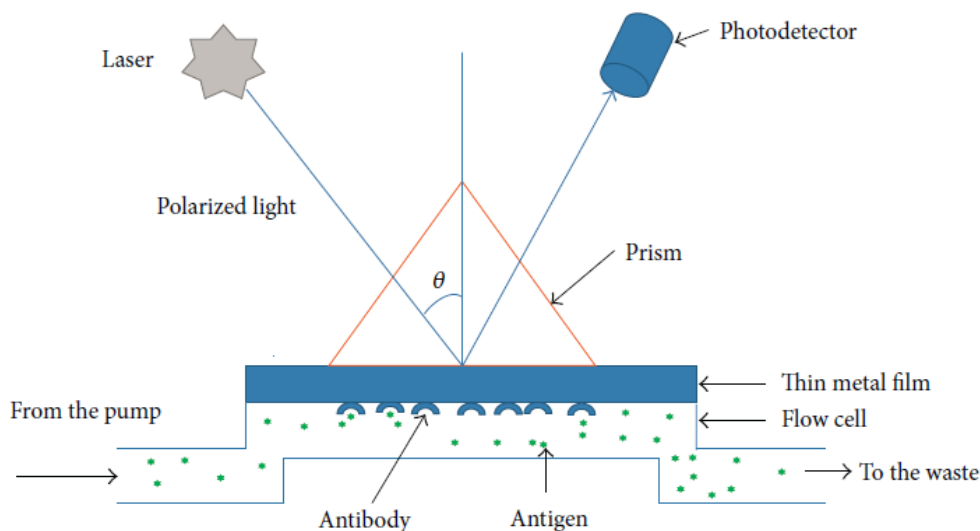


Figure 1.10 Working principle of surface plasmon resonance sensor. Reprinted from ref. ¹

1.3 Magnetic particles

Recently, nano-biotechnology, which integrates nanoscience with molecular biology and biomedicine, has attracted great attention in the field of biological analysis.⁶¹ Nanoparticles of various shapes, sizes, and compositions, have been developed and extensively utilized for the fabrication of chemical and biological sensors.⁶²⁻⁶³

Among these nanomaterials, magnetic particles have drawn particular interest because they have good biocompatibility and can be easily separated from reaction mixture with the aid of an external magnet. Iron oxide particles, for instance, have been widely used in immunoassay,⁶⁴⁻⁶⁵ protein and enzyme immobilization,⁶⁶⁻⁶⁷ cell separation,⁶⁸ DNA hybridization⁶⁹⁻⁷⁰ and drug delivery.⁷¹ In this section, the preparation of magnetic particles, surface modification and their applications in the field of biological analysis will be briefly reviewed.

1.3.1 Synthesis of magnetic particles

Many kinds of magnetic particles have been synthesized, including iron oxides (Fe_3O_4 and Fe_2O_3), MFe_2O_4 ($\text{M} = \text{Co}, \text{Mn}, \text{Ni}$ and Mg), FePt , FeCo , CoPt , $\alpha\text{-Fe}$, Co and Ni nanoparticles.⁷² The most commonly used magnetic nanoparticles in bioanalysis could be

1 Theoretical Background

iron oxides, because they can be easily prepared and functionalized and are considered as biocompatible. Thus, much of the following discussion focuses on iron oxide particles.

To date, various methods have been reported for the preparation of magnetic particles, including physical methods such as electron beam lithography and gas-phase deposition, microbial methods and chemical methods like sol-gel synthesis, hydrothermal reaction, flow injection synthesis, sonochemical decomposition reaction and chemical coprecipitation.⁷³ Several representative and widely used methods are introduced and discussed here.

1.3.1.1 Chemical coprecipitation

Chemical coprecipitation is perhaps the simplest and the most efficient method for the synthesis of iron oxide particles (Fe_3O_4 or $\gamma\text{-Fe}_2\text{O}_3$), which is based on coprecipitation of iron compounds.⁷³ A base (e.g., NH_4OH or NaOH) is added to an aqueous solution of Fe^{3+} and Fe^{2+} salts and black Fe_3O_4 NPs immediately form through reaction 1.1. The magnetite nanoparticles (Fe_3O_4 NPs) are not very stable under ambient conditions, which can be easily oxidized to maghemite ($\gamma\text{-Fe}_2\text{O}_3$) by oxygen in air (reaction 1.2) or dissolved in an acidic solution (reaction 1.3).⁷⁴



Furthermore, small amount of oxygen in water could oxidize the Fe^{2+} ions to Fe^{3+} as shown in reaction 1.4, which is favorable for the formation of $\text{Fe}(\text{OH})_3$ (reaction 1.5) and $\gamma\text{-Fe}_2\text{O}_3$ (reaction 1.6). Thus, the magnetic nanoparticles prepared by chemical coprecipitation could be a mixture of Fe_3O_4 , $\gamma\text{-Fe}_2\text{O}_3$ and $\text{Fe}(\text{OH})_3$.



The Fe_3O_4 NPs can be further oxidized by iron(III) nitrate in acidic medium to convert them into Fe_2O_3 . The formed maghemite particles are ferrimagnetic, which also display strong magnetic property. More importantly, the maghemite particles are chemically stable in both alkaline and acidic media.⁷⁵

Using the chemical coprecipitation method, a large scale of iron oxide nanoparticles can be prepared at one time. The morphology and size of magnetic particles depend on the reaction conditions, including the $\text{Fe}^{2+}/\text{Fe}^{3+}$ ratio, reaction temperature, pH value and ionic strength.

1.3.1.2 Thermal decomposition

In order to prepare magnetic nanoparticles with a narrow size distribution, thermal decomposition of metal complexes is utilized. The metal complexes decompose under high temperature in high-boiling organic solvents containing stabilizing surfactants. Organometallic compounds are used as precursors, such as metal acetylacetonates, $[\text{M}(\text{acac})_n]$, ($\text{M} = \text{Fe}, \text{Mn}, \text{Co}, \text{Ni}, \text{Cr}$, $n = 2$ or 3 , $\text{acac} = \text{acetylacetonate}$), iron oleate and $\text{Fe}(\text{CO})_5$. Fatty acids, oleic acid and hexadecylamine are used as stabilizing surfactants. In addition, a reducing agent such as 1,2-hexadecanediol and 1,2-tetradecanediol is often used. The ratio of metal precursor to stabilizing agent and reaction temperature greatly affect the size, morphology and monodispersity of the generated NPs.⁷⁵

Monodisperse MFe_2O_4 ($\text{M} = \text{Fe}, \text{Co}, \text{Mn}$) nanoparticles were prepared by Sun et al.⁷⁶ using metal acetylacetonate precursors, as shown in Figure 1.11. The particle size can be tuned from 3 to 20 nm by changing experimental conditions or by seed-mediated growth. Furthermore, the formed hydrophobic nanoparticles can be transformed into hydrophilic ones by adding bipolar surfactants, allowing the preparation of stable aqueous nanoparticle suspensions.

1 Theoretical Background

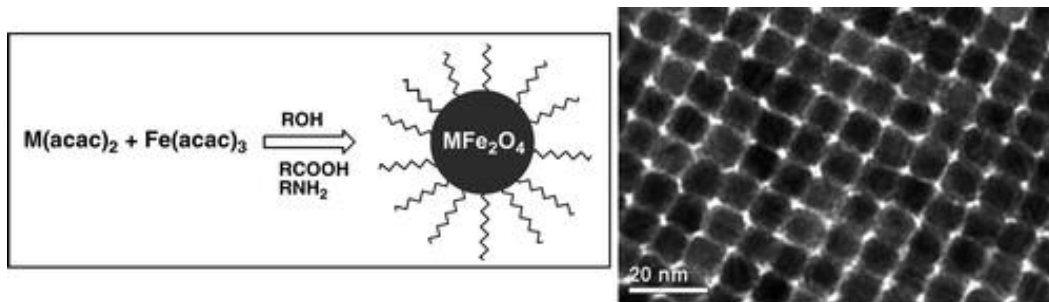


Figure 1.11 The preparation of monodisperse MFe_2O_4 nanoparticles. Reprinted from ref.⁷⁶

Monodisperse iron oxide nanoparticles were prepared by Hyeon et al. using $[Fe(CO)_5]$ or iron oleate precursors (Figure 1.12).⁷⁷⁻⁷⁸ As much as 40 g of monodisperse nanocrystals can be prepared in a single reaction. In addition, one-nanometer-scale size-controlled synthesis of iron oxide nanoparticles was achieved.⁷⁹ It was demonstrated that the thermal decomposition of $[Fe(CO)_5]$ at relatively low temperature induced nucleation while the decomposition of iron oleate at a higher temperature was responsible for the growth. Other magnetic nanoparticles such as iron nanocubes, cobalt nanoparticles, FePt nanoparticles and FePt- Fe_3O_4 heterodimer nanoparticles can also be prepared using thermal decomposition method.⁷⁵

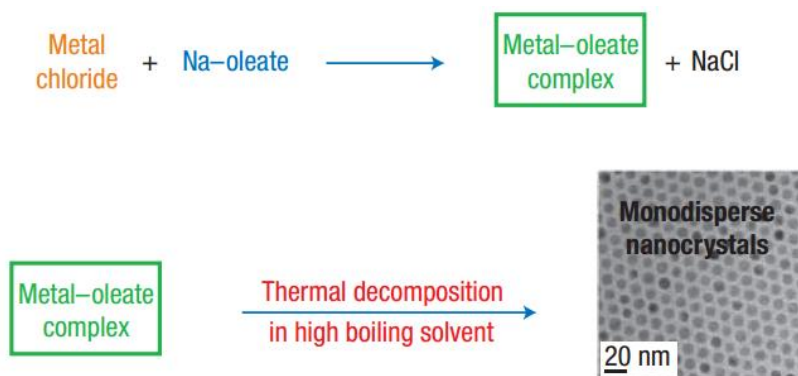


Figure 1.12 Schematic illustration of the synthesis of monodisperse nanocrystals using iron oleate as precursor. Reprinted from ref.⁷⁸

1.3.1.3 Solvothermal synthesis

A general solvothermal method for nanocrystal synthesis was developed by Li's group, which is suitable for the preparation of a serial of nanoparticles, including noble metal,

semiconductors, rare earth fluorescence and magnetic nanoparticles.⁸⁰ This strategy involved a general phase separation and transfer mechanism. Nanoparticles formed at the interfaces of the liquid, solid, and solution phases. Using this method, hydrophobic Fe₃O₄ and CoFe₂O₄ nanoparticles were prepared with very uniform size of about 9 and 12 nm, respectively. In addition, hydrophilic magnetic microspheres were also prepared by the same group.⁸¹ A mixture containing FeCl₃, ethylene glycol, sodium acetate, and polyethylene glycol was sealed in a PTFE-lined stainless-steel autoclave, and then heated to and maintained at 200°C for 8-72 h. Monodisperse ferrite spheres were obtained with tunable sizes in the range of 200-800 nm. In this reaction, ethylene glycol served as a high-boiling-point reducing agent and polyethylene glycol was utilized as a surfactant against particle aggregation. Although well-crystallized magnetic particles can be prepared through solvothermal synthesis, this reaction is usually conducted under high-temperature and high-pressure conditions. And long reaction time from hours to days is required.

Other strategies, like microemulsion, electrochemical deposition, sonochemical decomposition and aerosol/vapor-phase method were also reported for the preparation of magnetic particles. Among these approaches, chemical coprecipitation and thermal decomposition are the most frequently utilized methods. Both methods are suitable for preparation on a large scale. In terms of simplicity of the synthesis, chemical coprecipitation seems the best method. Particles prepared by coprecipitation are hydrophilic. In terms of size and morphology control of the nanoparticles, thermal decomposition is the preferred route, where the particles obtained are hydrophobic.^{72, 75}

1.3.2 Surface modification

Because of the high surface area to volume ratio of nanoparticles, small particles tend to agglomerate to reduce the surface energy. In addition, bare magnetic nanoparticles are highly chemically active, which can be easily oxidized in air. So surface modification is required to stabilize the particles against degradation and prevent the aggregation. It is realized by coating the particles with inorganic layer like silica, gold or graphite, or

1 Theoretical Background

organic species like surfactants or polymers. Furthermore, magnetic nanoparticles can be encapsulated into polymeric shells (Figure 1.13).^{73, 82} The polymeric shells not only hold the magnetic nanoparticles apart against attractive forces, but also provide functional groups like terminal amine or carboxyl moieties for further conjugation with bioactive molecules.

After surface modification, various molecules like drug, fluorophore, antibody, peptide and DNA/RNA can be immobilized onto the surface of magnetic particles (Figure 1.14).⁸³ The biofunctionalized magnetic particles are then utilized for different purposes, e.g., magnetic resonance imaging, drug delivery, cell labeling and separation, DNA detection and immunoassays.⁶¹

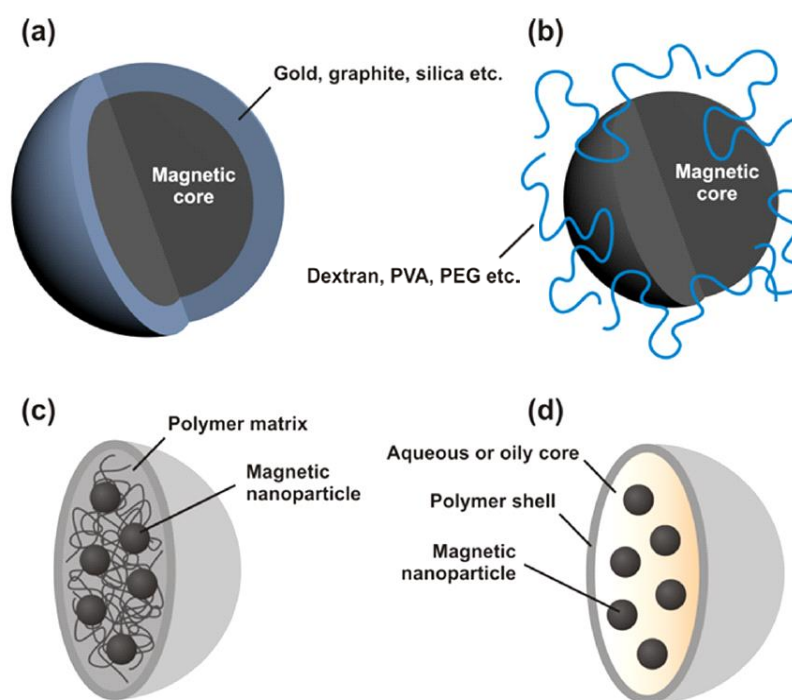


Figure 1.13 Schematic illustration of the stabilization of magnetic nanoparticles by surface coating with inorganic (a) or organic materials (b) or by encapsulation into nanospheres (c) or nanocapsules (d). Reprinted from ref.⁷³

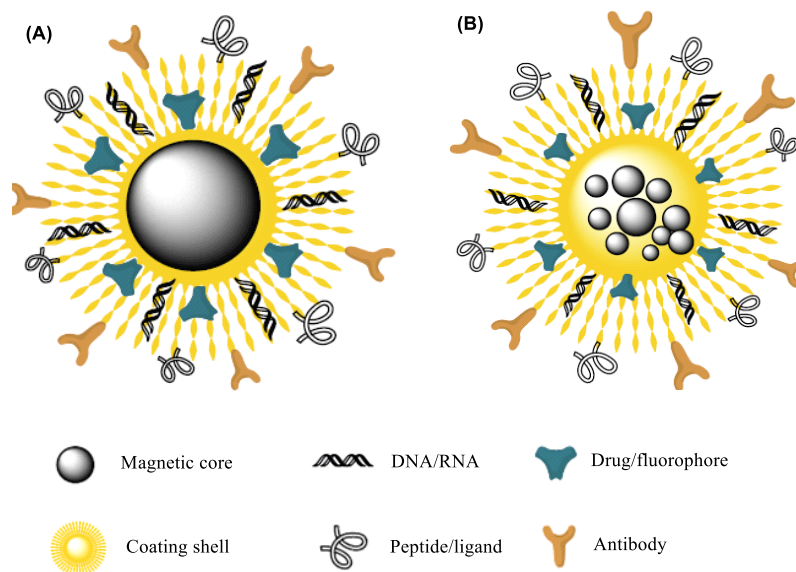


Figure 1.14 Scheme of functionalized magnetic particles with a single core (A) or a group of them (B).

Reprinted from ref.⁸³

1.3.3 Applications of magnetic particles

This section focuses on their applications in analytical chemistry. According to the properties of magnetic particles, they can be either used as solid carrier for fast separation or used as signal reporter in bioanalysis.

1.3.3.1 Serving as carrier

Magnetic particles have a large surface area, diffuse freely in the reaction mixture and more importantly, they can be easily separated using an external magnet. So they are ideal solid carriers. Combining magnetic particles with signal tags such as enzymes,⁸⁴ noble metal nanoparticles,⁸⁵⁻⁸⁶ fluorescent nanoparticles^{33, 87} and carbon nanotubes,⁸⁸ numerous analytes including proteins, DNA and small molecules can be detected.⁸⁹⁻⁹¹ Figure 1.15 shows a sandwich assay for the detection of DNA using magnetic particles for multiple separations. Specifically, the target DNA was captured in a sandwich format by biofunctionalized gold and magnetic nanoparticles. The resulting sandwich complexes were magnetically separated. Then fluorescent DNA probes complementary to the barcode DNA (P2) were immobilized onto the AuNPs. After magnetic separation to remove unbound Cy3-labeled probes, the fluorescence signal of the sandwich complex

1 Theoretical Background

was analyzed, allowing the quantitative analysis of target DNA. As low as 1 pM of DNA could be detected using this method.⁹²

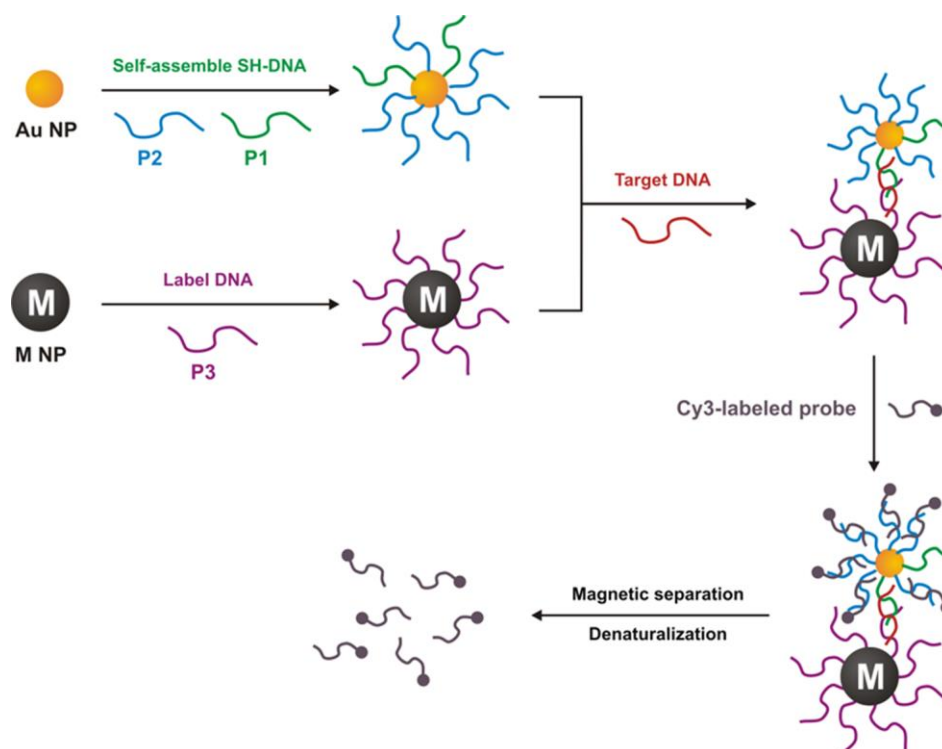


Figure 1.15 Schematic representation of amplified fluorescence detection of DNA based on magnetic separation. Reprinted from ref.⁷³

1.3.3.2 Serving as signal tag

Magnetic particles can be also utilized as signal reporter. In 2007, Gao et al. reported that magnetite nanoparticles (Fe_3O_4 NPs) possess intrinsic peroxidase-like activity, which opens up a wide range of new applications.⁹³ As seen in Figure 1.16, Fe_3O_4 NPs can catalyze the oxidization of different peroxidase substrates with the aid of H_2O_2 , including 3,3,5,5-tetramethylbenzidine (TMB), 3,3'-diaminobenzidine (DAB) and *o*-phenylenediamine (OPD), producing a significant color change. Compared with natural peroxidase, the Fe_3O_4 NPs were much more stable. Their catalytic activity kept almost unchanged after incubation at a range of temperatures (4-90°C). The high catalytic activity of Fe_3O_4 NPs, as well as their low cost, makes them an ideal alternative to peroxidase.

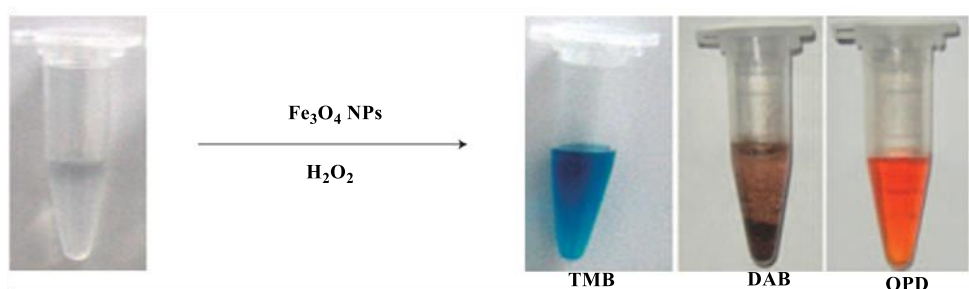


Figure 1.16 Fe_3O_4 NPs catalyze oxidation of peroxidase substrates in the presence of H_2O_2 to produce different color reactions. Reprinted from ref.⁹³

This special catalytic property of Fe_3O_4 particles has been utilized for the detection of H_2O_2 and glucose.⁹⁴ In addition, the Fe_3O_4 NPs can be used for the labeling of antibody, which has been utilized for the detection of proteins, rotaviruses and breast cancer cells (Figure 1.17).⁹⁵⁻⁹⁶

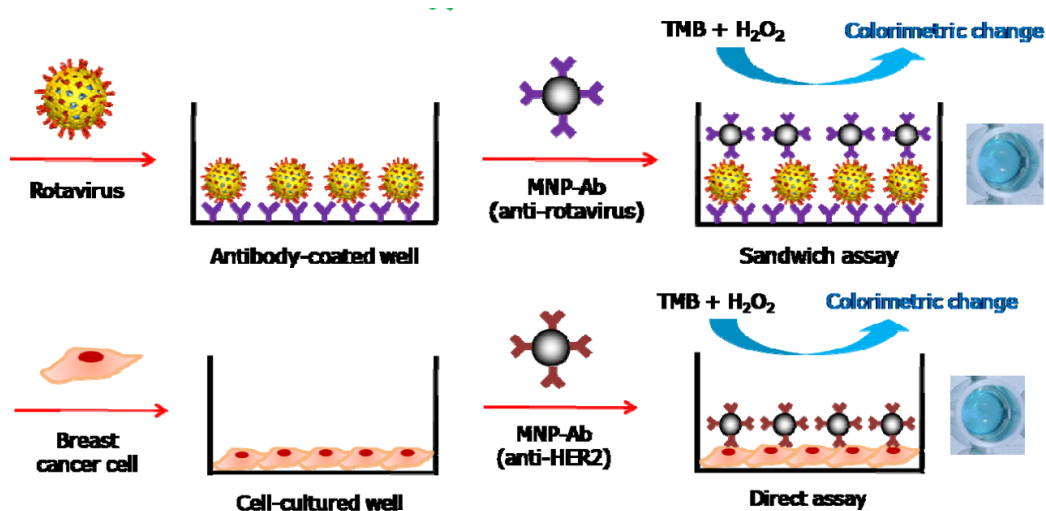


Figure 1.17 The principle of immunoassays for the detection of rotaviruses and breast cancer cells using Fe_3O_4 NPs as enzyme mimics. Reprinted from ref.⁹⁵

Tong et al. developed a nanocrystal-based amplification strategy for protein detection using iron oxide nanoparticles.⁹⁷ As shown in Figure 1.18, iron oxide nanoparticle-labeled antibody bound to the target molecules (i.e., antigen), and then the nanoparticles were dissolved by acid into individual metal ions (Fe^{2+}) that were further stoichiometrically converted to chromophores. Despite tiny in size, one nanoparticle contains thousands to millions of metal atoms. Thus, extremely high signal amplification was realized. In

1 Theoretical Background

contrast, only limited tags are conjugated to the antibody due to steric hindrance, so amplification factor is relatively low in direct amplification. Although high enhancement can be achieved in enzymatic reaction, the amplification is often nonlinear and the activity of natural enzymes may change during storage. The established iron oxide nanoparticle-linked immunosorbent assay allowed the detection of disease markers in low picomolar level with a wide dynamic range.

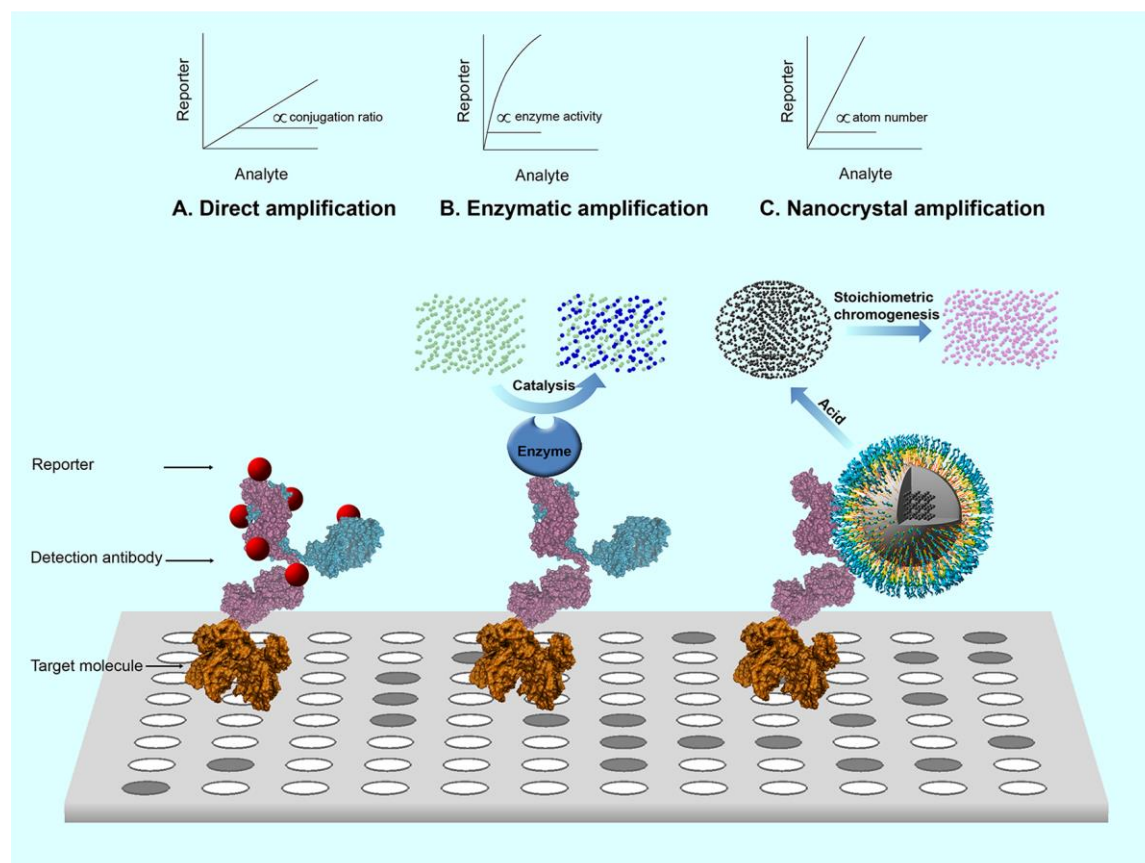


Figure 1.18 Schematic representation of different signal amplification schemes. Reprinted from ref.⁹⁷

Magnetic nanoparticles with different size display great difference in saturation magnetization. Based on this, a sensing platform that combines magnetic separation and magnetic relaxation switching (MS-MRS) has been developed for one-step detection of bacteria and viruses with high sensitivity and reproducibility.⁹⁸ As illustrated in Figure 1.19, a magnetic field of 0.01 T was applied to separate large magnetic beads (250 nm) from small ones (30 nm) and then the transverse relaxation time (T_2) of the water molecules around the 30 nm magnetic beads (MB30) was measured as the signal readout

of the immunoassay. The change of T_2 was proportional to the concentration of analyte. The use of magnetic nanoparticles integrates target enrichment, extraction and detection into one step, which can be completed within 30 min. This method allows the detection of *S. enterica* in milk as low as 100 cfu/mL.

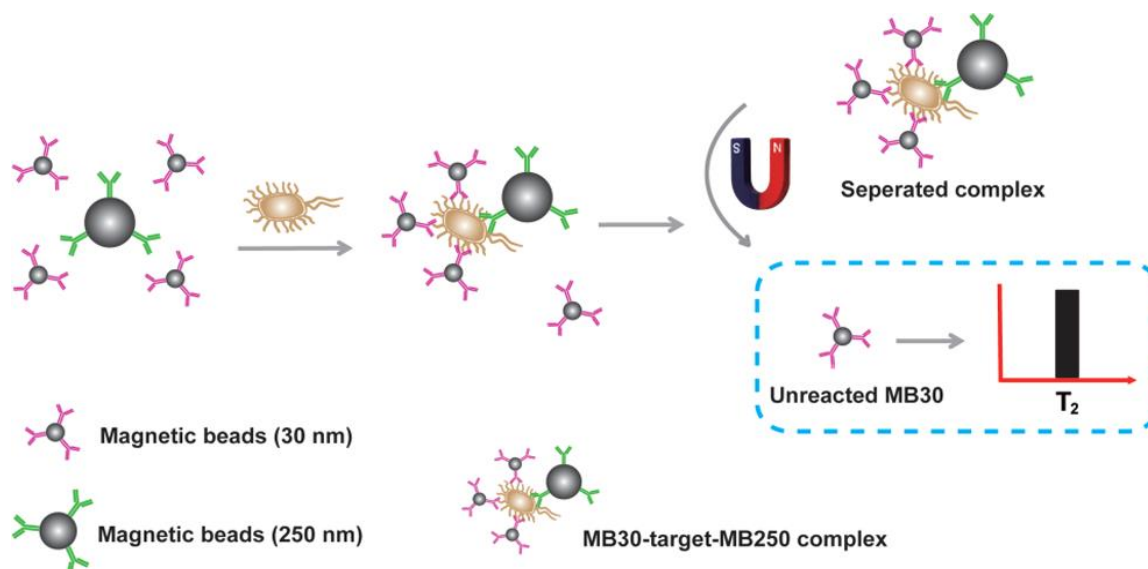
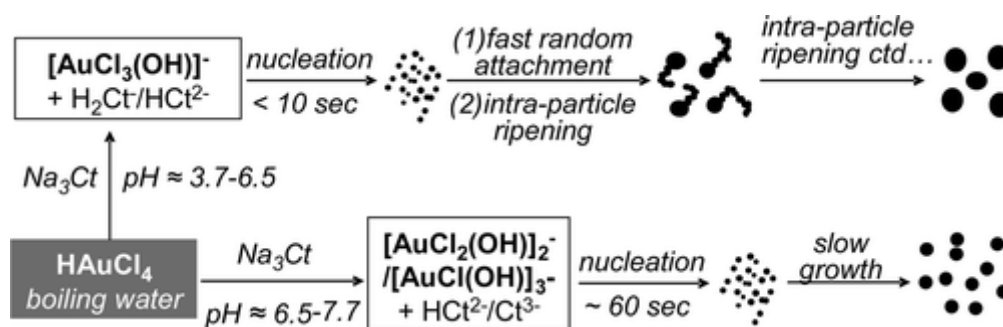


Figure 1.19 Schematic illustration of the MS-MRS sensor. Reprinted from ref.⁹⁸

The integration of magnetic nanoparticles with different analytical techniques has opened new avenues for sensing, purification, and quantitative analysis, which makes magnetic nanoparticles a powerful tool in medicine, bioanalysis and environmental chemistry.

1.4 Gold nanoparticles

Gold nanoparticles (AuNPs) have attracted great attention in the bioanalytical field owing to their unique physical and chemical properties, such as easy preparation, simplicity of modification, superior compatibility and excellent optical property.^{62, 99} They are frequently employed as labels for different biological receptors, including enzymes, antibodies, aptamers/DNA, and other biomolecules,⁶³ which have been utilized for the detection of a wide variety of analytes.¹⁰⁰⁻¹⁰¹ In this section, the preparation of AuNPs, their optical properties and applications in analytical chemistry will be introduced and discussed.



Scheme 1.2 Scheme of reaction pathways for synthesis of AuNPs by citrate reduction under different pH values. Reprinted from ref.¹⁰⁴

AuNPs with different sizes (16-147 nm) can be prepared using this method by varying the ratio of sodium citrate and HAuCl₄. For AuNPs smaller than 30 nm, nearly spherical particles with narrow size distribution were obtained. But deviations from a spherical shape and a broad size distribution, as well as low reproducibility were often observed for the preparation of AuNPs larger than 30 nm. So other methods such as seeded growth synthesis were developed for the preparation of large particles.

1.4.1.2 Seeded growth synthesis

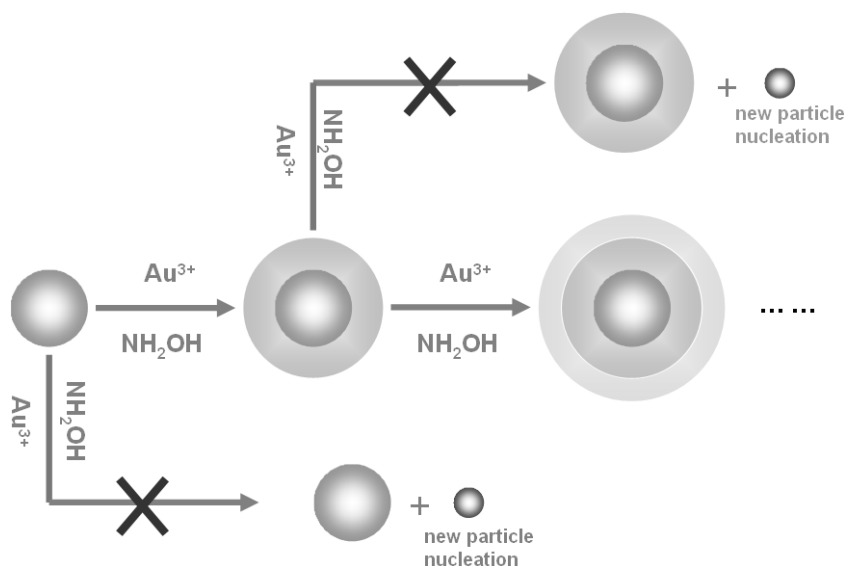


Figure 1.20 Scheme of step-by-step growth method for the synthesis of large AuNPs. Reprinted from ref.¹⁰⁵

Seeded growth methods have been developed for the synthesis of large AuNPs (> 30 nm).¹⁰⁶⁻¹⁰⁸ Generally small gold colloids (< 10 nm) prepared by citrate reduction are used

1 Theoretical Background

as seeds, which are grown to larger sizes based on surface-catalyzed reduction of Au^{3+} (Figure 1.20). Different reducing reagents can be used, such as sodium citrate, ascorbic acid and hydroxylamine. In the presence of small gold colloids, all gold atoms formed are deposited onto the surface of seeds, where the secondary nucleation is effectively avoided. This size of resulting AuNPs can be controlled by changing the ratio between seeds and gold salts. In addition, the grown AuNPs could be also used as seeds for further enlargement. AuNPs up to 200 nm with a uniform quasi-spherical shape and a narrow size distribution can be prepared using the step-by-step growth method.

1.4.2 Optical properties of AuNPs

When a metal nanoparticle is exposed to light, the electromagnetic field of incoming light induces a collective coherent oscillation of the free electrons (conduction band electrons) around the particle surface, resulting in a charge separation with respect to the ionic lattice. And thereby a dipole oscillation is formed along the direction of the electric field of the light (Figure 1.21). The amplitude of the dipole oscillation reaches maximum at a particular frequency, called surface plasmon resonance (SPR).¹⁰⁹

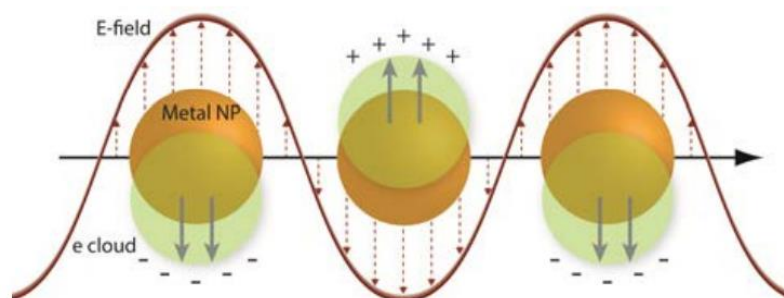


Figure 1.21 Schematic illustration of localized surface plasmon resonance induced by an external electrical field.¹⁰⁹

For Ag and AuNPs, the SPR frequency falls in the visible region of the spectrum. Taking 15-nm AuNPs for example, the SPR effect causes a strong absorption of light in the blue-green portion of the spectrum (~520 nm) while red light is reflected. Thus, the solution of AuNPs takes on deep-red. With the increase of particle size, the SPR peak shifts to longer

wavelengths (Table 1.2). Orange-red light is then absorbed while blue light is reflected, resulting in solutions with a pale blue or purple color.

In addition, AuNPs have extremely high molar extinction coefficient, which makes them ideal chromophore and fluorescence quencher. As listed in Table 1.2, with the increase of particle size, the molar extinction coefficient increased exponentially. In contrast, the molar extinction coefficient of traditional colored compounds is very low, e.g. $3.9 \times 10^4 \text{ M}^{-1}\text{cm}^{-1}$ for oxidized TMB.

Table 1.2 Optical properties of AuNPs with different size.¹¹⁰

Size (nm)	λ (SPR) (nm)	Extinction Coefficient ($\text{M}^{-1}\text{cm}^{-1}$)
5	515-520	1.10×10^7
10	515-520	1.01×10^8
15	520	3.67×10^8
20	524	9.21×10^8
30	526	3.36×10^9
40	530	8.42×10^9
50	535	1.72×10^{10}
60	540	3.07×10^{10}
80	553	7.70×10^{10}
100	573	1.57×10^{11}

1.4.3 Applications of AuNPs

AuNPs are extensively utilized in analytical chemistry. Taking advantage of special optical and chemical properties of AuNPs, a variety of detection platforms have been developed. A short introduction and discussion about these applications are presented in the following part.

1 Theoretical Background

1.4.3.1 Serving as carrier

Owing to the large surface area of AuNPs, they are frequently modified with different molecules, like fluorescent dyes,¹¹¹⁻¹¹² proteins¹¹³⁻¹¹⁴ and DNA¹¹⁵⁻¹¹⁶ to construct specific nanoprobe, which are utilized for the detection of various analytes.^{62, 100} For instance, active biomolecules like enzymes,^{113, 117} artificial DNazymes¹¹⁸ and enzyme-labeled antibodies¹¹⁹⁻¹²⁰ were immobilized on gold surface, which can efficiently catalyze the specific substrates to generate a distinguishable signal change, and thereby the signal was greatly amplified. As another example, AuNPs were used as carrier for accommodating DNA reporter molecules,^{116, 121} and DNA-based amplification could be conducted, e.g. bio-barcode assays.

1.4.3.2 Colorimetric assays based on aggregation of AuNPs

The SPR properties of AuNPs highly depend on particle size, shape and dispersion state. AuNPs appear red when the interparticle distances are substantially larger than the average particle diameter. But as the interparticle distances decrease to less than approximately the average particle size, the color changes to purple or blue. This red-to-blue (purple) color change provides a colorimetric sensing platform which can be observed directly by naked eyes or monitored by UV-vis spectrophotometer.¹²² As shown in Figure 1.22, the AuNPs are first functionalized with special affinity ligands like antibody, DNA or chelating agent. In the absence of target analyte, the functionalized AuNPs are well dispersed and the color is red. In the presence of analytes, the affinity ligands on the surface of AuNPs interact with the targets, inducing the aggregation of AuNPs, and the color changes to blue. This sensing system is simple and fast, which has been employed for the detection of a number of analytes, including thiol compounds, metal ions, proteins and DNA.⁶² But these colorimetric methods often suffer from relatively low sensitivity because of the lack of signal amplification.

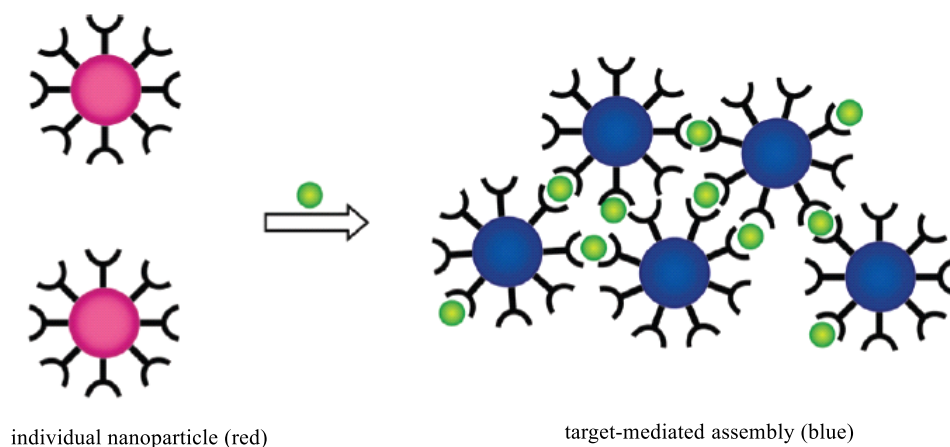


Figure 1.22 Schematic illustration of red-to-blue colorimetric sensing of target using AuNPs functionalized with affinity ligands. Reprinted from ref.⁶²

This colorimetric strategy was also used as the readout in immunoassays.¹²³ As shown in Figure 1.23, ALP-labeled antibodies are subjected to immunoreaction, where ALP enables the hydrolysis of ascorbic acid-phosphate, thus producing ascorbic acid. Cu(II) is then converted into Cu(I) by ascorbic acid. The formed Cu(I) acts as a catalyst that induces aggregation of AuNPs functionalized with azide and alkyne groups, which can be seen as a color change. And similar detection system has been developed for the detection of HIV in blood serum of infected patients.¹²⁴

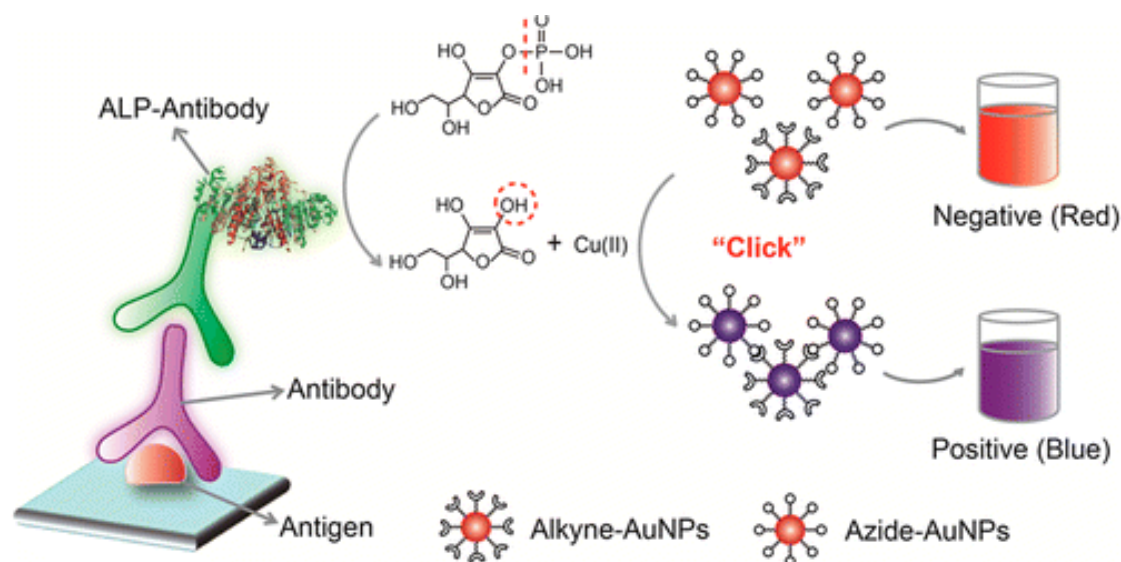


Figure 1.23 Schematic representation of enzyme-triggered click reaction inducing the aggregation of AuNPs. Reprinted from ref.¹²³

1.4.2.3 Fluorescence assays based on FRET

Because of their extraordinary high molar extinction coefficient and broad energy bandwidth, AuNP can effectively quench the fluorescence of nearby fluorophores via Förster resonance energy transfer (FRET). Sensors based on FRET between fluorophores and AuNPs have been developed for the detection of metal ions, small molecules, DNA and proteins.¹²⁵ Figure 1.24 shows the principle of a FRET immunosensor. Antigen labeled with fluorescein isothiocyanate (FITC) specifically reacted with AuNPs-labeled antibody. The fluorescence of FITC was quenched by AuNPs. In the presence of target antigen, the fluorescence quenching effect was inhibited because of the competitive binding. As low as 42 pM of immunoglobulin M (IgM) could be detected using the homogeneous immunoassay.¹²⁶

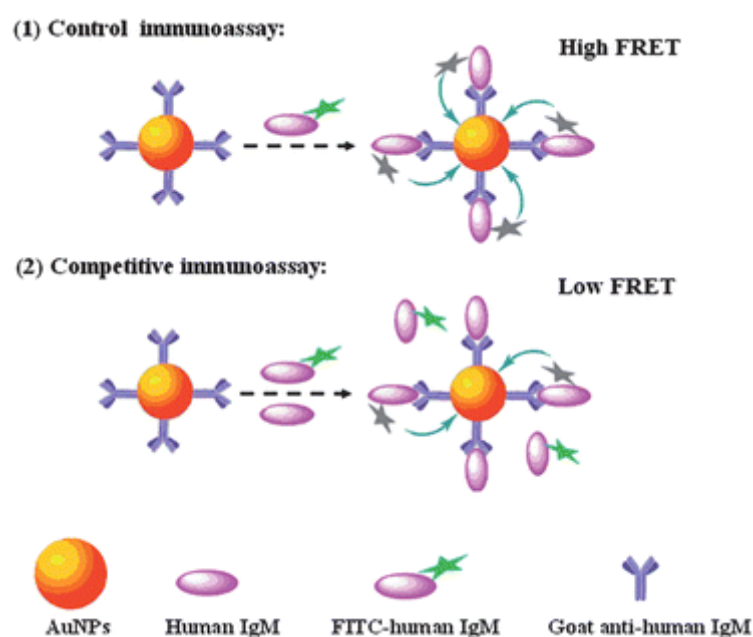


Figure 1.24 Schematic illustration of the determination of human IgM based on FRET immunosensor.

Reprinted from ref.¹²⁶

Due to the large size of antibody (~10 nm), the efficiency of FRET between fluorophores and AuNPs is limited. Improvement could be made by directly coating AuNPs with fluorophores. Recently, Liu et al. developed an ultrasensitive AuNP-based fluorescence-activatable probe,¹¹² as shown in Figure 1.25. Making use of the large surface area of

AuNPs and their high quenching efficiency, thousands of rhodamine B isothiocyanate (RBITC) molecules were immobilized on one AuNP, where their fluorescence was totally quenched. The RBITC-coated AuNPs were further conjugated with antibodies. After immunoreaction, the fluorescence was activated by the addition of cysteamine. Ultrahigh sensitivity was achieved for the detection of prostate-specific antigen (PSA).

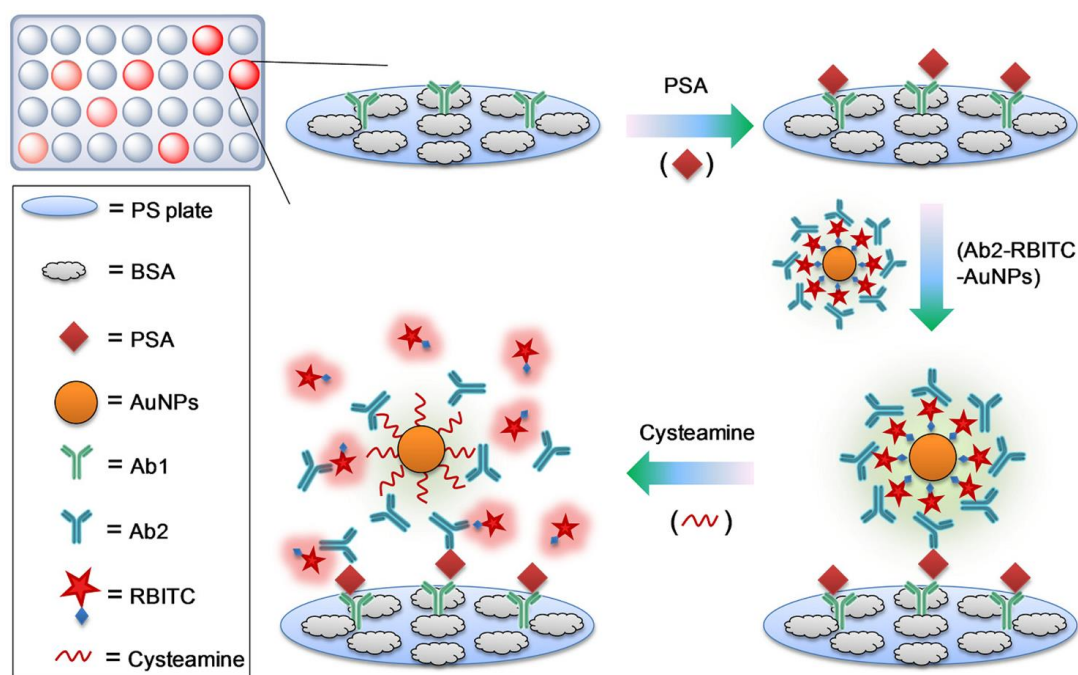


Figure 1.25 Scheme of the AuNP-based fluorescence immunoassay for PSA performed in 96-well PS plates. Reprinted from ref.¹¹²

1.4.3.4 Silver/Gold staining

AuNPs can be utilized as seeds for silver enlargement where the reduction and deposition of silver ions are catalyzed by the AuNPs. The so-called silver staining method has been well developed and extensively applied in biomolecular detection.¹²⁷ Figure 1.26 shows a colorimetric assay for the detection of virus based on enzyme-induced silver enlargement. In the presence of ALP, *p*-aminophenyl phosphate was enzymatically converted into a reducing agent *p*-aminophenol that reduced Ag^+ to Ag^0 in the presence of AuNPs. The formed Ag atoms deposited onto the surface of AuNPs, resulting in a color change of the suspension. Compared with AuNPs, Ag/AuNPs had a much larger molar extinction

1 Theoretical Background

coefficient. Thus, high sensitivity was achieved for the detection of H9N2 avian influenza virus with a LOD of 17.5 pg/mL.¹²⁸

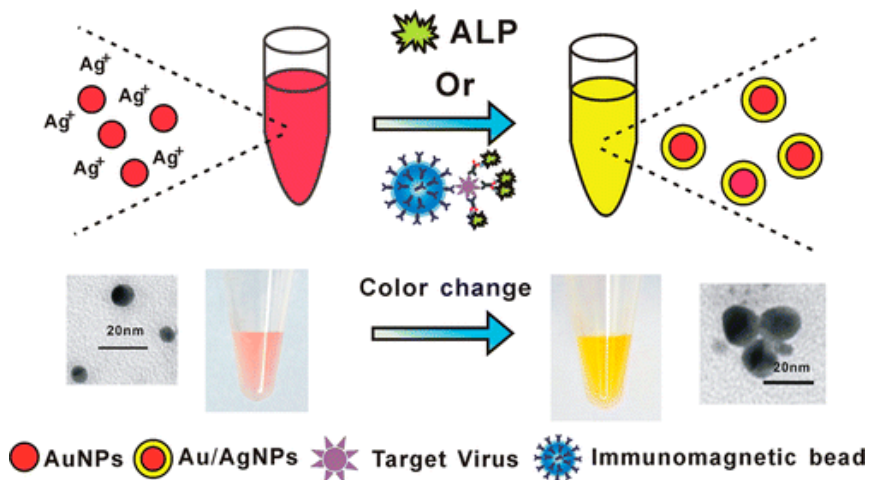


Figure 1.26 Schematic illustration of enzyme-induced silver staining as a signal amplification strategy for the detection of avian influenza virus particles. Reprinted from ref.¹²⁸

However, as a disadvantage, the silver salt is usually sensitive to pH, phosphates, chloride ions and natural light, which limits its practical application. As an alternative, the gold staining, i.e., using gold salt for catalytic enlargement of AuNPs, has solved these problems. The gold staining methods have been widely used for the detection of a variety of targets such as proteins and DNA.¹²⁹⁻¹³¹ Figure 1.27 shows a microarray-based scanometric assay using gold staining for signal amplification. As mentioned above, the molar extinction coefficient of AuNPs increases exponentially with the increase of particle size. Thus, after gold enlargement, the signal (absorbance) is enhanced greatly. Moreover, multiple rounds of metal development can be realized by using the enlarged AuNPs as seeds for further enlargement.

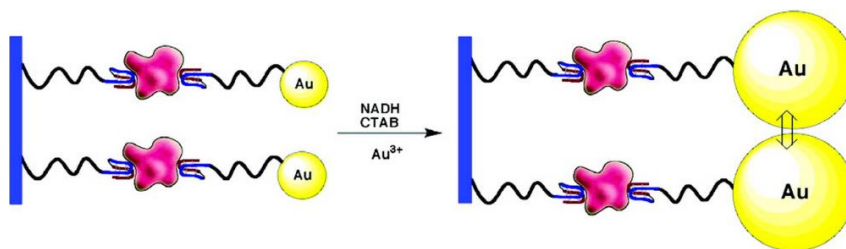


Figure 1.27 Schematic representation of chip-based scanometric assay using gold staining for signal amplification. Reprinted from ref.¹³⁰

But this technique is mostly applied onto solid substrates like glass slides and nitrocellulose strips, therefore, strict control of the reaction conditions are required to obtain acceptable reproducibility.

1.4.3.5 Enzyme-like activity of AuNPs

Recently, Chuang et al. found that heavy metal ions, such as Hg^{2+} , Ag^+ , Pb^{2+} and Bi^{3+} , could greatly enhance the catalytic activity of citrate-capped AuNPs.¹³² As shown in Figure 1.28, the formation of Au-M alloys on the AuNPs surfaces endows the generated bimetallic nanoparticles strong peroxidase-like activity towards the oxidation of Amplex UltraRed (AUR) reagent. In contrast, the activity of unmodified AuNPs towards AUR oxidation is very low. This enzyme-like activity has been used for fluorescent detection of metal ions, acetylcholine and thrombin.¹³³⁻¹³⁵

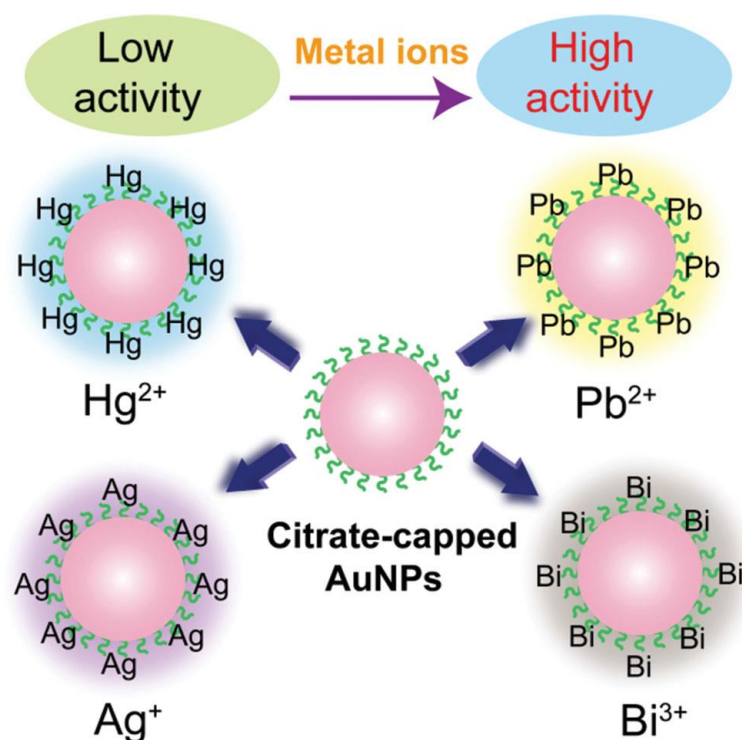


Figure 1.28 The metal ions enhanced peroxidase-like activity of citrate-capped AuNPs. Reprinted from ref. ¹³²

In addition, AuNPs can catalyze the reduction of organic compounds like 4-nitrophenol in the presence of NaBH_4 . An electrochemical detection for proteins was developed by Yang et al. using this reaction for signal amplification,¹³⁶ as illustrated in Figure 1.29.

1 Theoretical Background

AuNPs catalyzed the reduction of 4-nitrophenol to 4-aminophenol (AP) which were further electrochemically oxidized to *p*-quinone imine (QI) via an electron mediation of ferrocene. The oxidized QI is then reduced back to AP by NaBH₄. The oxidation current of AP was greatly amplified during this process, and thereby ultrasensitive detection was realized.

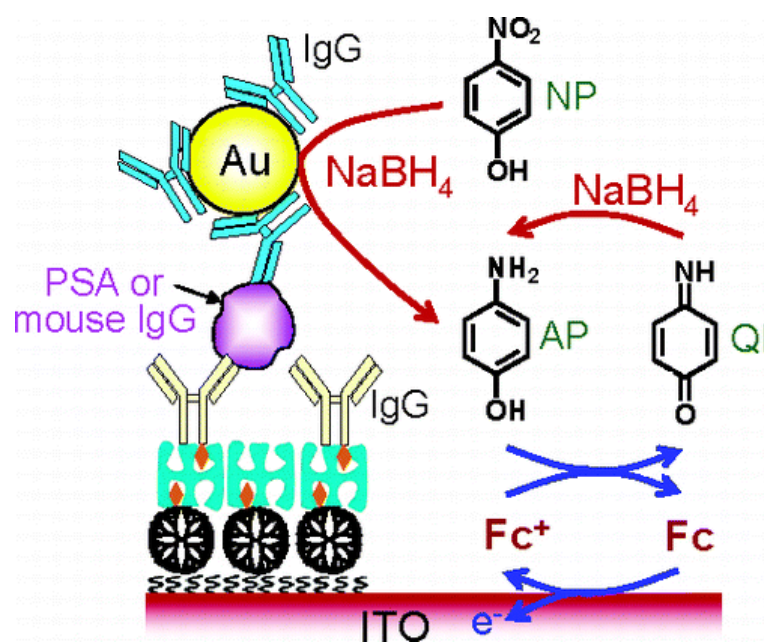


Figure 1.29 Schematic illustration of electrochemical detection of proteins using catalytic reduction of 4-nitrophenol by AuNPs for signal amplification. Reprinted from ref.¹³⁶

When 4-nitrophenol is reduced, its absorbance decreases significantly, which has been used in colorimetric assays for the detection of chloramphenicol residue and human chorionic gonadotropin.¹³⁷⁻¹³⁸ AuNPs can also catalyze the decoloration of other colored dyes, such as methyl orange and methylene blue, which were utilized for signal amplification in colorimetric detection of thrombin.¹³⁹⁻¹⁴⁰

1.5 Nanoparticle-based immunoassays for aflatoxins

Nanoparticles have been frequently utilized in aflatoxins analysis. Compared with traditional methods such as instrumental analysis and ELISA, nanoparticle-based immunoassays are generally fast, easy to operate, cost-effective and highly sensitive. Different analytical techniques were employed in such immunoassays. In this section, we introduced some typical nanoparticle-based immunoassays for aflatoxins developed in recent years.

1.5.1 Colorimetric detection

In 2008, Tudorache et al. developed a magnetic particle-based ELISA for AFB1 determination.⁸⁴ The use of magnetic particles as solid support of the antibody facilitated the fast separation of immune complexes, and thereby reducing the testing time. As low as 1 ppt AFB1 could be detected under optimized conditions.

Recently, Ying's group developed a homogeneous colorimetric immunoassay for AFB1 based on competitive dispersion of gold nanorods,¹⁴¹ as illustrated in Figure 1.30. In the absence of AFB1, *anti*-AFB1 served as a linker to induce the aggregation of gold nanorods, resulting in large decrease in absorbance at 709 nm. The aggregation was competitively inhibited in the presence of AFB1, allowing the determination of AFB1 in a linear range from 0.5 to 20 ng/mL. Although not so sensitive compared with ELISA, the homogeneous assay is attractive because tedious separation and washing steps are eliminated.

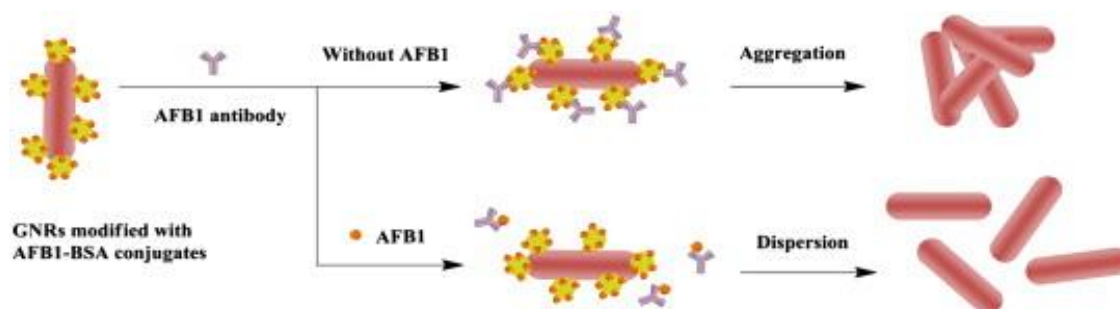


Figure 1.30 AFB1 sensing based on competitive dispersion of gold nanorods. Reprinted from ref.¹⁴¹

1.5.2 Fluorescent detection

Homogeneous fluorescence immunoassay for AFB1 has been developed by Xu et al. based on FRET between different-sized quantum dots (QDs),¹⁴² as seen in Figure 1.31. Two kinds of QDs with different emission (i.e. QSA₅₃₀ and QSH₆₂₀) were coated with AFB1 and antibody, respectively. FRET occurred between these two QDs in the absence of AFB1, and the green fluorescence of QSA₅₃₀ was quenched by QSH₆₂₀. With the increase of AFB1, the FRET effect was inhibited, resulting in a decrease in red fluorescence and an increase in green fluorescence. A dynamic range of 0.06-5 ng/mL with a LOD of 0.04 ng/mL was obtained for AFB1 determination in rice extracts.

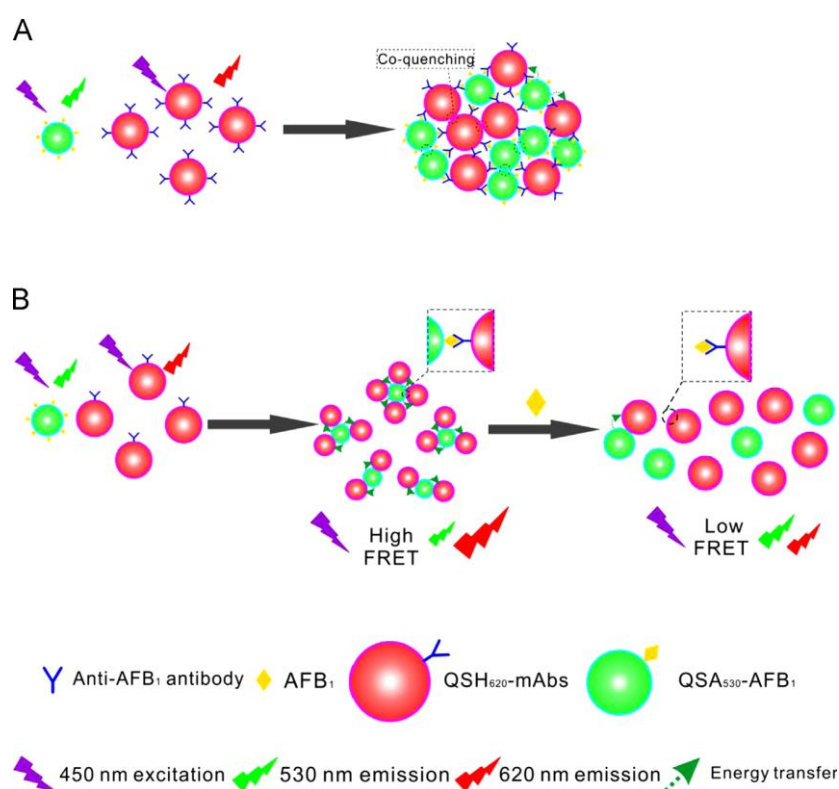


Figure 1.31 Schematic illustration of the competitive homogenous QDs-FRET immunosensing strategy for the determination of AFB1. Reprinted from ref.¹⁴²

Magnetic bead-based luminescent immunoassays were also developed for AFB1, using either biofunctionalized upconversion nanoparticles⁹¹ or rhodamine B-doped silica nanoparticles³³ as signal probes. Recently, Tang's group developed a novel fluorescence immunoassay strategy for sensitive detection of AFB1 using functionalized magnetic

mesoporous silica nanoparticles (MMSN) and AuNPs.¹¹³ As shown in Figure 1.32, mannose-conjugated MMSN was capped with biotinylated concanavalin A (Con A) which encapsulated rhodamine B within the pores of MMSN, and then the biotinylated *anti*-AFB1 was immobilized through streptavidin-biotin interactions. AuNPs coated with BSA-AFB1 conjugate and invertase were employed as immunosensing probes, which competed with target AFB1 for binding with the immobilized antibody on MMSN. After magnetic separation, the carried invertase converted sucrose into glucose which displaced the Con A-antibody complex from the MMSN, and thereby the encapsulated rhodamine B molecules were released, producing a strong fluorescence signal. The fluorescence intensity was inversely proportionally to AFB1 concentration from 0.01 to 5 ng/mL with a LOD of 8 pg/mL. Although highly sensitive, the assay procedure is really complicated.

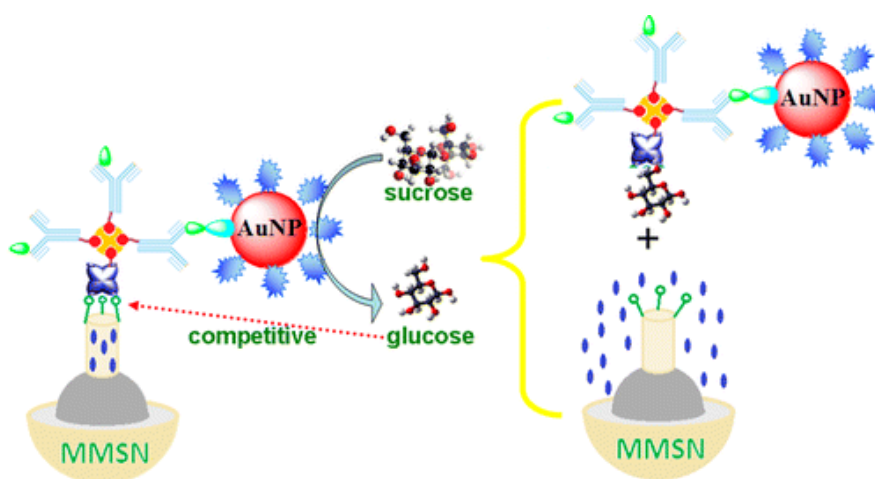


Figure 1.32 Schematic representation of the fluorescence immunoassay based on target-induced displacement reaction accompanying cargo release from MMSNs. Reprinted from ref.¹¹³

1.5.3 Light scattering detection

AuNPs are capable of scattering light. For instance, the scattered light intensity of AuNPs is about 10^5 times stronger than a fluorescein molecule and 100-1000 times stronger than a polymer bead.⁹⁹ Based on this, a magnetic particle-based immunoassay for AFB1 was developed using dynamic light scattering (DLS) as the readout (Figure 1.33).¹⁴³ Free AFB1 and AFB1-AuNPs competitively bound with antibodies immobilized on magnetic particles. After magnetic separation, the supernatant containing unbound AuNPs was

1 Theoretical Background

directly measured by DLS instrument. Because color development step was eliminated, the described method was very fast with a total assay time of ~ 20min.

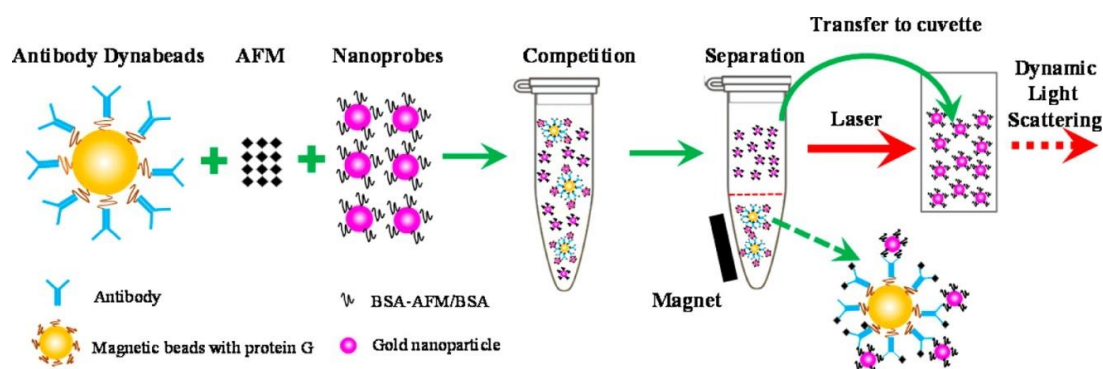


Figure 1.33 Magnetic particle-based immunoassay for AFM1 using DLS as the readout. Reprinted from ref.¹⁴³

Surface-enhanced Raman scattering (SERS) technique has also been utilized for aflatoxins analysis. Very recently, Ko et al. designed an SERS-based immunoassay for AFB1 using silica-encapsulated hollow AuNPs as SERS-encoding nanoprobes. Quantitative determination of AFB1 was realized by monitoring the intensity change of the characteristic peaks of Raman reporter molecules. The detection could be completed in 30 min with a LOD of 0.1 ng/mL.¹⁴⁴

1.5.4 Electrochemical detection

In 2009, our group developed a sensitive and reusable electrochemical immunoassay for AFB1 in food.¹⁴⁵ AFB1-BSA-modified magnetic nanoparticles consisting of a CoFe_2O_4 core with a silica shell doped with Prussian blue nanoparticles were attached on the surface of an indium tin oxide (ITO) electrode, while AuNPs coated with HRP-labeled *anti*-AFB1 were employed as recognition probes. Using a competitive immunoassay format, 0.05-12 ng/mL of AFB1 could be detected with a LOD of 6.0 pg/mL.

The sensitivity was further improved using a target-induced displacement strategy, as illustrated in Figure 1.34. Multifunctional silica beads doped with HRP-thionine were coated with *anti*-AFB1 and Con A. The silica beads were immobilized on dextran-modified glassy carbon electrode (GCE) through the dextran-Con A interactions. AuNPs

functionalized with BSA-AFB1 conjugate and invertase were employed as the trace tag. A competitive immunoreaction occurred for the immobilized antibodies on the electrode between free AFB1 in sample and AuNP-labeled BSA-AFB1. The carried invertase catalyzed the hydrolysis of sucrose into glucose. And the immobilized silica beads were displaced from the surface of electrode by the generated glucose, resulting in a decrease in catalytic efficiency of HRP towards thionine-H₂O₂ system. The electrochemical signal was proportional to AFB1 concentration and a lower LOD (2.7 pg/mL) for AFB1 was achieved.¹⁴⁶

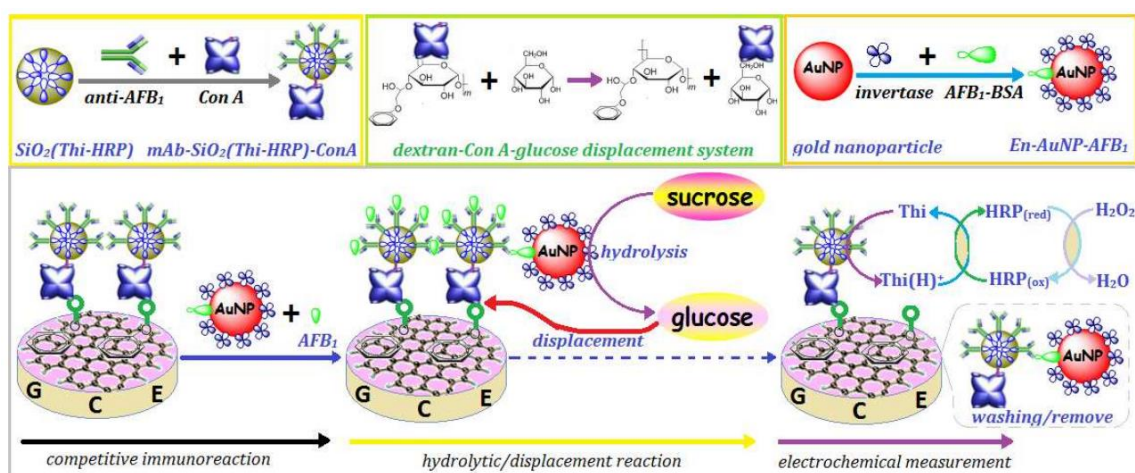


Figure 1.34 Schematic illustration of electrochemical immunoassay for AFB1 based on target-induced displacement reaction. Reprinted from ref.¹⁴⁶

1.5.5 Other methods

Other method, like chemiluminescence technique, was also utilized for the analysis of aflatoxins.¹⁴⁷ In addition, a novel immunosensing platform for AFB1 was recently developed by Tang's group using a portable personal glucometer (PGM) as the readout. Different from conventional immunoassays which use aflatoxin conjugate as a competitor, in the new system polyethylenimine (PEI) was utilized as a pseudo-hapten. As shown in Figure 1.35, two nanomaterials were utilized, including PEI-functionalized mesoporous silica nanocontainers (PEI-MSN) and antibody-conjugated AuNPs (Ab-AuNPs). Initially numerous glucose molecules were entrapped within the pores of MSN by Ab-AuNPs. Upon target AFB1 introduction, Ab-AuNPs were displaced from the surface of MSN,

1 Theoretical Background

resulting in the opening of molecular gates. And thereby the encapsulated glucose molecules could release from the pores, which were quantitatively measured by a PGM. The method could detect AFB₁ in the range of 0.01-15 $\mu\text{g}/\text{kg}$ with a LOD of 5 ng/kg .¹⁴⁸

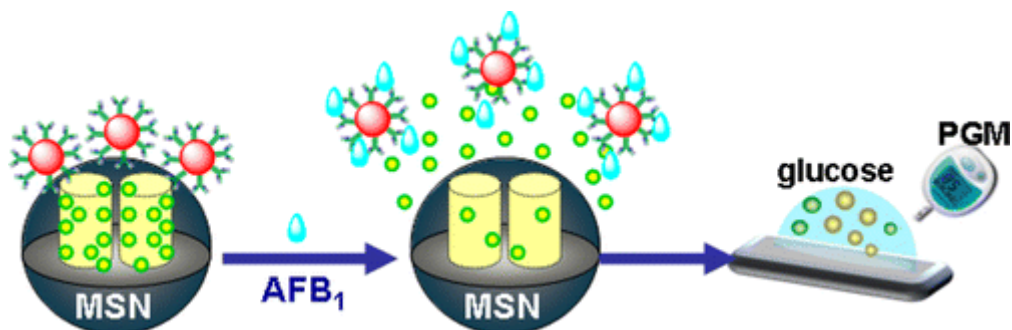


Figure 1.35 Glucometer-based detection for AFB₁ using MSN and AuNPs. Reprinted from ref.¹⁴⁸

1.6 Outline of this thesis

Numerous immunological methods have been developed for aflatoxins analysis. In order to achieve high sensitivity, different strategies were utilized. For instance, complicated nanostructures, such as mesoporous silica nanocontainers and magnetic core-shell nanomaterials, were used for multifunctional signal transduction. Although high sensitivity is achieved, the sophisticated preparation procedure of these nanomaterials is a main problem. Furthermore, deviations are accumulated during multi-step synthesis, which may result in low reproducibility. Apart from nanomaterials, enzymes are extensively utilized in immunoassays for catalytic amplification. However, the preparation and purification of enzyme conjugates are generally time-consuming and expensive. In addition, as a kind of proteins, enzymes tend to denature under environmental changes, which will increase the uncertainties of assay.

Hence, to overcome these limitations, we used simple nanomaterials, including AuNPs and magnetic particles, combined with immunoassays for the analysis of aflatoxins. Figure 1.36 illustrates the principle of the established immunoassays. AFB₁-BSA-modified magnetic beads (AFB₁-BSA-Fe₃O₄; MBs) were employed as immunosensing probe and *anti*-AFB₁ antibody coated AuNPs (Ab-AuNPs) were used for immunological

recognition of AFB1 and for signal transduction. Specifically, free AFB1 in sample competed with AFB1-BSA-Fe₃O₄ for binding with the AuNP-labeled antibodies. After magnetic separation of the formed AuNPs-MBs immune complexes, the supernatant containing unbound AuNPs was utilized for further experiments. Due to the extremely high molar extinction coefficient of AuNPs, the absorbance of the supernatant can be directly read out using a UV-vis spectrophotometer (Section 3.1). In addition, because AuNPs possess special catalytic properties, they were utilized as artificial enzyme for signal amplification. Homogeneous gold staining (Section 3.2) and AuNP-catalyzed uranine reduction (Section 3.3) were performed to improve the sensitivity.

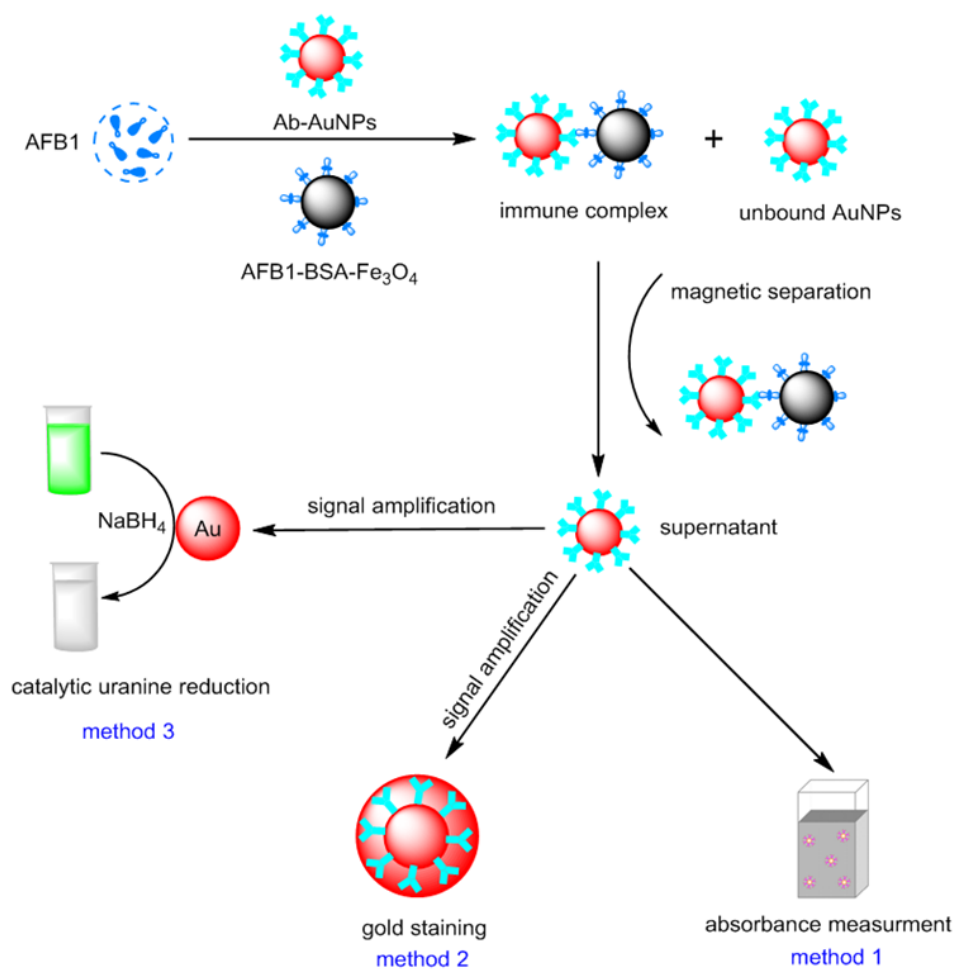


Figure 1.36 Schematic illustration of magnetic bead-based immunoassays for AFB1 using Ab-AuNPs.

1 Theoretical Background

2 Experimental Section

2 Experimental Section

2.1 Materials and instrumentation

2.1.1 Chemicals

The following chemicals and solvents were used without further purification.

Acetonitrile (271004, Sigma-Aldrich, Steinheim)

AFB1- BSA Conjugate from *Aspergillus flavus* (A6655, Sigma-Aldrich, Steinheim)

Aflatoxin B1 (32754, Sigma-Aldrich, Steinheim)

3-Aminopropyltriethoxysilane (APTES, 09324, Sigma-Aldrich, Steinheim)

Ammonia ($\text{NH}_3 \cdot \text{H}_2\text{O}$, 221228, Sigma-Aldrich, Steinheim)

Bovine serum albumin (BSA, A-2153, Sigma-Aldrich, Steinheim)

Buffer solutions (pH 3.0-9.0, Carl Roth, Karlsruhe)

Cetyltrimethylammonium bromide (CTAB, 9161.1, Roth, Karlsruhe)

Chloroform (288306, Sigma-Aldrich, Steinheim)

Dimethylaminopyridine (DMAP, 107700, Sigma-Aldrich, Steinheim)

Ethanol (34852, Sigma-Aldrich, Steinheim)

Ethanolamine (0342.1, Carl Roth, Karlsruhe)

Ferrous sulfate heptahydrate ($\text{FeSO}_4 \cdot 7\text{H}_2\text{O}$, 215422, Sigma-Aldrich, Steinheim)

Fluorescein sodium salt (F6377, Sigma-Aldrich, Steinheim)

Fumonisin B1(32936, Sigma-Aldrich, Steinheim)

Glutaraldehyde (820603, Merck, Darmstadt)

Glycine (33226, Sigma-Aldrich, Steinheim)

Gold(III) chloride hydrate (50790, Sigma-Aldrich, Steinheim)

Iron (III) chloride hexahydrate ($\text{FeCl}_3 \cdot 6\text{H}_2\text{O}$, 31232, Sigma-Aldrich, Steinheim)

L-Asorbic acid (95210, Sigma-Aldrich, Steinheim)

2 Experimental Section

L-Tryptophan (T0254, Sigma-Aldrich, Steinheim)

Melamine (125350050, Acros Organics, Geel, Belgium)

Methanol (34860, Sigma-Aldrich, Steinheim)

Mouse monoclonal *anti*-aflatoxin antibody 1F2 (IWC, TUM, Munich)

4-Nitroaniline (185310, Sigma-Aldrich, Steinheim)

Ochratoxin A (O1877, Sigma-Aldrich, Steinheim)

Polyethylene glycol 8000 (PEG-8000, 0263.1, Carl Roth, Karlsruhe)

Potassium carbonate (K_2CO_3 , 4928, Merck, Darmstadt)

Sodium borohydride ($NaBH_4$, 71321, Sigma-Aldrich, Steinheim)

Sodium chloride ($NaCl$, HN00.2, Carl Roth, Karlsruhe)

Sodium citrate tribasic dihydrate (71402, Sigma-Aldrich, Steinheim)

Sodium dihydrogen phosphate dihydrate ($Na_2HPO_4 \cdot 2H_2O$, 6345, Merck, Darmstadt)

Sodium dodecyl sulfate (SDS, 436143, Sigma-Aldrich, Steinheim)

Sodium hydroxide ($NaOH$, P031.2, Carl Roth, Karlsruhe)

Sodium phosphate dibasic dihydrate ($Na_2HPO_4 \cdot 2H_2O$, 71638, Sigma-Aldrich, Steinheim)

Sodium thiosulfate ($Na_2S_2O_3$, 217263, Sigma-Aldrich, Steinheim)

T-2 Toxin, liquid in Acetonitrile, 99 % (B-MYC0540-1, LGC Standards, Wesel)

Trichloroacetic acid (T6399, Sigma-Aldrich, Steinheim)

Tween-20 (8.22184.2500, Merck, Darmstadt)

Milk and pulverized maize samples were purchased from a local market in Munich.

Phosphate buffer solution (PBS) was prepared by using 0.2 M NaH_2PO_4 and 0.2 M Na_2HPO_4 and then diluted to the corresponding concentration.

2.1.2 Instrumentation

Ultrapure water was produced using reverse osmosis with UV treatment (Milli-RO 5 Plus, Milli-Q185 Plus, Millipore, Eschborn, Germany).

UV-vis absorption spectra were measured on a Specord 250 Plus UV-vis spectrophotometer (Analytik Jena, Jena, Germany).

Resonance light scattering (RLS) spectra were measured on a RF-5301 PC spectrofluorometer (Shimadzu Europe GmbH, Duisburg, Germany) by simultaneously scanning the excitation and emission monochromators from 300 to 800 nm with $\Delta\lambda = 0$ nm and sensitivity set to low.

Fluorescence spectra were collected on the RF-5301 PC spectrofluorometer. The excitation wavelength was 493 nm with slit widths of both excitation and emission light kept at 3 nm and sensitivity set to low.

The microtiter plate (Ref. 655201, Greiner, Frickenhausen, Germany) was read with a Synergy HT plate reader (Bio-Tek, Bad Friedrichshall, Germany).

Dynamic light scattering (DLS) measurements were performed on a NANO-flex particle size analyzer (Microtrac, Meerbusch, Germany).

2.2 Colorimetric immunoassay for AFB1

2.2.1 Preparation of AFB1-BSA-Fe₃O₄

Fe₃O₄ MBs were synthesized according to a previously reported method.⁸⁸ In brief, 1.35 g of FeCl₃·6H₂O and 0.695 g of FeSO₄·7H₂O were dissolved in 25 mL of water. The solution was heated at 85°C for 10 min. Then 2 mL of ammonia (28% in water) was added. After stirring at 85°C for 30 min, the obtained black particles were separated using an external magnet and washed thoroughly with water and ethanol. The particles were dried at 120°C for 30 min. Then 60 mg of Fe₃O₄ particles were dispersed in 10 mL of ethanol under ultrasonic treatment for 15 min. 100 μL of water and 200 μL of APTES were added. The suspension was shaken for 5 h at room temperature. The APTES-

2 Experimental Section

modified Fe_3O_4 particles ($\text{NH}_2\text{-Fe}_3\text{O}_4$) were separated and washed thoroughly to get rid of any physically adsorbed APTES. The amino-functionalized particles were dispersed in 4 mL water.

One milliliter of $\text{NH}_2\text{-Fe}_3\text{O}_4$ (~15 mg/mL) was washed and dispersed in 1 mL of phosphate buffer solution (PBS, pH 8.0, 50 mM). Then 0.5 mL of glutaraldehyde (25% in water) was added and the suspension was shaken for 1 h at 100 rpm. The aldehyde-activated particles were separated, washed and re-dispersed in 1 mL of 50 mM PBS (pH = 8). Finally 50 μL of AFB-BSA (1.5 mg/mL in water) was added and the suspension was well mixed and then shaken overnight. To block free sites on MBs' surface, 100 μL of BSA solution (50 mg/mL) was added and the mixture was shaken for another 1 h. The obtained AFB1-BSA- Fe_3O_4 particles were washed five times with water, dispersed in 5 mL water and stored at 4°C when not in use. The concentration of AFB1-BSA- Fe_3O_4 was ~3 mg/mL. Figure 2.1 illustrates the preparation process.

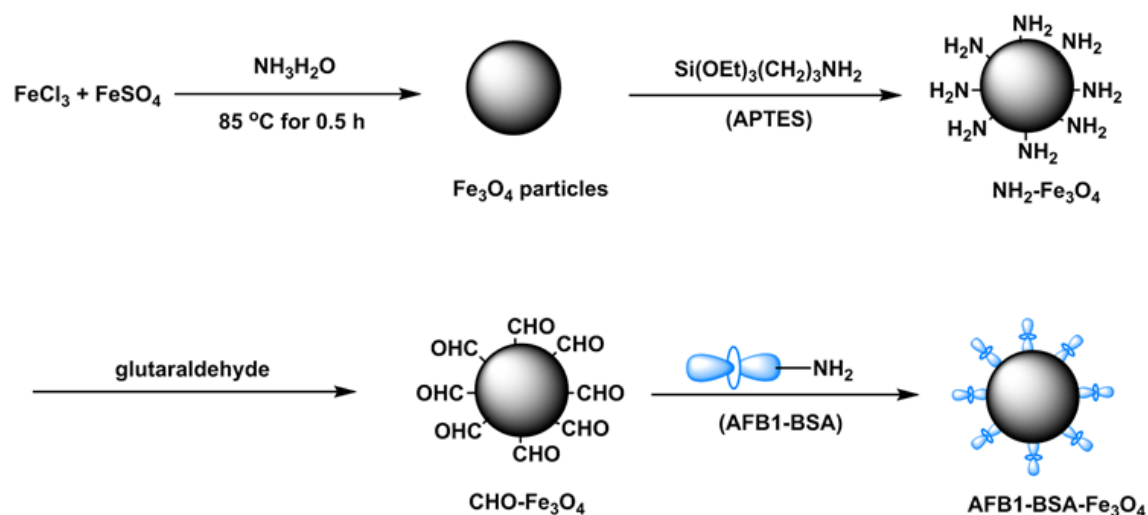


Figure 2.1 Schematic illustration of the preparation and modification of magnetic particles.

2.2.2 Preparation of Ab-AuNPs

AuNPs were prepared according to the Frens method.¹⁰³ To avoid any unwanted nucleation and aggregation during the synthesis, all glassware and stirrer were cleaned thoroughly with aqua regia ($\text{HNO}_3\text{-HCl}$, 1:3, v/v), and then washed with water before use. Briefly, a solution of sodium citrate was quickly added to a boiled HAuCl_4 solution

(0.01%, 50 mL) under vigorous stirring. The color changed from yellow over black to red and the solution was kept boiling and stirred for further 15 min. Then the colloidal solution was cooled to room temperature and filtered through a syringe filter with pore size of 220 nm. The obtained AuNPs were stored at 4°C in the refrigerator. Different size AuNPs were prepared by changing the amount of sodium citrate. The AuNPs were characterized by UV-Vis spectroscopy and DLS measurements.

Ab-AuNPs were prepared following a previously reported procedure with a few modifications.¹⁴⁹ Figure 2.2 represents the fabrication of Ab-AuNPs. First, the pH value of AuNPs solution was adjusted to 8~9 by adding 0.1 M K_2CO_3 . 50 μ L of *anti*-AFB antibody (1 mg/mL in 10 mM PBS containing 0.8% NaCl) was added to 5 mL of pH-adjusted AuNPs solution. After incubation for 1 h at room temperature, 570 μ L of 5% BSA was added to block any free binding sites on AuNPs' surface. 1 h later, Tween-20 was added to a final concentration of 0.1% (w/v) for stabilizing the AuNPs. The excess antibody, BSA and Tween-20 were removed by centrifugation at 9500 g for 15 min at 4°C. The pink supernatant was carefully removed. The oily ruby sediment was washed twice and finally dispersed in 4 mL washing solution (5 mM PBS, pH 7.4, 0.1% PEG-8000). The antibody modified AuNPs were stored at 4°C.

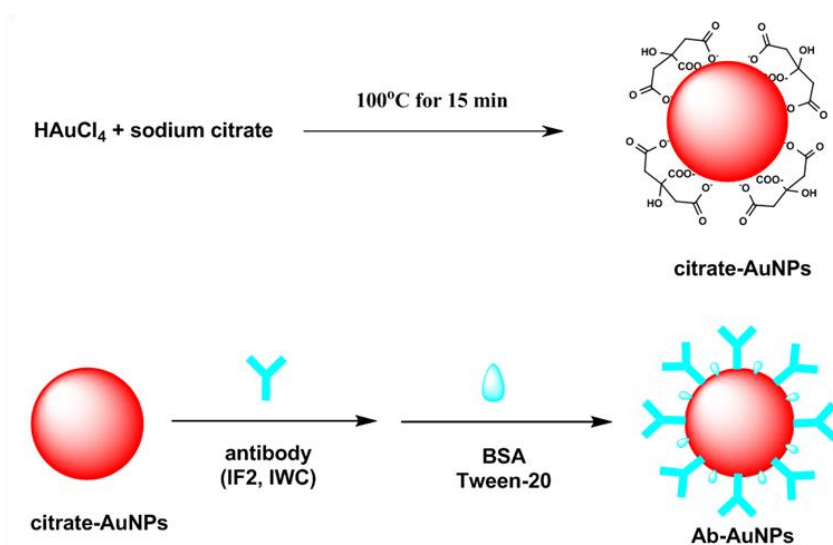


Figure 2.2 Schematic illustration of the preparation of Ab-AuNPs.

2.2.3 Optimization and detection procedures

General procedure for the detection of AFB1: 100 μL of AFB1 standard solution in 50 mM PBS at varied concentrations were mixed with 100 μL of Ab-AuNPs, and then 20 μL of AFB1-BSA- Fe_3O_4 suspension (~ 3 mg/mL) were added. The mixture was well mixed and incubated at room temperature for 30 min with a rotation speed of 200 rpm on a shaker. After magnetic separation of the formed immune-complexes (i.e., *anti*-AFB1-AuNP-AFB1-BSA- Fe_3O_4), the supernatant was directly transferred into a cuvette for UV-vis measurements. The absorbance maximum was recorded and final absorbance was calculated by subtracting the absorbance of the corresponding blank samples. Each immunoassay was conducted three times to determine the reproducibility.

To study the influence of AuNP size on the performance of AFB1 detection, antibody-modified AuNPs with three different sizes were used. To investigate the effect of pH value on testing results, AFB1 standard solutions were prepared in three different pH buffers: 6.0, 7.4 and 8.2 at 50 mM. To test the influence of incubation time on the immunoassay, mixed solution with 20 μL AFB1-BSA- Fe_3O_4 , 100 μL Ab-GNPs (34.8 nm) and 100 μL PBS (50 mM, pH 7.4) were incubated for 2 to 60 min and separated at corresponding time.

To evaluate the selectivity of the developed approach, OTA, T-2 toxin, FB1 and their mixtures with AFB1 were tested. The concentration of all other mycotoxins used was 20 ng/mL, while the concentration of AFB1 was 1 ng/mL.

2.2.4 Preparation of maize samples

1 g of the pulverized maize samples was spiked with AFB1 (in methanol) at concentrations of 0, 5, 10, 20 and 50 $\mu\text{g}/\text{kg}$, respectively. The spiked samples were kept overnight at room temperature in a light-protected fume hood to evaporate methanol. Then the spiked samples were extracted with 5 mL of methanol-water (80:20, v/v) by vortex mixing for 3min and then centrifugated at 1920 g for 15 min. The supernatant was 20-fold diluted with PBS (50 mM, pH = 7.4) for colorimetric assays.

2.3 Controlled growth of immunogold for signal amplification

Ab-AuNPs and MBs were prepared and characterized as described above. The AuNPs with size of 35 nm were used. The concentration of AuNPs and MBs was estimated to be 0.36 nM and ~4 mg/mL, respectively.

2.3.1 Preparation of gold growth solution

General procedure: 25 μ L of 0.1 M HAuCl₄ was added to 10 mL of 100 mM CTAB in water. The mixture was heated in a water bath and mixed until all the precipitates were dissolved. Then 100 μ L of 100 mM AA solution was added. The solution changed immediately from clear orange to colorless. The growth solution was ready for use after cooling down to room temperature.

To study the influence of CTAB on gold enhancement, CTAB solution with different concentrations (0, 5, 10, 25, 50, 75, 100 mM) was used to prepare the gold growth solution. To investigate the effect of AA, solutions were tested with different final concentrations (0.5, 0.55, 0.6, 0.75, 1, 2, 5, 10 mM). Volumes of 10, 25 and 40 μ L of HAuCl₄ were used to evaluate the influence of gold concentration.

2.3.2 Growth of AuNPs in aqueous phase

The immunogold nanoparticles (~0.18 nM Ab-AuNPs in 25 mM PBS, pH 7.4, 0.05% PEG-8000) were used as gold seeds for the enlargement. Generally, 50 μ L of gold seeds were added to 1.0 mL of the growth solution. The absorption spectra were measured after 30 min. The kinetics of the AuNP growth was quantitatively monitored by UV-vis and RLS spectroscopy. To study the influence of immunogold concentration, different amounts of gold seeds (10-50 μ L) were added to 1.0 mL growth solution for gold enhancement.

2.3.3 Analysis of maize samples

Pulverized maize samples (1 g) were spiked with AFB1 at different concentrations (0, 4, 8, 20 and 40 μ g/kg). The spiked samples were kept at room temperature under dark

2 Experimental Section

condition for 3 h to evaporate methanol used to prepare AFB1 standards and then extracted with 4 mL of methanol/water (80:20, v/v) by vortex mixing for 2 min and then centrifugated at 1920 g for 15 min. The supernatant was then 20-fold diluted with PBS (50 mM, pH = 7.4) for quantitative analysis.

2.3.4 Assay procedure

The AFB1 standard solutions with different concentrations were prepared in 50 mM PBS (pH 7.4). A volume of 50 μ L of AFB1 standards/samples was injected into a 0.5-mL Eppendorf tube, then 50 μ L of Ab-AuNPs and 15 μ L of MBs suspension (~4 mg/mL) were added successively. The mixture was well mixed and incubated under shaking for 30 min. After removing the formed MBs-AuNPs immune complexes by magnetic separation, 100 μ L of supernatant solution containing unbound AuNPs was transferred into 1.0 mL gold growth solution and the mixture was incubated at room temperature for 20 min. Then 100 μ L of 10 mM Na₂S₂O₃ was added to stop the reaction and the absorbance of the enlarged AuNPs was measured on UV-vis spectrophotometer. The absorbance at 565 nm (533 nm for AuNPs without gold staining) was recorded and final absorbance was calculated by subtracting the absorbance of the corresponding blank samples. Error bars were standard deviations across at least three repetitive assays.

2.4 AuNP-catalyzed uranine reduction for signal amplification

AuNPs with different size were prepared according to the method described above with slight modification. Briefly, 50 mL of deionized water was heated to boiling while stirred vigorously. Then 120 μ L of HAuCl₄ solution (0.1 M in water) was added. After 1 min, an aqueous solution of trisodium citrate (1 wt %) was added. A change of color occurred from yellow over black to red. The solution was kept boiling and stirred for further 15 min. Then the colloid solution was cooled to room temperature and stored at 4°C in the refrigerator. The gold content was about 47.3 mg/L. The particle size can be tuned by changing the amount of trisodium citrate, which was estimated by dynamic light scattering (DLS) measurements.

2.4.1 Catalytic reduction of uranine

The sodium borohydride solution (100 mM) was always freshly prepared by dissolving 37.8 mg of NaBH₄ in 10 mL water and used immediately. Uranine (200 μM) was prepared newly every day from a stock solution (2 mM in water) by 10-fold dilution with water.

For the AuNP-catalyzed reduction of uranine, a mixture containing 2.58 mL of ultrapure water, 120 μL of uranine (200 μM) and 300 μL of NaBH₄ (100 mM) was first prepared in a 4-mL PMMA cuvette (Ref 67.755, Sarstedt, Nümbrecht, Germany). Then 20 μL of citrate-AuNPs was rapidly added to the uranine solution. The fluorescence spectrum was measured at 1-min intervals for 15 min on the RF-5301 PC spectrofluorometer.

To study the influence of nanoparticle size on the catalytic reaction, AuNPs with different size (16, 25, 34 nm) were used. To test the effect of AuNP concentration, 0/10/20/50 μL of 16-nm AuNPs were added. To investigate the effect of NaBH₄, solutions were tested with different final concentrations (0, 5, 10, 15 mM). Aggregated AuNPs were prepared by adding 100 μL of 1M NaCl to 1 mL of 16-nm AuNPs. Then 50/55 μL of dispersed/aggregated AuNPs were tested. For the study of the effect of surfactants, 1.0 mL of 16-nm AuNPs were added to 100 μL of 1 wt % surfactant solution, incubated for 30 min and then 22 μL of surfactant-coated AuNPs were added to the uranine-NaBH₄ solution.

For the corresponding absorption measurements, the final concentration of uranine and NaBH₄ was 20 μM and 10 mM, respectively, with a total volume of 3 mL, while other conditions were kept all the same.

2.4.2 Detection of melamine

Initially, 5 mL of 16-nm AuNPs colloid solution was diluted with 20 mL of deionized water to give a final volume of 25 mL. Different amount of melamine (50 μL) was added into 0.5 mL of the above AuNPs suspension. After 15 min, the reaction mixture was 10-fold diluted with water to stop the reaction. 100 μL of the diluted AuNPs was transferred

2 Experimental Section

into the well of a microtiter plate, followed by the addition of 80 μL of 100 μM uranine and 20 μL of 100 mM NaBH_4 . The fluorescence intensity ($\lambda_{\text{ex}}/\lambda_{\text{em}} = 485/528 \text{ nm}$) was measured every 2 min for 30 min on the microplate reader. All the measurements were conducted in triplicate. Error bars represented standard deviations across three assays.

Several amino compounds were measured to evaluate the selectivity, including ammonia, ethanolamine, glycine, tryptophan, 4-nitroaniline and DMAP. The concentration of melamine was 0.25 mg/L while that of other amino compounds was 5 mg/mL. The catalytic reaction time was 30 min.

For the detection of melamine in milk samples, 2 mL of milk was pipetted into a 15-mL centrifuge tube, followed by the addition of 0, 6, 10, 20, 50, 100 and 200 μL of 1 g/L melamine stock solution (in water). The concentrations of melamine in milk were 0, 3, 5, 10, 25, 50 and 100 mg/L, respectively. Then, 2 mL of water, 1 mL of 10% (w/v) trichloroacetic acid solution and 1 mL of chloroform were added. The mixture was vortexed for 30 s, ultrasonically treated for 15 min and then centrifugated at 4500 g for 10 min to separate the deposit. 3 mL of supernatant was transferred into another centrifuge tube and adjusted to pH 7.0 with 2M of NaOH. The solution was centrifugated at 20800 g for 15 min to remove the deposit again and stored at 4°C for future treatment. 100 μL of the milk extract was diluted with 900 μL of acetonitrile. White precipitation was formed immediately, which was removed by centrifugation at 20800 g for 20 min. The final solution was used for detection. 100 μL of melamine- CH_3CN solution was added into 1 mL of 5-fold diluted 16-nm AuNPs to induce the aggregation. The following procedure was the same as that described for the detection of melamine in water.

2.4.3 Detection of AFB1

Ab-AuNPs and AFB1-BSA- Fe_3O_4 were prepared and characterized as described above. AFB1 solutions with various concentrations were prepared in 50 mM PBS (pH 7.4). 50 μL of AFB1 standard was transferred to a 0.5-mL tube, followed by the addition of 50 μL of Ab-AuNPs and 15 μL of MBs suspension ($\sim 3 \text{ mg/mL}$, before use, the MBs were

washed three times with water). The mixtures were incubated at room temperature under shaking for 30 min. After magnetic separation of the formed MBs-AuNPs immune complexes, 50 μL of supernatant solution containing unbound AuNPs was transferred into the well of a microtiter plate. 50 μL of 100 μM uranine and 50 μL of 100 mM NaBH_4 were added successively. The fluorescence intensity ($\lambda_{\text{ex}}/\lambda_{\text{em}} = 485/528$ nm) was measured every 2 min for 20 min on the microplate reader. All the measurements were conducted in triplicate. Error bars were standard deviations across three assays.

To evaluate the selectivity of the established method, T-2 toxin, FB1, OTA and their mixtures with AFB1 were tested. The concentration of all other toxins used was 20 ng/mL, while that of AFB1 was 1 ng/mL. The catalytic reaction time was 10 min.

To simulate the analysis of a real sample, aflatoxin-free maize extract was used to prepare the AFB1 solutions. Briefly, 5 g of pulverized maize samples and 1 g of NaCl were placed in a 50-mL centrifuge tube, followed by the addition of 20 mL of methanol-water (80:20, v/v). The sample was extracted by vortex mixing for 2 min and then centrifugated at 3645g for 15 min. 1 mL of supernatant was diluted with 19 mL of PBS (50 mM, pH 7.4) and later used as diluent solution for the preparation of AFB1 samples. Then the samples were analyzed in a similar way as described above. The only change was that the supernatant containing unbound immunogold nanoparticles was diluted (1:1, v/v) with PBS (25 mM, pH 7.4) before signal amplification. In addition, a certain amount of AFB1 was spiked into pulverized maize powders, then extracted and analyzed in accordance with the above described procedure to determine the recoveries.

2 Experimental Section

3 Results and Discussion

3 Results and Discussion

3.1 Colorimetric immunoassay for AFB1

Magnetic beads (MBs) are biocompatible, diffuse freely in the reaction mixture and can be easily separated with the aid of an external magnet, so they have been widely used in bioanalysis. MB-based assays have been developed by combining MBs with recognition elements such as enzymes, Au or Ag nanoparticles and quantum dots. These assays are usually fast and simple to operate, which offers a promising platform for the detection of various analytes.⁷³

Different analytical techniques were employed in MB-based assays, such as colorimetry,¹¹⁷ fluorescence,¹⁵⁰ light scattering,¹⁵¹ electrochemistry¹⁵² and chemiluminescence.⁶⁴ Among these methods, colorimetric assay has gained considerable attention due to its incomparable advantages such as simplicity, practicality, rapidness and no requirement to utilize expensive or challenging instruments. AuNPs are extensively used in such colorimetric assays owing to their special physical and chemical properties. For instance, AuNPs serve as carrier to load active biomolecules like enzymes and DNA reporters, thereby achieving enzymatic or DNA-based signal amplification.¹⁵³ Further, AuNPs are used as seeds for catalytic deposition of silver or gold, followed by scanometric or absorbance detection.^{127, 130} As another example, AuNPs can catalyze the decoloration of organic dyes like methyl orange and methylene blue to generate colorimetric signals.¹³⁹⁻¹⁴⁰

Although high sensitivity was achieved, the color development step in these assays indeed increased the complexity of assay. Obvious absorbance change might be also obtained even without amplification, because AuNPs themselves have extremely high extinction coefficient. Liu et al. developed a sandwich assay for DNA detection utilizing AuNPs probes and MBs to recognize and capture the target DNA where the supernatant solution containing unbound AuNPs was directly submitted to absorption measurements.¹⁵⁴ A similar double-bead sandwich immunoassay was developed for protein detection, which proved a simple tool for bioanalysis.¹⁵⁵

3 Results and Discussion

Herein, we utilized the double-bead system in competitive immunoassay for the detection of AFB1. Figure 3.1 shows the principle of the colorimetric immunoassay. AFB1-BSA- Fe_3O_4 MBs were employed as capture probe, while *anti*-AFB1 antibody-coated AuNPs (Ab-AuNPs) were used as detection probe for immunological recognition of AFB1, as well as for signal transduction. Specifically, AFB1-BSA- Fe_3O_4 competed with target AFB1 for binding with the AuNP-labeled antibodies. The amount of Ab-AuNPs bound onto MBs decreased with increasing AFB1 concentration because of competitive inhibition. After magnetic separation of the generated AuNPs-MBs immune complexes using an external magnet, the supernatant containing unbound AuNPs was measured directly by using a UV-vis spectrophotometer. Obviously, the absorbance of supernatant was directly proportional to the concentration of AFB1.

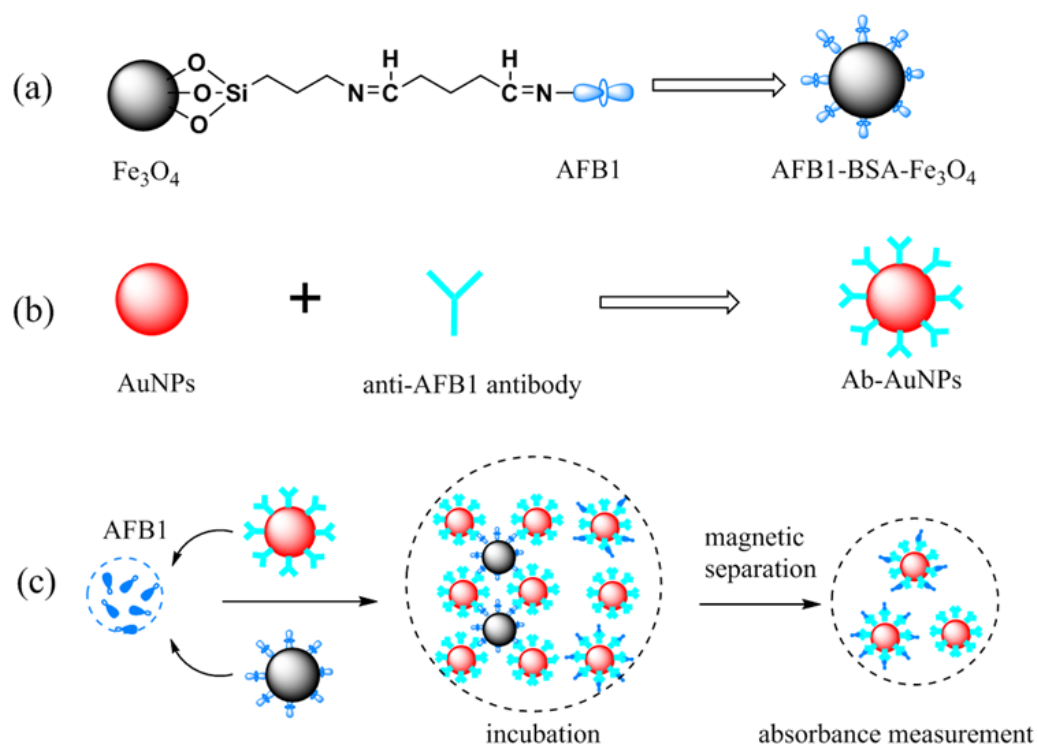


Figure 3.1 Schematic illustration of the preparation of (a) AFB1-BSA- Fe_3O_4 , (b) Ab-AuNPs, and (c) principle of the competitive colorimetric immunoassay for AFB1 detection.

To construct a double-bead competitive immunoassay, antibody and antigen are generally immobilized on different particles, respectively. If MBs are utilized as solid carrier for antibody, usually the surface of MBs is first modified by linker proteins such as protein A,

G and streptavidin, to avoid activity loss of antibody after immobilization. In contrast, the activity of an antibody will be only minimal affected when it is labeled directly with colloidal gold. In this assay, the stability of AFB1-BSA on MBs is much higher compared to the antibody. Therefore, also in consideration of the cost and complexity, we immobilized antibodies on AuNPs while AFB1-BSA molecules were covalently linked to MBs.

3.1.1 Characteristics of AuNPs

AuNPs of different sizes were prepared through the reduction of HAuCl_4 by sodium citrate. The particle size was determined by DLS. As shown in Table 3.1, the average size of AuNPs could be well tuned by the amount of reduction reagent. As the volume of sodium citrate decreasing from 1 to 0.5 mL, the particle size grows from 25.3 to 49.0 nm, and the surface plasmon resonance peak, λ (SPR), shows red shifts from 524 to 538 nm, which is consistent with the reported results.¹⁵⁶

Table 3.1 The preparation and physical properties of AuNPs.

Sample	HAuCl_4 (0.01%)	Sodium citrate (1%)	Citrate-stabilized		Antibody-coated	
			Size	λ (SPR)	Size	λ (SPR)
AuNP 1	50 mL	1 mL	25.3 nm	524 nm	44.0 nm	529 nm
AuNP 2	50 mL	0.75 mL	34.8 nm	529 nm	55.4 nm	533 nm
AuNP 3	50 mL	0.5 mL	49.0 nm	538 nm	74.2 nm	543 nm

When the volume of sodium citrate was fixed (0.75 mL), with the increase of HAuCl_4 concentration, the absorbance of gold colloidal solution increased correspondingly (Figure 3.2A). This is because more AuNPs were formed. Meanwhile, the absorption maxima shifted slightly to longer wavelength (Figure 3.2B), which indicates there was an increase in particle size.¹⁵⁶ All these results demonstrated that the size of AuNPs was determined by the molar ratio between sodium citrate and HAuCl_4 . With the increase of citrate/gold ratio, the particle size decreased.

3 Results and Discussion

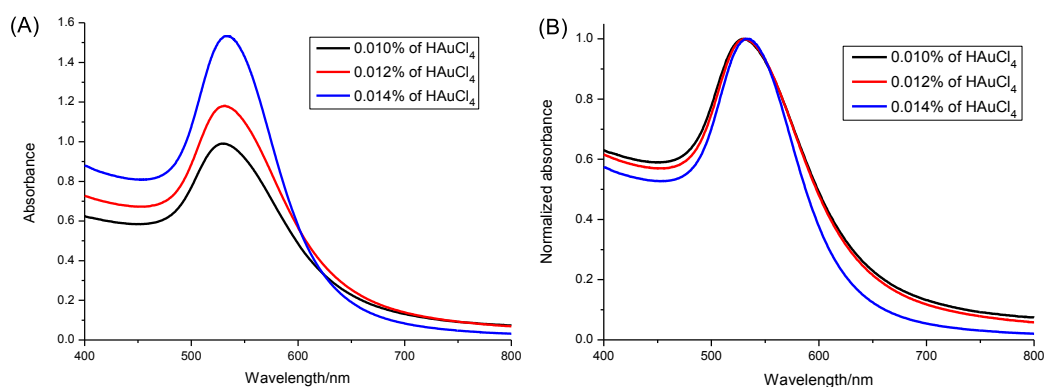


Figure 3.2 UV-Vis absorption spectra of AuNPs prepared by using different amount of HAuCl₄.

The obtained AuNPs were then conjugated with *anti*-AFB1 antibodies. The association of antibody to the colloidal surface was possibly due to direct coupling of functional groups of protein with gold through electrostatic interactions and coordination effect, such as cysteine, NH₃⁺-lysine residues and imidazole groups on antibody.¹¹⁷ As shown in Figure 3.3, the absorption maximum of Ab-AuNPs was red shifted compared with unmodified AuNPs. This is because the refractive index changed around the particle surface. In addition, the hydrodynamic diameter of AuNPs increases correspondingly (Table 3.1). The thickness increase, of ~10 nm, is almost equal to the size of antibody, which indicates successful attachment of antibodies on the colloidal surface.

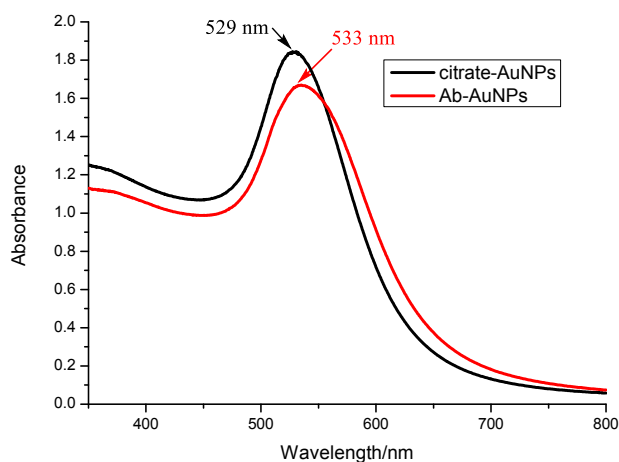


Figure 3.3 UV-Vis absorption spectra of AuNPs and Ab-AuNPs.

The stability of the prepared AuNPs was investigated. The colloidal solutions of citrate-AuNPs and BSA-AuNPs were diluted with phosphate buffer. As seen in Figure 3.4A, when the final concentration of phosphate was above 40 mM, the absorption spectra of citrate-AuNPs became broader and a new peak appeared around 700 nm, indicating the AuNPs aggregated.¹²² This is because the citrate-AuNPs were dispersed in water mainly through ionic repulsion of citrate ions on the surface of AuNPs. The negative charges were screened at high ionic strength, and the colloidal stability decreased greatly, resulting in the aggregation of particles. Coating AuNPs with proteins (BSA and antibody) can counter this behavior, since the particles experienced steric repulsion in addition to ionic repulsion. As shown in Figure 3.4B, the absorption of BSA-AuNPs changed little in the presence of phosphate, demonstrating the high stability of AuNPs after conjugation with proteins.

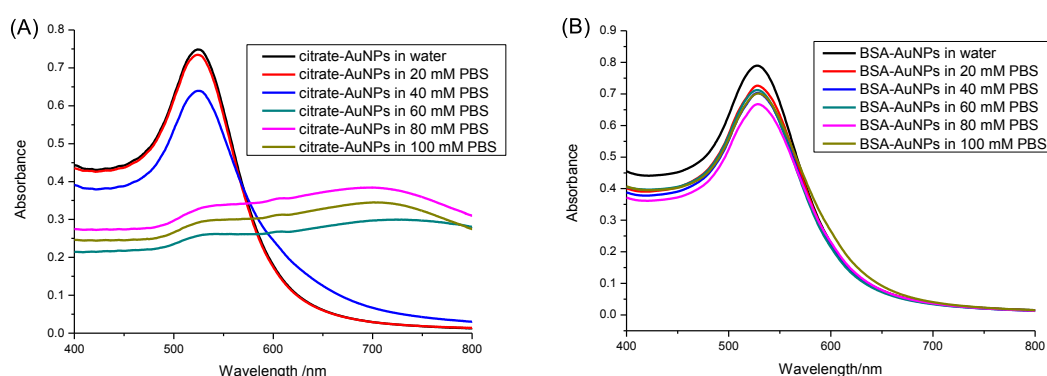


Figure 3.4 Absorption spectra of citrate -AuNPs and BSA-AuNPs in different concentrations of PBS.

3.1.2 Characteristics of MBs

The Fe₃O₄ MBs were prepared by chemical coprecipitation, since this method is very simple and suitable for the synthesis on a large scale. Ammonium hydroxide was added to induce the coprecipitation of trivalent and divalent iron compounds under heating. The obtained magnetic particles were washed thoroughly with water and ethanol to remove all the reaction reagents, and then functionalized with APTES to introduce amino groups. The generated silica layer can prevent the particles from oxidization. Then aldehyde groups were introduced through the reaction with glutaraldehyde. Finally AFB1-BSA conjugates were

3 Results and Discussion

covalently immobilized on the surface of MBs through the cross-linking of glutaraldehyde. The MBs not only serve as solid carrier, yet facilitate the rapid separation of immune complexes.

Figure 3.5 shows the picture of Fe_3O_4 suspension. The prepared magnetic particles were black and could be well dispersed in water. Using a magnet, the MBs can be easily separated and a very clear solution was obtained. This is very important because if MBs could not be totally removed, they would interfere with the following absorbance measurements.

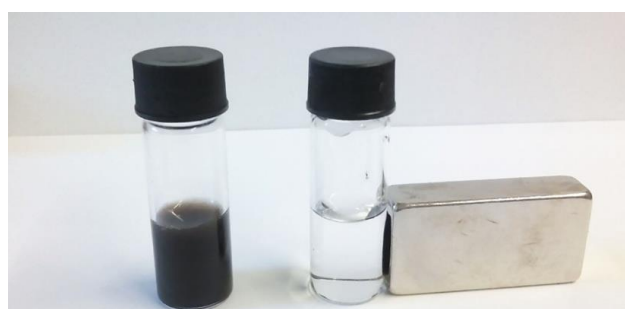


Figure 3.5 Picture of Fe_3O_4 suspension with and without magnetic separation.

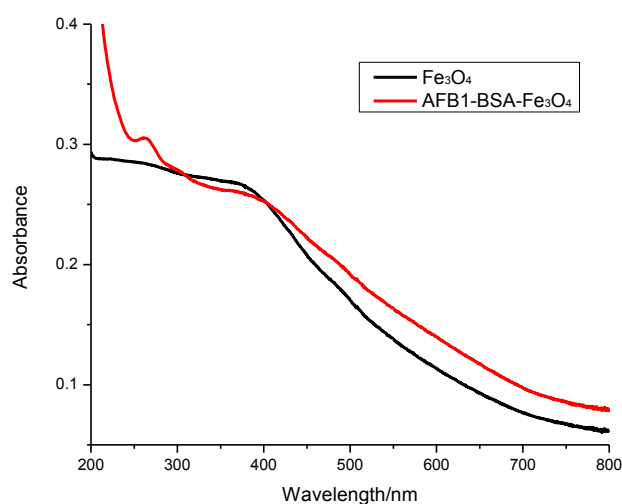


Figure 3.6 UV-Vis absorption spectra of Fe_3O_4 and AFB1-BSA- Fe_3O_4 particles.

As shown in Figure 3.6, bare Fe_3O_4 particles had a very broad absorption from 200 to 800 nm. After reaction with AFB1-BSA conjugate, an obvious absorption peak appeared between 250 and 300 nm, which indicates the successful immobilization of protein on the

surface of magnetic particles. The average size of AFB1-BSA-Fe₃O₄ was ~3.3 μm as determined by DLS. The larger size might be ascribed to agglomeration of small particles under heating.

3.1.3 Optimization of experimental conditions

The prepared AFB1-BSA-Fe₃O₄ and Ab-AuNPs were then utilized in immunoassay for the detection of AFB1. The performance of the developed immunoassay could be greatly affected by parameters such as temperature, incubation time and pH. So the experimental conditions were optimized.

To simplify the analytical procedure, all experiments were conducted at room temperature. First the effect of incubation time was studied. Figure 3.7 shows the absorbance changes of supernatant after different incubation times when Ab-AuNPs were incubated with AFB1-BSA-Fe₃O₄ in PBS (pH = 7.4, 50 mM). The absorbance decreased with increasing incubation time, which indicates that functionalized AuNPs could gradually bind with the magnetic beads via antigen-antibody reaction, leading to a lower concentration of AuNPs in bulk solution after magnetic separation. During the first 30 min, the absorbance decreased rapidly while it changed less between 30 and 60 min. Due to limited diffusion of biofunctionalized nanoparticles, the final equilibrium of the immunoreaction might not be reached within 30 min. Nevertheless, a 30 min incubation was chosen in this study because there was only a small difference of absorbance between 30 and 60 min.

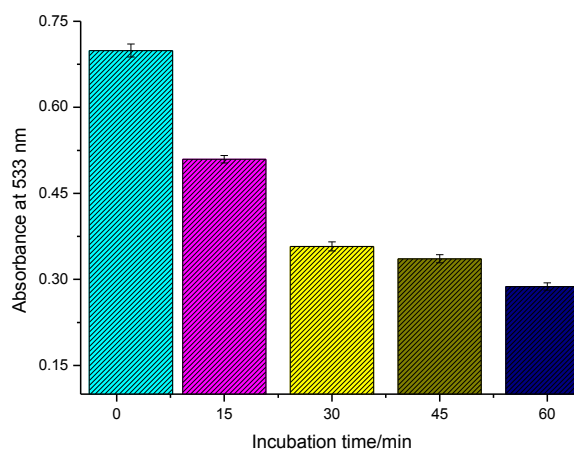


Figure 3.7 The effect of incubation time on the absorbance of supernatant.

3 Results and Discussion

The net charges of biomolecules (antibody and AFB1-BSA) are affected by the pH value (Figure 3.8). The possible interactions between AFB1 and antibody such as hydrogen bond and hydrophobic interaction might also change at different pH.¹⁵⁷ So the influence of pH was investigated. As the isoelectric point of AFB1 antibodies is ~pH 7.0 and the isoelectric point of BSA is ~pH 4.7, the antibodies are positively charged, while BSA molecules are negatively charged at pH 6.0. This could lead to nonspecific adsorption of Ab-AuNPs to AFB1-BSA-Fe₃O₄ particles' surface via electrostatic attractions, which causes a relatively low sensitivity, as shown in Figure 3.9. When the pH was too high (pH = 8.2), there might be electrostatic repulsions between Ab-AuNPs and AFB1-BSA-Fe₃O₄ particles since both antibody and BSA were negatively charged, which also gave a lower sensitivity. The highest sensitivity was obtained at pH 7.4, when antibodies carried almost no net charges. Thus, PBS buffer with pH 7.4 was used for following quantitative analysis.

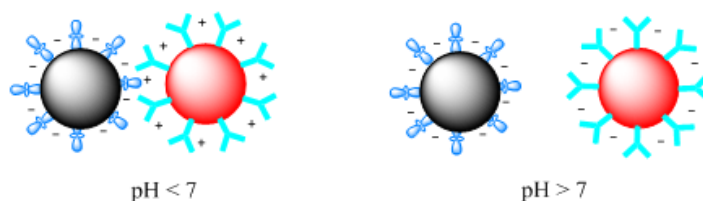


Figure 3.8 Schematic illustration of the surface charges of two types of particles under different pH values.

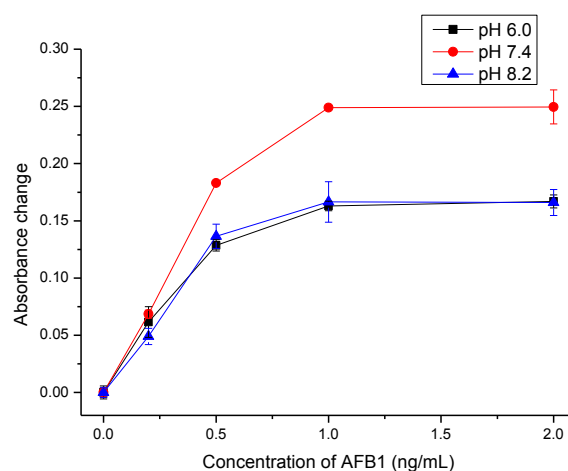


Figure 3.9 Optimization of pH value for the detection of AFB1.

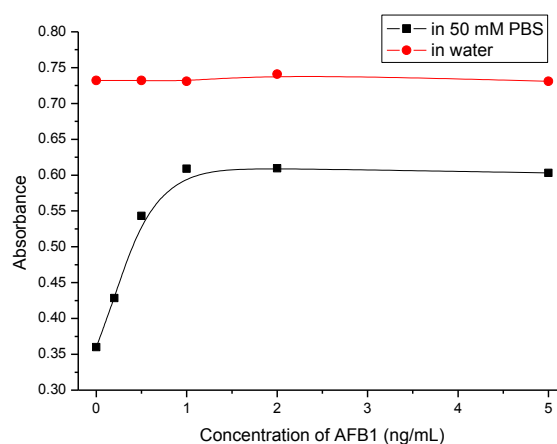


Figure 3.10 Dose-response curves for the detection of AFB1 in water and 50 mM PBS.

In addition, we studied the influence of ionic strength. AFB1 standards were prepared in pure water and then analyzed. Surprisingly, the absorbance of supernatant kept almost unchanged for AFB1 at varied concentrations (Figure 3.10). It seems the antibody did not work. But previous ELISA had demonstrated that the monoclonal 1F2 antibody against AFB1 indeed worked in pure water. This might be because both AFB1-BSA-Fe₃O₄ and Ab-AuNPs were negatively charged in water, electrostatic repulsions occurred between these two kinds of particles. So a certain ionic strength was required to reduce such repulsions. On the other hand, if the ionic strength was too high, some antibodies might be exfoliated from AuNPs because they were non-covalently immobilized on gold surface mainly through electrostatic interactions. Thus, phosphate buffer with a moderate concentration (50 mM) was used. As shown in Figure 3.10, a good dose response curve was obtained in 50 mM PBS. Therefore, 50 mM PBS was used for the following studies.

3.1.4 Influence of AuNP size on the immunoassay

Since the SPR characteristic of AuNPs is dependent on the AuNP radius, the effect of the AuNP size on the assay sensitivity was investigated. There are two opposite trends, which favor large and small AuNPs, respectively. That is, with the increase of particle size, the extinction coefficient of AuNP increases exponentially. The removal of a single, large

3 Results and Discussion

AuNP will lead to a larger absorbance change compared to the removal of smaller ones. On the other hand, due to the larger surface-to-volume ratio of smaller AuNPs, they are more effectively functionalized with antibodies. Further, because of the smaller steric hindrance when binding with magnetic beads, smaller AuNPs might give better response. Based on this consideration, we tested AuNPs of different sizes for the detection of AFB1. The corresponding dose–response curves are shown in Figure 3.11. The three kinds of AuNPs gave similar response. With the increase of AFB1 concentration, the absorbance of supernatant increased correspondingly. The saturation level was obtained at a concentration of ~ 1 ng/mL AFB1. At this concentration the absorbance change at SPR was 0.11, 0.25 and 0.13 for AuNPs of 25.3, 34.8 and 49.0 nm, respectively. Since 34.8 nm AuNPs gave the largest signal change, they were used in further experiments.

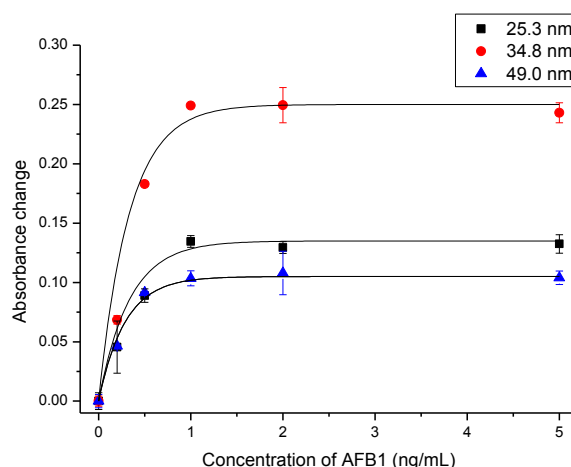


Figure 3.11 Dose-response curves for the detection of AFB1 using different size of AuNPs.

3.1.5 Measurement of AFB1

AFB1 in PBS at different concentrations (0, 20, 50, 100, 200, 500, 800 ng/L) were quantitatively analyzed under optimal conditions, i.e., 20 μ L of AFB1-BSA-Fe₃O₄ (3 mg/mL), 100 μ L of Ab-AuNPs (34.8 nm) at pH 7.4 with incubation time of 30 min. Figure 3.12A shows the absorption spectra of supernatant after magnetic separation. With the increase of AFB1 concentration, the absorbance at 533 nm increased correspondingly. The absorbance change at 533 nm was linear to AFB1 concentration in the range of 20 to

800 ng/L ($\Delta\text{Abs} = 2.87 \times 10^{-4}C_{\text{AFB1}} + 0.00298$) with a correlation coefficient of 0.992 (Figure 3.12B). The detection limit was calculated to be 12 ng/L based on three times of signal-to-noise ratio.

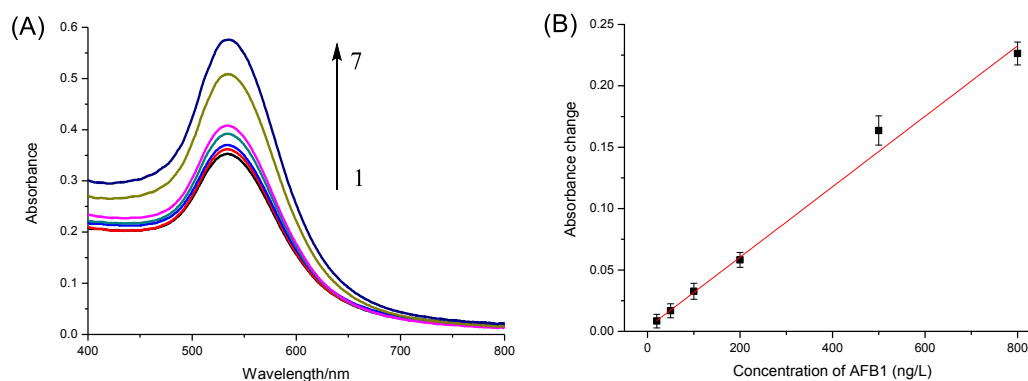


Figure 3.12 (A) UV-Vis absorption spectra of supernatant after magnetic separation with different concentrations of AFB1 (from sample 1 to 7: 0, 20, 50, 100, 200, 500, 800 ng/L) (B) the relationship between absorbance changes and AFB1 concentration ($m = 5$, $n = 6$).

The detectable concentration range is about one order of magnitude lower than that of MB-based fluorescence immunoassay (0.5–30 ng/mL)³³ and homogeneous immunoassay based on competitive dispersion of gold nanorods (0.5–20 ng/mL) using the same antibody.¹⁴¹ Although the developed method is not as sensitive compared to some other ELISAs or electrochemical immunosensors, its simplicity and applicability are indeed attractive.

The selectivity and specificity of the established approach was also investigated. OTA, FB1, T-2, and their mixture with AFB1 were analyzed by the developed immunoassay. As indicated in Figure 3.13, the presence of other mycotoxins caused very small signal change, while the signal change was almost the same as AFB1 alone compared with that of mixtures containing AFB1 and the interfering agents, indicating a negligible impact of the other tested mycotoxins.

3 Results and Discussion

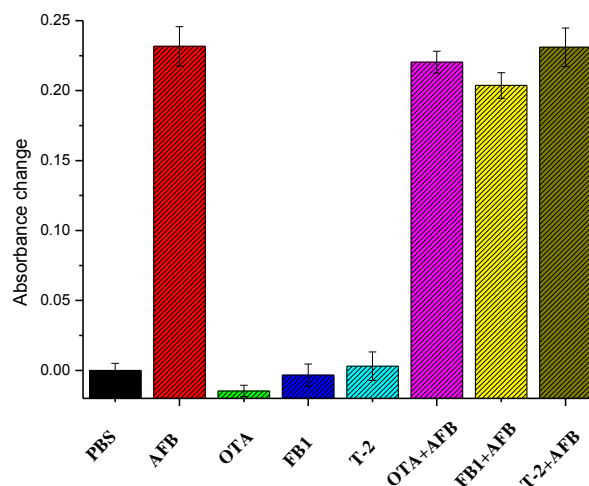


Figure 3.13 The selectivity of AFB1 determination using the developed immunoassay.

The reproducibility of the immunoassay was evaluated by calculating the intra- and inter-batch variation coefficients (CVs, $n = 3$). Experimental results indicated that the CVs of the assays using biofunctionalized nanoparticles from the same batch were 5.0%, 1.6%, and 1.7% at 0.1, 0.2, and 0.8 ng/mL AFB1 levels, respectively, while the CVs of the assays using particles from different batches were 11.6%, 8.7%, and 3.0% at the above-mentioned analyte concentrations.

3.1.6 Analysis of AFB1 spiked maize samples

To further evaluate analytical reliability and possible application of the established assay, maize samples artificially spiked with AFB1 were analyzed. Non-spiked sample extract dilution was used as blank and AFB1 concentration in maize samples were determined from the calibration curve. The testing results are listed in Table 3.2. Acceptable recovery was obtained in the range of 92.8% to 122.0%. Thus, the established immunoassay could be useful for the determination of AFB1 in real samples.

Table 3.2 The detected results of AFB1 in maize samples and recoveries ($n = 3$).

In Spiked Sample ($\mu\text{g}/\text{kg}$)	After Dilution (ng/L)	Detected Concentration (ng/L)	Recovery (%)
5	50	57.7	115.4 ± 23.0
10	100	122.0	122.0 ± 16.4
20	200	192.1	96.1 ± 12.1
50	500	464.2	92.8 ± 8.1

3.1.7 Summary

In summary, we have demonstrated the feasibility of a competitive colorimetric immunoassay for the determination of AFB1 using AFB1-BSA-modified magnetic particles as capture probe and biofunctionalized AuNPs as signal probe. The whole assay is simple, time-saving and cost-effective, owing to rapid separation by the use of magnetic particles and no requirement of color development step. The proposed double-bead method allows the detection of AFB1 within the low ng/L range in PBS and real maize sample extract. This method could be easily extended for the detection of other mycotoxins since the biofunctionalization process is very simple and generally applicable. Multiple-analyte detection could be established by simultaneously using different metal nanoparticles such as gold nanorods and silver nanoparticles.

3.2 Homogeneous gold staining for signal amplification

Silver and gold staining methods have been well developed and extensively utilized for the detection of various targets such as proteins and DNA.^{127, 129} Compared with silver staining, gold staining has several attractive features. For example, gold enlargement reagents are compatible with physiological buffers and less sensitive to pH, while silver ions precipitate with phosphate, chloride ions and hydroxyl ions.¹⁵⁸ Further, the autonucleation is minimal for gold enlargement, and thus the background is usually lower than that of silver staining.¹⁵⁹ But gold enhancement is mostly used in heterogeneous chip-based assays on solid substrates, such as glass slides and nitrocellulose strips,^{130, 160} which require the immobilization of biomolecules to the solid surface (Figure 3.14 A). And strict control of reaction conditions is needed to obtain acceptable reproducibility.

Several homogeneous gold growth methods have been developed to solve these problems.^{90, 158} The AuNPs were enlarged in aqueous HAuCl₄ solution using ascorbic acid or hydroxylamine hydrochloride as reducing reagents and surfactants like cetyltrimethylammonium bromide (CTAB) as stabilizer (Figure 3.14 B). The detection is generally simple, highly sensitive and cost-effective. But a long reaction time is often

3 Results and Discussion

required for homogeneous gold nanogrowth.¹⁶¹ Since the gold enlargement is time-dependent, the reaction continues until all the gold ions in growth solution are exhausted. Significantly, we recently found that sodium thiosulfate can efficiently stop the reaction, which makes the homogeneous gold staining more controllable and convenient.



Figure 3.14 Schematic illustration of chip-based (A) and homogeneous gold staining (B).

In this section, controlled growth of AuNPs in aqueous solution was studied in-depth by UV-vis spectroscopy and resonance light scattering (RLS) technique, using CTAB as stabilizing surfactant and ascorbic acid (AA) as reducing agent. The controlled gold staining was then used for signal amplification in competitive immunoassay. The principle of the immunoassay is illustrated in Figure 3.15. Biofunctionalized MBs and free AFB1 molecules competitively bind to AuNP-labeled antibodies. After magnetic separation, the supernatant containing unbound AuNPs was directly submitted for gold enlargement. The final absorbance depends on the amount of immunogold nanoparticles added, which is directly proportional to the concentration of AFB1 in the sample. Since MBs were removed from the reaction mixture, they did not participate in the subsequent gold enlargement. After signal amplification, the sensitivity of the immunoassay increased distinctly. To the best of our knowledge, this is the first time that homogeneous gold staining was applied to a competitive immunoassay.

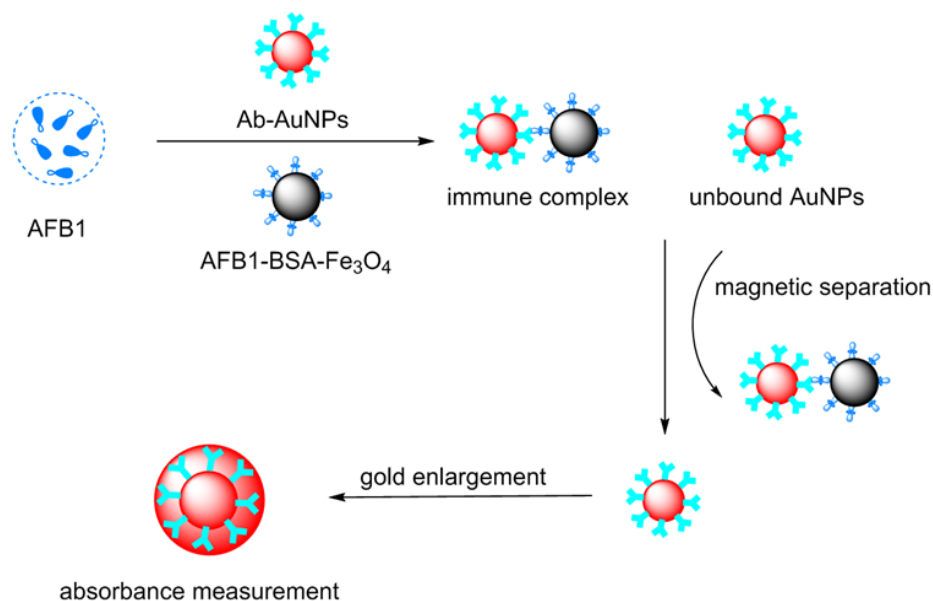
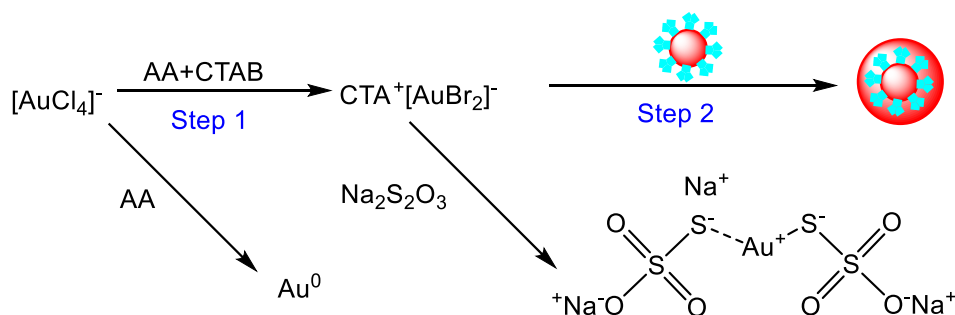


Figure 3.15 Schematic illustration of homogeneous gold staining for amplified optical detection of AFB1.

3.2.1 Proposed mechanism of gold enlargement

The proposed mechanism of the homogeneous growth of AuNPs is illustrated in Scheme 3.1. The immunogold nanoparticles act as self-catalysts while the CTAB serves as a surfactant to stabilize the enlarged nanoparticles. Ascorbic acid was employed as the reducing agent for the gold enlargement.



Scheme 3.1 Proposed mechanism of gold enlargement in aqueous phase.

As an electrolyte, CTAB molecules dissociated into $\text{CH}_3(\text{CH}_2)_{15}(\text{CH}_3)_3\text{N}^+$ (CTA^+) and Br^- species (Eq. 3.1). And HAuCl_4 dissociated into $[\text{AuCl}_4]^-$ and H^+ ions in aqueous solution (Eq. 3.2). Then a multi-step ligand exchange reaction occurred between HAuCl_4 and CTAB, where $[\text{AuCl}_4]^-$ was converted into $[\text{AuBr}_4]^-$ (Eq. 3.3), resulting in the formation

3 Results and Discussion

of perfect transparent and stable orange-yellow colored complex.¹⁶²⁻¹⁶³ As shown in Figure 3.16, chloroauric acid solution had very low absorption between 350 nm and 800 nm. In the presence of CTAB, a significant absorption peak appeared at 416 nm with a shoulder around 470 nm, which was ascribed to the absorption of $[\text{AuBr}_4]^-$. Meanwhile, the generated $[\text{AuBr}_4]^-$ could be stabilized by CTA^+ to form $\text{CH}_3(\text{CH}_2)_{15}(\text{CH}_3)_3\text{N-AuBr}_4$ complex (Eq. 3.4).

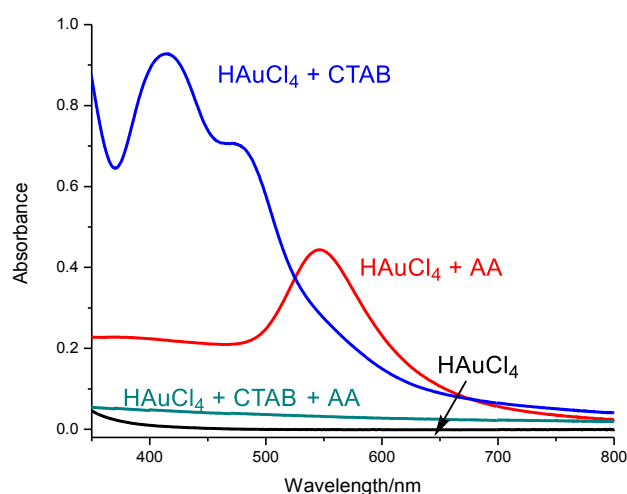
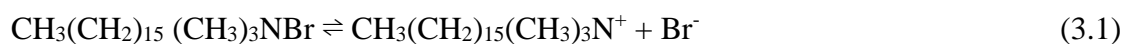


Figure 3.16 UV-vis absorption of HAuCl_4 , $\text{HAuCl}_4+\text{CTAB}$, $\text{HAuCl}_4+\text{CTAB}+\text{AA}$ and HAuCl_4+AA .

After the addition of AA, the Au^{3+} ions were rapidly reduced to Au^+ ions as shown in Scheme 3.2. The formed Au^+ species were stabilized by CTAB (CTA-AuBr_2), which could not be further reduced in the absence of AuNPs. CTA-AuBr_2 species were colorless and had very low absorption in the range 350-800 nm (cyan line in Figure 3.16). In contrast, the Au^{3+} ions were directly reduced to Au^0 without the stabilization of CTAB.

3 Results and Discussion

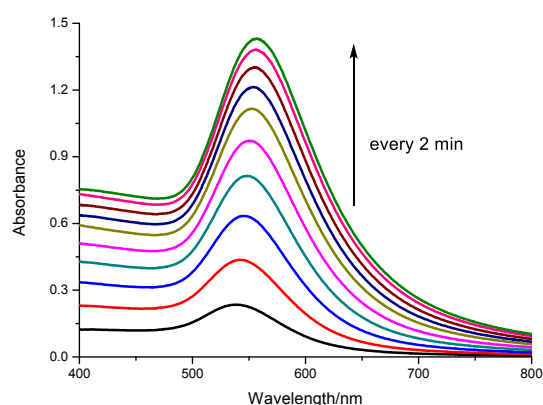


Figure 3.17 UV-vis absorption spectra of the enlarging AuNPs recorded every 2 min.

3.2.2 Controlled growth of immunogold in aqueous solution

In order to optimize the gold enlargement, several experimental parameters were investigated in detail, including the concentrations of CTAB, AA and HAuCl_4 .

Typically, the CTAB used in this study not only stabilizes the reduced Au^+ ions but also is crucial for preventing the aggregation of enlarged AuNPs, which is very significant for assays based on optophysical properties of the nanostructures (e.g. absorption, light scattering). As shown in Figure 3.18, with the decrease of CTAB concentration, the absorption spectrum became broader and the maximum absorption was red-shifted. This might be attributed to the enlarged AuNPs aggregated at low concentration of CTAB due to high surface energy. Thus, a high concentration of CTAB, 100 mM, was used in further experiments.

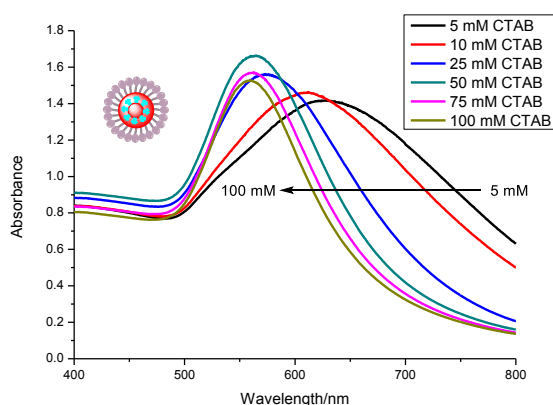


Figure 3.18 Effect of CTAB concentration on the absorbance of enlarged AuNPs (0.25 mM HAuCl_4 and 1 mM AA were utilized for the preparation of gold growth solution).

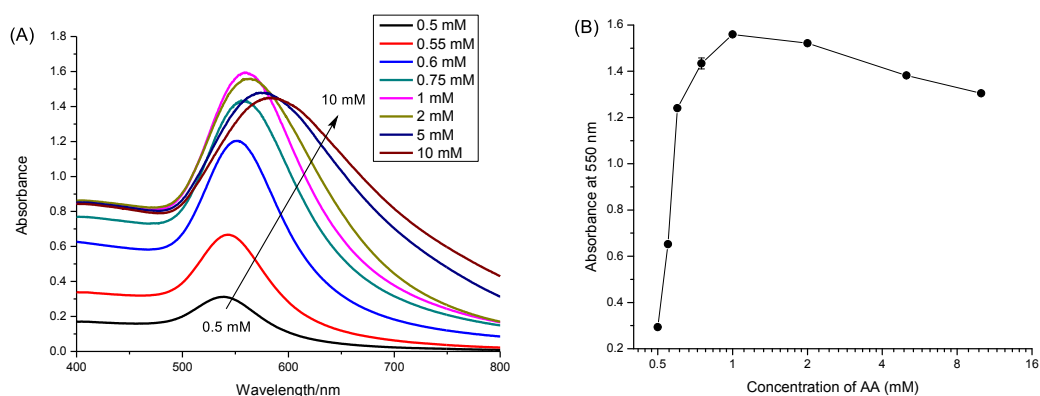


Figure 3.19 (A) Effect of AA concentration on the absorption spectra of enlarged AuNPs. (B) Absorbance at 550 nm versus the concentration of AA ($m = 3$, $n = 8$). (100 mM CTAB and 0.25 mM HAuCl₄ were utilized for the preparation of gold growth solution).

The AA reduced Au³⁺ to Au⁺, and the Au⁺ species were further reduced to gold atoms in the presence of immunogold. A certain amount of AA was required to reduce all the gold ions. As shown in Figure 3.19, the absorbance increased rapidly when the AA concentration rose from 0.5 to 1 mM, and then decreased slightly in the range of 2-10 mM. The maximum absorbance occurred at 1 mM AA. Therefore, 1 mM AA was used for the following studies.

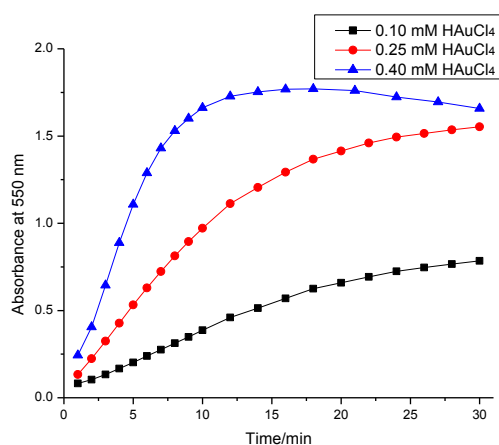


Figure 3.20 Time-dependent absorbance changes at 550 nm of the enlarged AuNPs using different HAuCl₄ concentration (100 mM CTAB and 1 mM AA were used for the preparation of gold growth solution).

3 Results and Discussion

The influence of the concentration of HAuCl_4 was also investigated as indicated in Figure 3.20. The absorbance at 550 nm was monitored by UV–vis spectroscopy. It is clearly seen that the gold enhancement was faster at higher concentration of HAuCl_4 . But at 0.4 mM HAuCl_4 , the absorbance decreased after 15 min. This might be caused by the enlarged AuNPs which were too big at high concentration of chloroauric acid and therefore, some particles precipitated, resulting in a decrease in the absorbance. Hence, 0.25 mM of chloroauric acid was selected for the following experiments.

The gold enlargement is time-dependent and normally the process will be catalyzed continuously until all the gold ions are exhausted. Thus, a long reaction time is required. Recently, we found that $\text{Na}_2\text{S}_2\text{O}_3$ can efficiently stop the reaction. As shown in Figure 3.21, after the addition of $\text{Na}_2\text{S}_2\text{O}_3$, the absorbance did not increase anymore and kept almost constant. This is because stable gold-sodium thiosulfate complex was formed (Scheme 3.1), which could not be reduced by AA and is well soluble in water. Thus, $\text{Na}_2\text{S}_2\text{O}_3$ solution was used as stop solution for gold enlargement.

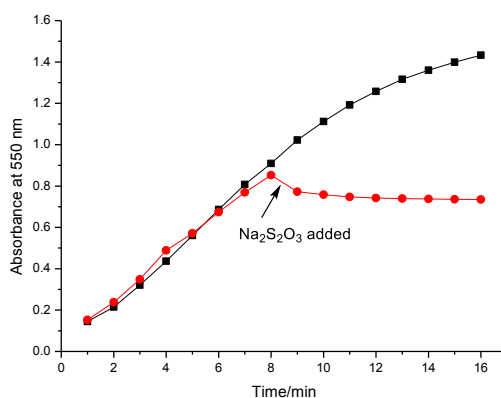


Figure 3.21 Time-dependent absorbance changes at 550 nm of the enlarged AuNPs using $\text{Na}_2\text{S}_2\text{O}_3$ as stop reagent. (100 mM CTAB, 0.25 mM HAuCl_4 and 1 mM AA were used for the preparation of gold growth solution).

The homogeneous growth of immunogold was then conducted under optimized conditions, i.e., 100 mM CTAB, 0.25 mM HAuCl_4 and 1 mM AA were utilized to prepare the growth solution and then different volumes of immunogold were added to 1

mL of growth solution for gold enhancement. Figure 3.22A shows the kinetics behavior of gold staining using different amounts of gold seeds. The absorbance increased faster at higher concentration of gold seeds. This is reasonable because AuNPs acted as a catalyst. The absorption spectra after 30 min were shown in Figure 3.22B. It can be clearly seen that final absorption intensity are highly dependent on and proportional to the initial concentration of immunogold (Figure 3.22C), which provides a quantitative basis for signal amplification.

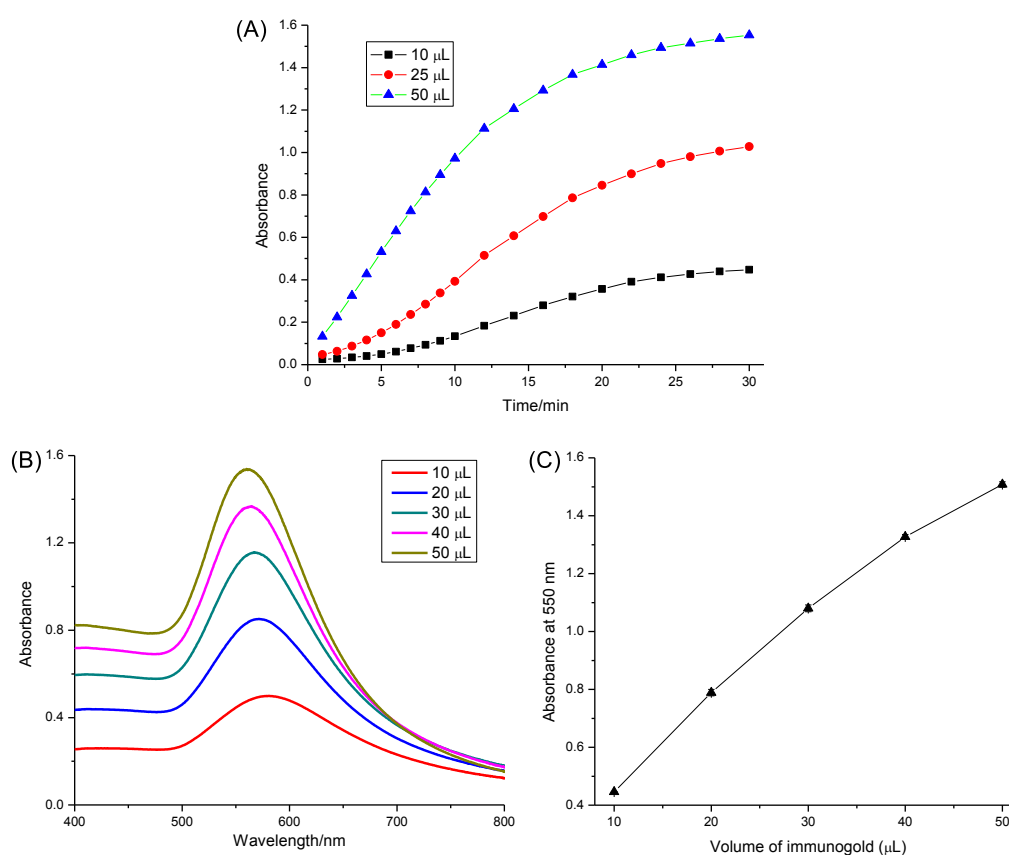


Figure 3.22 (A) Time-dependent absorbance changes at 550 nm upon analyzing different amounts of immunogold nanoparticles. (B) UV-vis absorption spectra after deposition of 30 min. (C) Absorbance at 550 nm of enlarged AuNPs vs. the amount of immunogold ($m = 3$, $n = 5$). Conditions: different amounts of immunogold were added to 1 mL of growth solution containing 100 mM CTAB, 1 mM AA and 0.25 mM HAuCl₄.

3.2.3 Monitoring the gold enlargement by RLS spectra

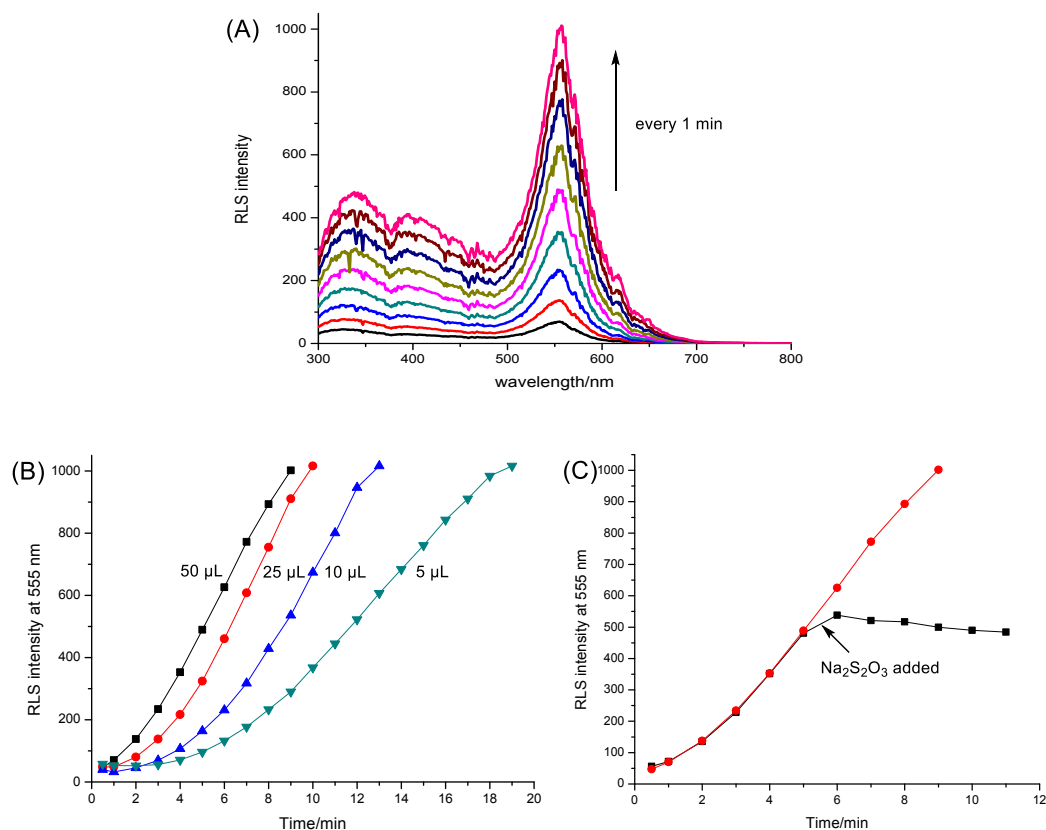


Figure 3.23 (A) RLS spectra of the enlarging AuNPs recorded every 1 min. (B) Time-dependent RLS intensity changes at 555 nm upon analyzing different amounts of immunogold nanoparticles. (C) Effect of $\text{Na}_2\text{S}_2\text{O}_3$ on RLS intensity.

The RLS spectra of enlarging AuNPs were also investigated. RLS occurs when the wavelength of incident light is close to that of the absorption band of metal nanoparticles.¹⁶⁴ AuNPs exhibit characteristic RLS peak at about 550 nm. The RLS intensity can be greatly enhanced with increasing particle size. As shown in Figure 3.23A, a typical RLS peak was observed around 555 nm. With the increase of deposition time, the RLS intensity increased dramatically. Different from the absorption band, the wavelength of RLS peak kept almost the same. Figure 3.23B shows the kinetic plots of RLS intensity at 555 nm versus time. The RLS intensity increased faster at higher concentration of immunogold. Similar to the absorption behavior, the RLS intensity did not increase when the gold enlargement was stopped by the addition of $\text{Na}_2\text{S}_2\text{O}_3$ (Figure

3.23C). Thus, RLS technique could be utilized as another tool for monitoring the gold enhancement.

3.2.4 Amplified optical detection of AFB1

After gold enlargement, the absorbance as well RLS intensity of AuNPs increased greatly. So we supposed the homogeneous gold staining could be utilized for signal amplification in the magnetic bead-based colorimetric immunoassay using Ab-AuNPs. As discussed above, the gold enlargement is time-dependent, so the influence of gold staining time was first investigated. The AFB1 standards were analyzed following the procedures described in the experimental section. After magnetic separation, 100 μ L of supernatant was added to 1 mL of growth solution containing 100 mM CTAB, 1 mM AA and 0.25 mM H₂AuCl₄. The absorbance at 565 nm of the enlarged AuNPs was measured. As shown in Figure 3.24A, because of continual growth of AuNPs, the absorbance at 565 nm increased gradually with the increase of reaction time. When the reaction time was fixed, with increasing AFB1 concentration, the absorbance also displayed a tendency to increase, indicating the signal was AFB1 concentration-dependent. The largest signal change was obtained at 20 min (Figure 3.24B). So 20 min of gold staining was fixed in this study. 100 μ L of 10 mM Na₂S₂O₃ was added to stop the enlargement.

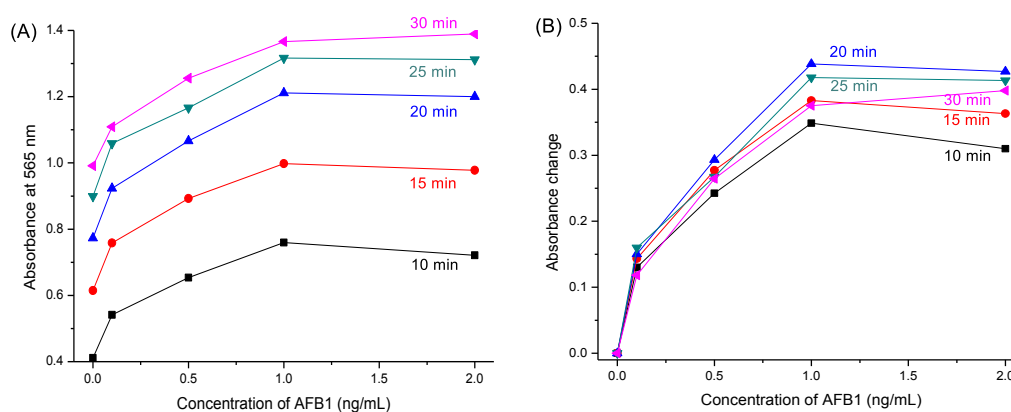


Figure 3.24 (A) Time-dependent absorbance changes at 565 nm of the supernatant after gold enhancement. (B) The dependence of absorbance change on AFB1 concentration after different staining times.

3 Results and Discussion

AFB1 standards were then quantitatively analyzed to make the calibration curve. Figure 3.25A shows the absorption spectra of supernatants after gold enhancement. With the increase of AFB1 concentration, the absorption intensity around 565 nm increased correspondingly, and the maximum absorption was slightly blue-shifted, which is ascribed to smaller enlarged AuNPs at higher concentration of immunogold. As seen in Figure 3.25B, a linear dependence between absorbance change at 565 nm and AFB1 level could be achieved in the dynamic range from 0.01 to 1 ng/mL (ppb). The regression equation could be fitted to $y = 0.45431 \times C_{[AFB1]} + 0.03182$ (ng/mL, $R^2 = 0.988$, $m = 6$, $n = 5$). The LOD was estimated to be 0.007 ng/mL (7 ppt) based on three times of signal-to-noise ratio.

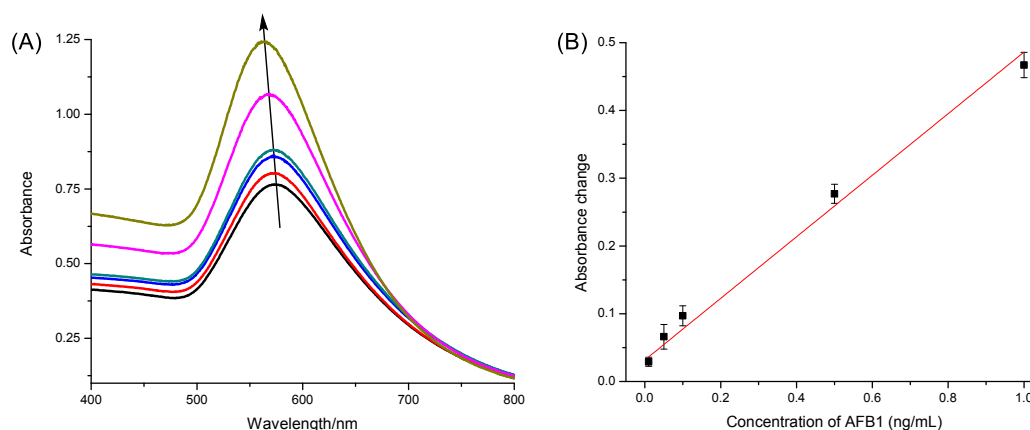


Figure 3.25 (A) UV-vis absorption spectra of supernatant after gold enlargement with different concentrations of AFB1 (from the bottom up: 0, 0.01, 0.05, 0.1, 0.5, 1 ng/mL) (B) The relationship between absorbance changes at 565 nm and AFB1 concentration.

The detectable concentration range of the developed assay is comparable with that obtained by an ELISA³¹ or an electrochemical immunosensor.¹⁴⁵ In addition, the sensitivity of proposed assay format is also high. Figure 3.26 shows the comparison of AFB1 detection without and with gold enlargement. After gold staining, the signal response increased distinctly. Taking 1 ng/mL AFB1 for example, the absorbance change is about 3.5 times of that without gold staining, which indicates that the sensitivity was

indeed improved after gold enhancement. Moreover, the method is relatively fast, with a total assay time of ~1 h.

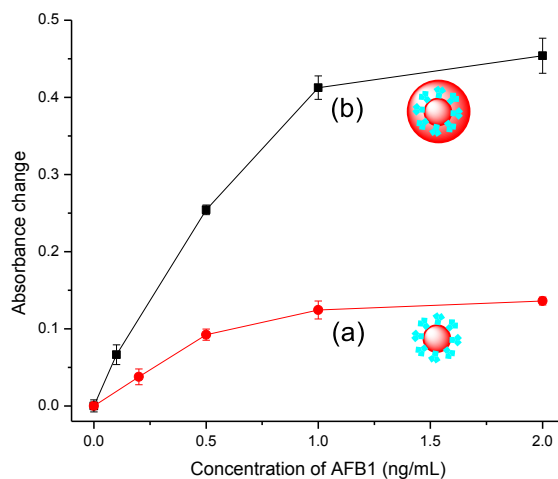


Figure 3.26 Response curves of the developed immunoassay toward AFB1 standards: (a) without and (b) with gold enlargement ($m = 3$, $n = 5$).

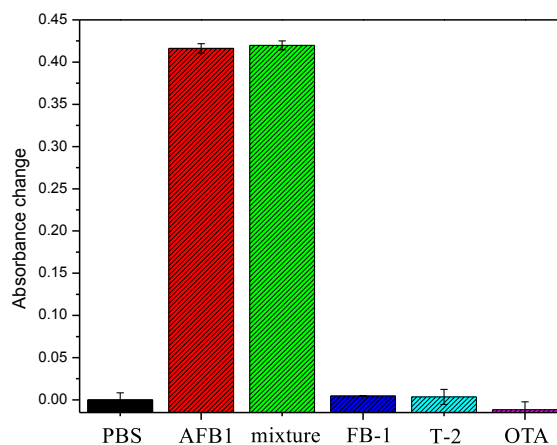


Figure 3.27 Specificity of the developed assay towards AFB1 (1 ng/mL), FB1 (20 ng/mL), T-2 toxin (20 ng/mL), OTA (20 ng/mL) and their mixture with AFB1 (20 ng/mL of FB1, T-2 and OTA, and 1 ng/mL of AFB1).

Further, the specificity of the developed immunoassay was evaluated using common mycotoxins as competitors, including FB1, T-2 toxin, OTA, and their mixture with AFB1.

3 Results and Discussion

As shown in Figure 3.27, a significant change in absorbance was only observed in the presence of AFB1, which demonstrated that the assay has a good selectivity toward AFB1 detection.

The feasibility of applying the established immunoassay for complex matrices was evaluated by the analysis of spiked maize samples. The results are summarized in Table 3.3. Satisfactory recoveries were obtained in the range of 90.7% to 115.1% with acceptable relative standard deviation. This analysis demonstrated that the established method could be used for quantitative monitoring of AFB1 in real samples.

Table 3.3 Analysis of spiked maize samples ($n = 3$).

In Spiked Sample ($\mu\text{g/kg}$)	After Dilution (ng/L)	Detected Concentration (ng/L)	Recovery (%)
4	50	51.5	103.1 ± 8.2
8	100	115.1	115.1 ± 13.2
20	250	255.6	102.2 ± 6.9
40	500	453.3	90.7 ± 2.1

The proposed method is simple, specific and highly sensitive. Furthermore, the established method does not require expensive or challenging equipments. This strategy is very attractive for mycotoxin determination because (1) the preparation and the bio-functionalization of the nanoparticles is simple and generally applicable; (2) taking advantages of the amplification effect of catalytic deposition of gold, as well as the extraordinarily high molar extinction coefficient of enlarged AuNPs, the gold enlargement-based colorimetric strategy exhibits high sensitivity; (3) the use of magnetic beads as solid carrier reduces the incubation time, and facilitates the rapid separation of immune complexes.

3.2.5 Summary

In summary, we have shown here the controlled growth of AuNPs using CTAB as stabilizing surfactant, AA as reducing agent, and $\text{Na}_2\text{S}_2\text{O}_3$ as stop reagent. SPR signature of the enlarged AuNPs and the kinetics of the gold enlargement were monitored by UV-vis spectroscopy and RLS technique. The absorbance as well as RLS intensity of the

enlarged AuNPs is highly dependent on the initial concentration of gold seeds. The controlled homogeneous gold enlargement was then utilized for signal amplification in competitive immunoassay for the first time. High sensitivity and satisfactory recoveries in spiked maize samples were achieved for the detection of AFB1. The total assay is simple, specific, sensitive, and could be easily transferred to the detection of other toxins and organic pollutants.

3.3 AuNP-catalyzed uranine reduction for signal amplification

AuNPs exhibit special catalytic properties, which have been utilized for signal amplification.¹³² As described in Section 3.2, AuNPs can serve as nanocatalyst for the deposition of Ag or Au, where the signal is amplified significantly after particle enlargement. In addition, AuNPs can catalyze the reduction of organic compounds like 4-nitrophenol in the presence of sodium borohydride, which was used for the detection of different proteins. But this catalytic reduction is only limited to several colored substances, including methyl orange, 4-nitrophenol and methylene blue.¹³⁹⁻¹⁴⁰

Compared with absorption measurements, fluorometry is generally simple, highly specific and sensitive, and therefore, is used for a variety of environmental, industrial, and biotechnology applications.¹⁶⁵⁻¹⁶⁶ A number of fluorescence biosensors have been developed based on energy transfer between fluorophores (donor) and AuNPs (acceptor), where AuNPs can effectively quench the fluorescence of nearby fluorophores.¹²⁵ But this system requires to be elaborately constructed because the quenching efficiency highly depends on the distance between the donor and acceptor. In addition, several fluorescence assays have been developed by utilizing the catalytic activity of Au-M (M = Hg, Pb, Ag) bimetallic nanoparticles.¹³³⁻¹³⁵ The formation of M–Au alloys on the AuNPs surfaces endows the generated bimetallic nanoparticles strong peroxidase-like activity towards the oxidation of Amplex UltraRed (AUR) reagent. In contrast, the activity of unmodified AuNPs towards AUR oxidation is very low. Here, we developed a more straightforward fluorescence system which directly used the intrinsic catalytic activity of AuNPs towards

3 Results and Discussion

the reduction of uranine. Specifically, in the presence of NaBH_4 , AuNPs can catalyze the reduction of uranine, producing a significant fluorescence change (Figure 3.28). The effects of NaBH_4 and AuNPs were studied in detail. The reaction rate highly depends on the concentration, size and dispersion state of AuNPs. The catalytic reaction was then utilized in signal amplification for detection of two harmful chemicals melamine (1,3,5-triazine-2,4,6-triamine) and AFB1 in food products based on different principles.

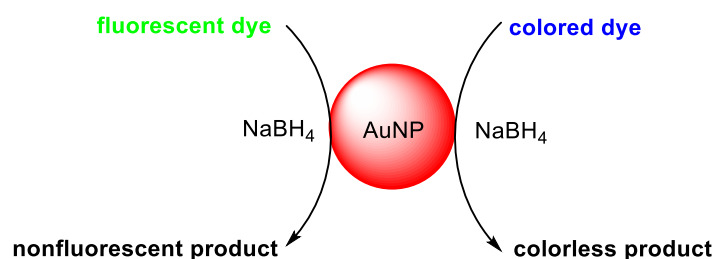
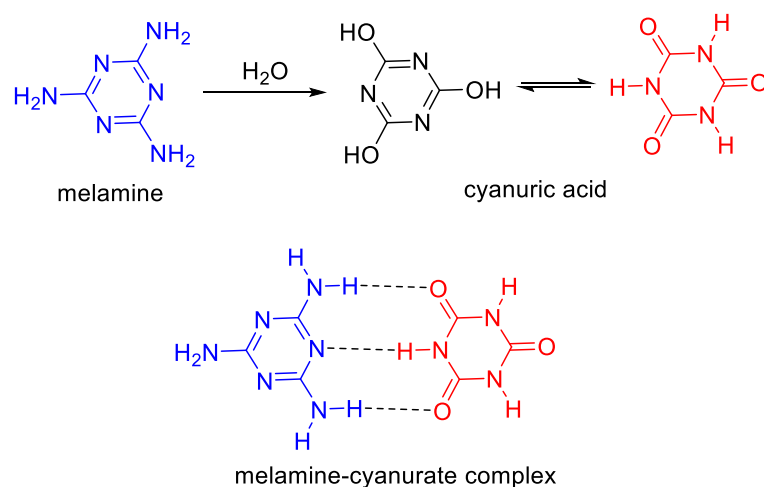


Figure 3.28 Schematic representation of AuNP-catalyzed reduction of dye by NaBH_4 .

Melamine contains a significantly high amount of nitrogen, which accounts for about 66% of its mass. Besides its industrial use for the production of polymers, adhesives, fertilizers and such, it has been artificially and illegally used as non-protein nitrogen additive, in order to increase the 'false' apparent protein content in milk products. The exposure to melamine may be particularly dangerous to human health, able to cause death in babies and children.¹⁶⁷ Specifically, melamine can be converted into cyanuric acid through hydrolysis. The generated cyanuric acid reacts with melamine to form an insoluble melamine-cyanurate which may cause the formation of stones in the urinary system (Scheme 3.3), resulting in acute renal failure by obstruction. Thus, to control the limit of melamine in milk products especially in infant formula, various analytical methods for the detection have been developed. Most of them are based on chromatographic techniques, such as HPLC and GC/MS. However, these methods lack on-site applicability and require skilled personnel, therefore have high operating costs, and are time consuming. Novel techniques have been developed using chemical sensors and biosensors.¹⁶⁷ Because of available amino groups, melamine can serve as linker to cause the aggregation of AuNPs.¹⁶⁸ In the present investigation it was shown that the catalytic activity towards uranine reduction of aggregated AuNPs decreased gradually,

resulting in different fluorescence signal after catalysis. Thereby a label-free fluorescent assay was established for the detection of melamine.



Scheme 3.3 Schematic illustration of the formation of melamine-cyanurate complex.

In addition, a magnetic bead-based fluorescence immunoassay was developed using the catalytic uranine reduction for signal amplification. The mycotoxin AFB1 was selected as the model analyte because of its extremely high toxicity and carcinogenicity and its possible presence in natural food samples, as mentioned above. AFB1-BSA-Fe₃O₄ and Ab-AuNPs were employed as capture and signal probe, respectively. AFB1 samples were incubated with AFB1-BSA-Fe₃O₄ and Ab-AuNPs. After magnetic separation of the formed MBs-AuNPs immune complexes, the supernatant containing unbound immunogold nanoparticles was utilized for catalysis. The reaction rate was dependent on the amount of immunogold which was proportional to the AFB1 concentration of the sample. To the best of knowledge, this is the first time that the intrinsic catalytic activity of AuNPs was harnessed in fluorescence detection.

3.3.1 AuNP-catalyzed uranine reduction

Figure 3.28 illustrates the reduction of dye catalyzed by AuNPs with the aid of sodium borohydride. Uranine, a type of xanthene dye, was used as the substrate owing to its high fluorescence quantum yield under alkaline conditions (0.92 in 0.1 M NaOH).¹⁶⁹ The catalytic process was investigated by fluorescence and UV-vis absorption spectroscopy.

3 Results and Discussion

As shown in Figure 3.29A, after the addition of AuNPs, the fluorescence peak of uranine around 514 nm decreased significantly. The reduction was very fast and finished within 10 min. Similar results were obtained for absorption measurements (Figure 3.29B). In contrast, the fluorescence intensity as well as absorbance of uranine kept almost the same in the absence of AuNPs (Figure 3.29C and D), which indicates that the reduction of uranine could not proceed even with a large excess of reducing reagent. These results demonstrate that AuNPs indeed act as a catalyst.

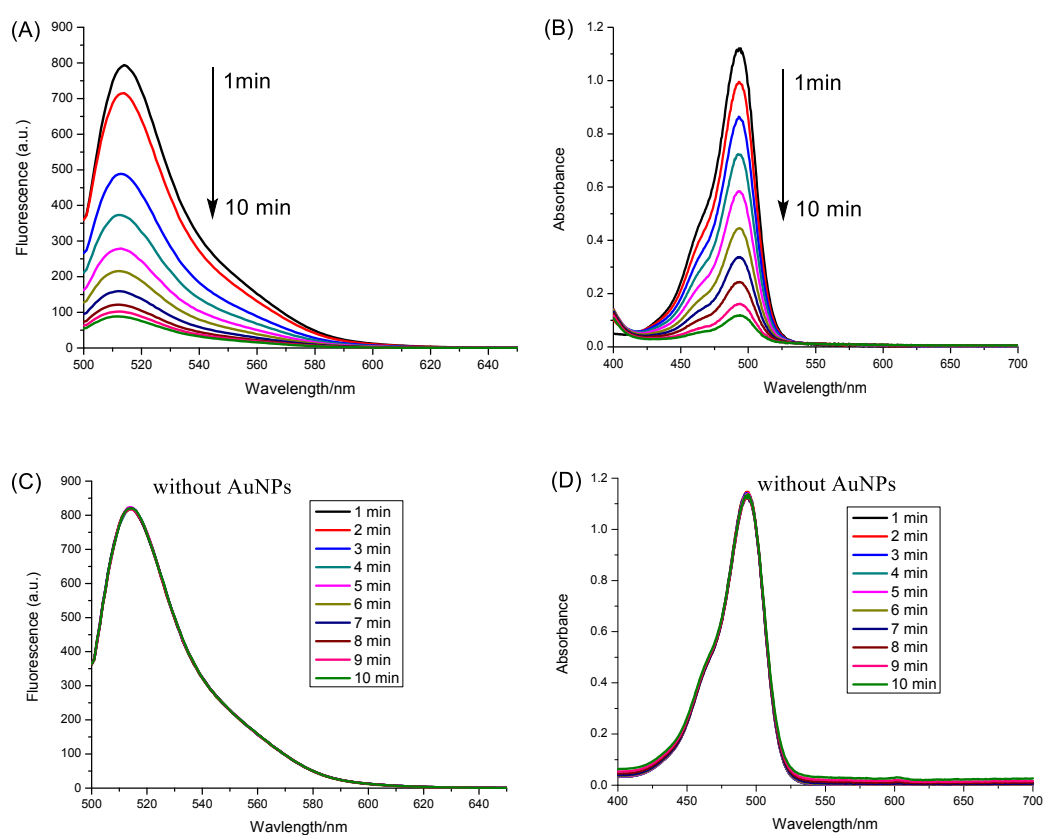


Figure 3.29 (A) and (C): Time-dependent fluorescence spectra of uranine/NaBH₄ (8 μ M/10 mM) with/without the addition of AuNPs. (B) and (D): Time-dependent UV-vis absorption spectra uranine/NaBH₄ (20 μ M/10 mM) with/without the addition of AuNPs.

The catalytic process could be explained by an electrochemical mechanism,¹⁷⁰ where the AuNP serves as an electron relay system for the oxidant and reductant. As illustrated in Figure 3.30, first BH₄⁻ ions and uranine molecules are adsorbed together onto the surface of AuNPs. Then electron transfer takes place between uranine and BH₄⁻ through the

AuNP. After receiving the electrons, the uranine molecules are reduced. During this process, the π - π conjugated structure of xanthene ring is destroyed. So the formed products are colorless and nonfluorescent. Meanwhile, NaBH_4 is converted into gaseous products B_2H_6 and H_2 , which causes the formation of air bubbles during reaction.

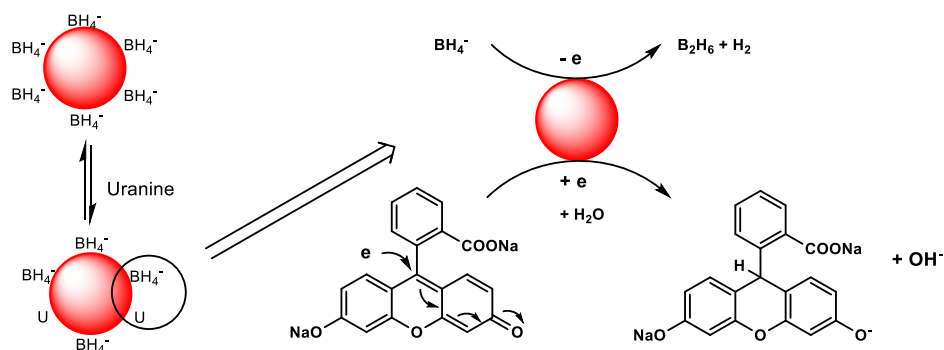


Figure 3.30 Proposed mechanism of AuNP-catalyzed uranine reduction.

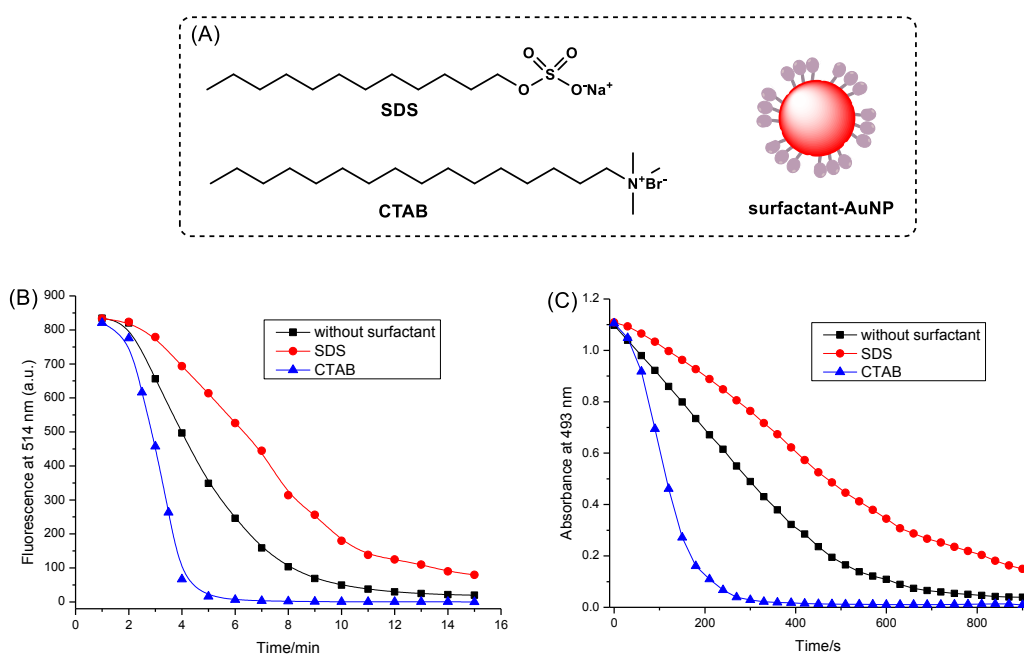


Figure 3.31 (A) The structure of SDS, CTAB and surfactant-AuNP. (B) Time-dependent fluorescence changes of uranine/ NaBH_4 solution (8 μM /10 mM) at $\lambda_{em} = 514$ nm after the addition of AuNPs with different surface coating. (C) Time-dependent absorbance changes of uranine/ NaBH_4 solution (20 μM /10 mM) at 493 nm after the addition of AuNPs with different surface coatings.

To verify the adsorption-based catalytic mechanism, the catalytic activity of AuNPs with different surface modification was measured. Cationic surfactant CTAB and anionic

3 Results and Discussion

surfactant sodium dodecyl sulfate (SDS) were utilized to coat the AuNPs (Figure 3.31A) by hydrophobic interaction, most probably. Although the surfactant molecules may block some of active sites on AuNP surfaces, the modified AuNPs still showed high catalytic ability. As shown in Figure 3.31B and C, compared with unmodified citrate-AuNPs, CTAB-AuNPs showed higher activity, while SDS-AuNPs displayed lower catalytic ability. This is because the substrates, BH_4^- and uranine, are both negatively charged, which tend to adsorb onto cationic CTAB-modified surface much better due to electrostatic attraction. In contrast, anionic SDS-modified surface inhibits the adsorption of reactants. Experimental data are in strong support of the proposed catalytic mechanism.

3.3.2 The role of NaBH_4

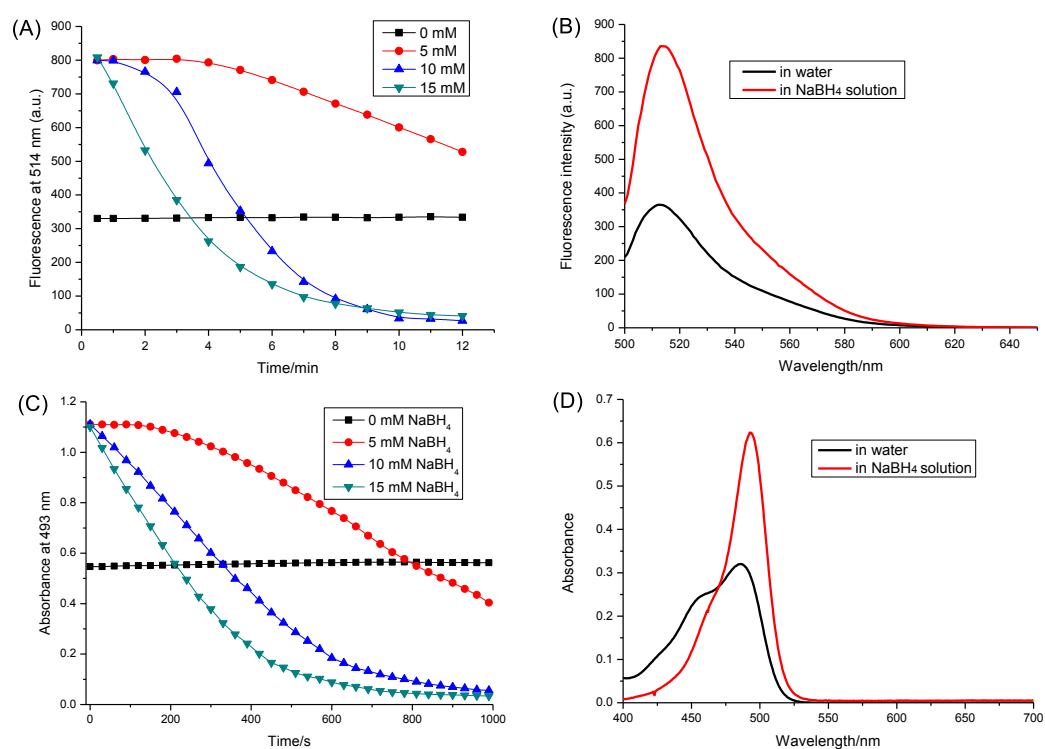


Figure 3.32 (A) and (C): The effect of NaBH_4 concentration on the catalytic reaction (uranine in 3 mL water, NaBH_4 with different concentrations and then 20 μL of 16 nm citrate-stabilized AuNPs was added. For fluorescence measurements, the concentration of uranine was 8 μM . For absorption measurements, the concentration of uranine was 20 μM . (B) and (D): Fluorescence and absorption spectra of uranine in water and NaBH_4 solution.

The influence of NaBH₄ on the catalytic reaction was investigated. As shown in Figure 3.32A and C, in the absence of NaBH₄, the fluorescence intensity and absorbance of uranine kept constant after the addition of AuNPs, which indicates the reaction did not proceed. With the increase of NaBH₄ concentration from 5 mM to 15 mM, the reaction rate was enhanced correspondingly. Interestingly, the initial fluorescence as well as absorbance of uranine in water was much lower than that in NaBH₄ solution. We further measured the corresponding fluorescence and absorption spectra without the addition of AuNPs. As seen in Figure 3.32B and D, NaBH₄ changed the fluorescence emission and absorption of uranine. This can be ascribed to partial hydrolyzation of NaBH₄, which shifted the pH value from 6.5 in water to 10.4, as shown in equation 3.5.



Uranine is very sensitive to pH change (Figure 3.33).¹⁷¹ With the increase of pH value, non-fluorescent fluorescein spirolactone (colorless) in water converts to the dianion form which displays strong green fluorescence (yellow colored) (Scheme 3.4).¹⁷¹ Thus, higher fluorescence and absorbance were observed in alkaline NaBH₄ solution. Furthermore, due to the large excess of NaBH₄, the solution pH was kept constant during the reaction process. In short, NaBH₄ not only serves as reducing reagent, but also controls the solution pH.

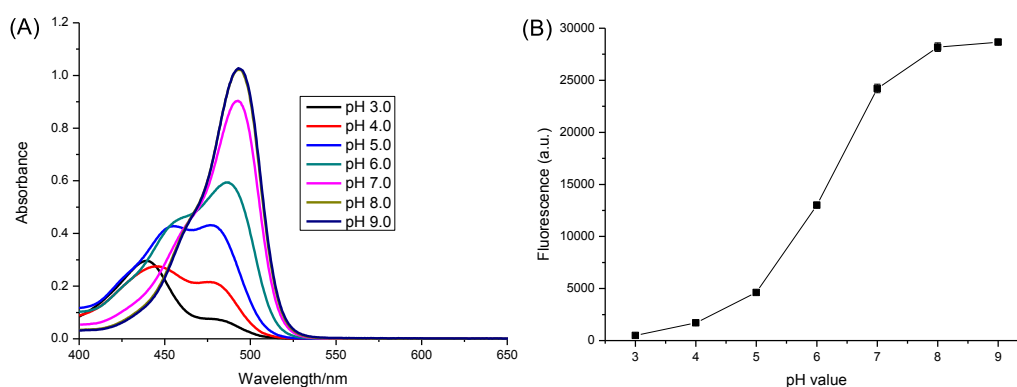
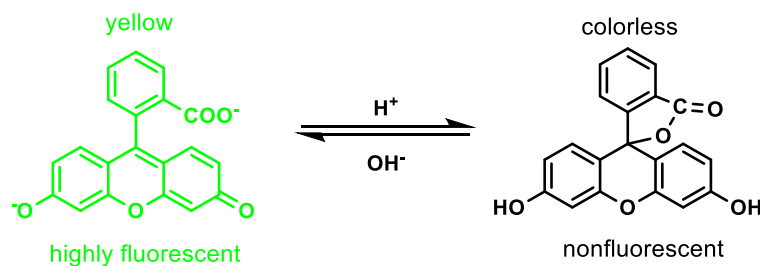


Figure 3.33 The effect of pH value on the absorbance and fluorescence of uranine. Conditions: 20 μM uranine in buffers with different pH value.

3 Results and Discussion



Scheme 3.4 Chemical structure conversion of uranine under different pH conditions.

3.3.3 The effect of AuNPs

The influence of AuNPs on the catalytic reaction was studied in detail. Figure 3.34 shows the kinetics behavior of uranine reduction using different amounts of AuNPs. It can be clearly seen that the reaction rate was highly dependent on the initial concentration of nanocatalyst, which was speeded up at high concentration of AuNPs.

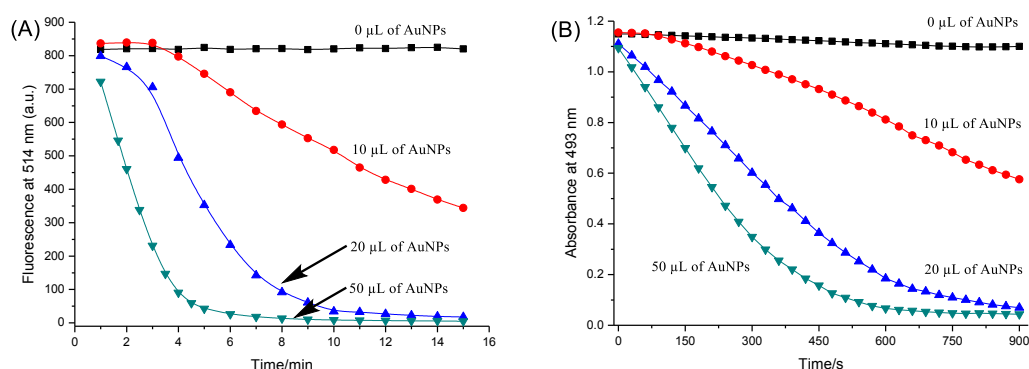


Figure 3.34 The effect of AuNP concentration on the catalytic reaction. Conditions: uranine (8 μM for fluorescence measurements, 20 μM for absorption measurements) and 10 mM NaBH_4 in 3 mL water, and then 16nm AuNPs with different volume were added.

As the properties of inorganic nanoparticles are often dependent on size, we studied the catalytic activity of AuNPs with different size (16, 25 and 34 nm). The size distribution of AuNPs was determined by DLS (Figure 3.35). As indicated in Figure 3.36, the AuNPs showed different levels of activity towards uranine reduction. The smaller the size, the higher is the catalytic activity. This may be because smaller AuNPs have a larger surface-to-volume ratio, which can interact more efficiently with substrates.

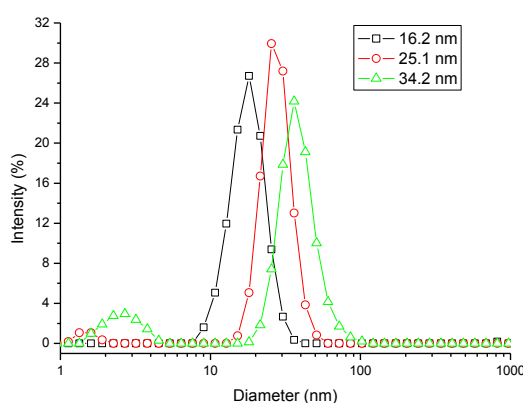


Figure 3.35 Size distribution of the prepared AuNPs determined by DLS.

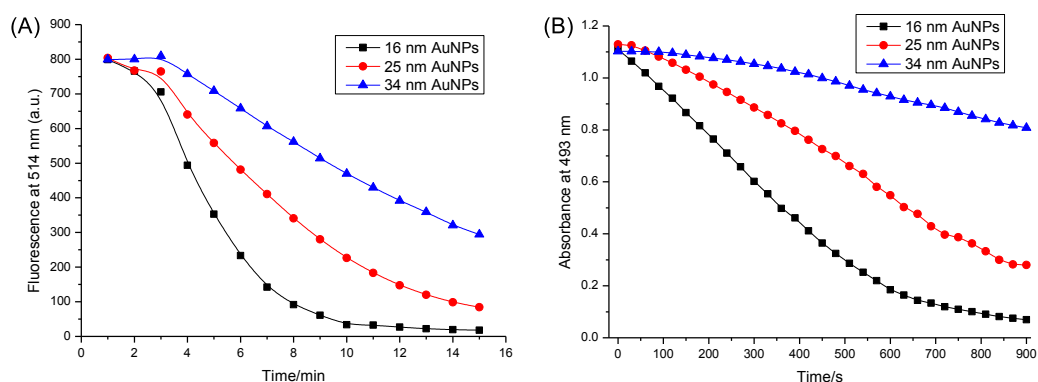


Figure 3.36 The effect of AuNP size on the catalytic reaction. Conditions: uranine ($8 \mu\text{M}$ for fluorescence measurements, $20 \mu\text{M}$ for absorption measurements) and 10 mM NaBH_4 in 3 mL water, and then $20 \mu\text{L}$ of AuNPs with different size were added.

The dispersion state of AuNPs may also affect their catalytic activity. So comparison between aggregated and dispersed AuNPs was made. Aggregated AuNPs were obtained by adding high concentration of NaCl to AuNPs solution ($100 \mu\text{L}$ of 1 M NaCl to 1 mL of AuNPs). As seen in Figure 3.37, after the addition of NaCl, the color changed from red to blue, and a broad absorption band appeared and shifted to longer wavelength, which indicates that the AuNPs did aggregate.¹²² Compared with dispersed AuNPs, the catalytic activity of aggregated AuNPs was much lower as shown in Figure 3.38. This may be because the total surface area decreased greatly when AuNPs aggregated, and a large number of active sites on gold surface were blocked sterically.

3 Results and Discussion

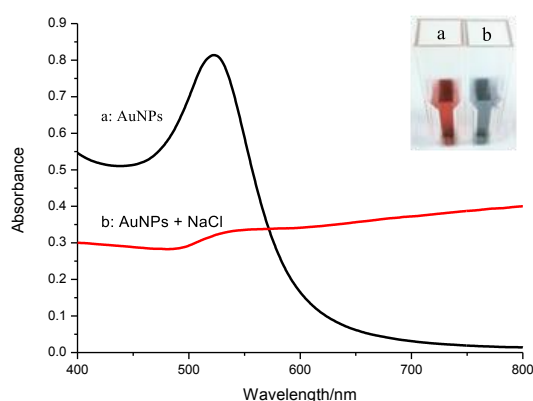


Figure 3.37 UV-vis absorption spectra of dispersed and aggregated AuNPs and corresponding picture.

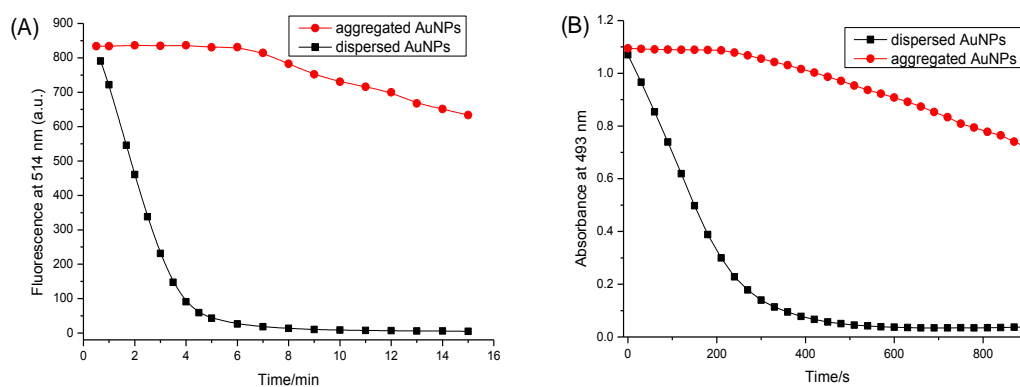


Figure 3.38 The influence of dispersion state of AuNPs on the catalytic reaction. Conditions: uranine (8 μM for fluorescence measurements, 20 μM for absorption measurements) and 10 mM NaBH_4 in 3 mL water, and then 50/55 μL of dispersed/aggregated AuNPs were added.

3.3.4 Detection of melamine

Because of the strong interaction between electron-rich nitrogen atoms and the electron-deficient surface of AuNPs, melamine containing multiple binding sites can cause the aggregation of AuNPs (Figure 3.39A). As shown in Figure 3.39B, with the increase of melamine concentration, the absorption of AuNPs around 530 nm decreased gradually, and a new peak around 700 nm appeared. Meanwhile, the color of colloidal solutions changed from red over purple to blue (Figure 3.39C), indicating the AuNPs aggregated in the presence of melamine.

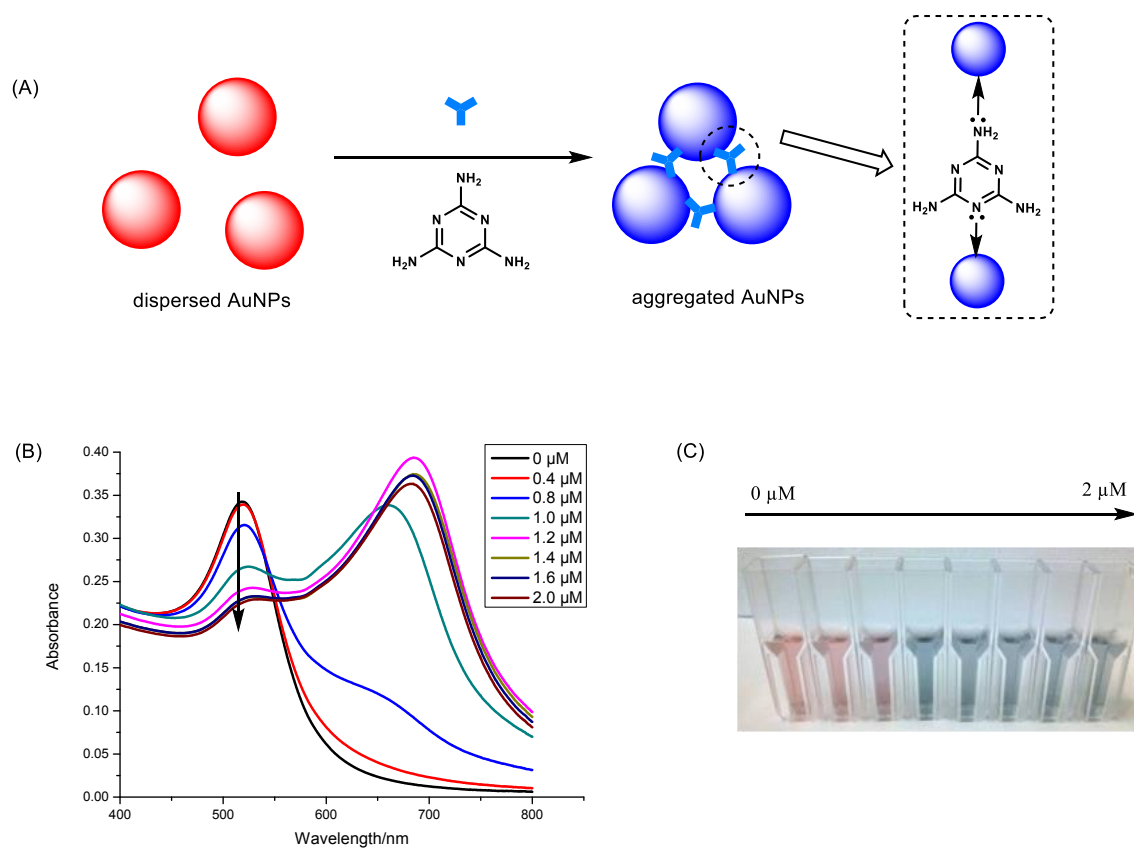


Figure 3.39 (A) Schematic illustration of the aggregation of AuNPs induced by melamine. (B) Absorption spectra of AuNPs after the addition of melamine with different concentrations and (C) corresponding picture. $[\text{Au}] = 9.46 \text{ mg/L}$.

As AuNPs aggregated, their catalytic activity towards the reduction of uranine decreased. And thereby an aggregation-based label-free fluorescent assay was established for the detection of melamine, as illustrated in Figure 3.40. The aggregated AuNPs were utilized to catalyze the reduction of uranine by NaBH_4 to induce a fluorescence change. With the increase of melamine concentration, AuNPs aggregated to a higher extent. Obviously, the fluorescence intensity is proportional to the melamine concentration.

3 Results and Discussion

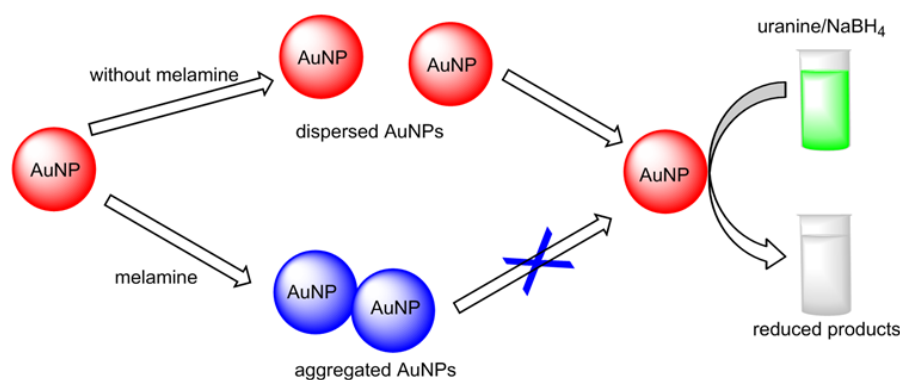


Figure 3.40 Schematic illustration of the proposed fluorescent detection of melamine based on AuNPs catalysis.

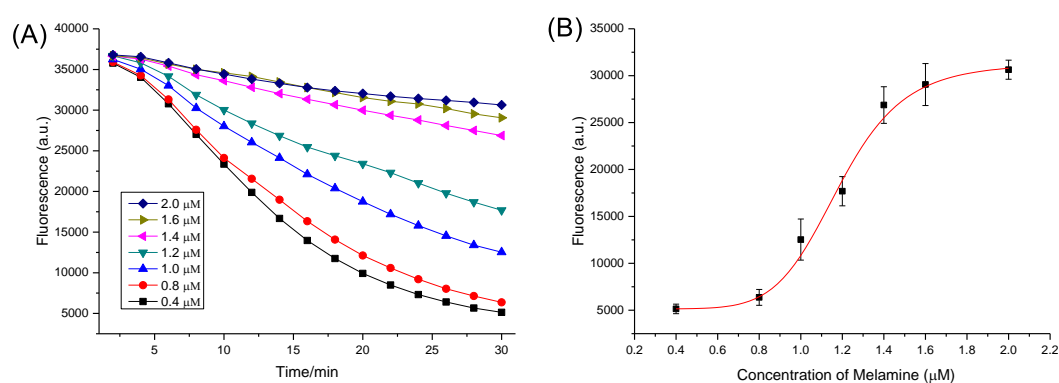


Figure 3.41 Kinetic-based fluorescent assay for melamine using AuNP-catalyzed uranine reduction ($\lambda_{ex}/\lambda_{em} = 485/528$ nm). (A) Time-dependent fluorescence changes corresponding to different concentrations of melamine. (B) The dependence of fluorescence intensity on melamine concentration.

The time-dependent reduction of uranine catalyzed by aggregated AuNPs, which was induced by melamine, was monitored on microplates by a reader. Because of continual reduction of uranine molecules, the fluorescence intensity decreased gradually with the increase of reaction time (Figure 3.41A). When the reaction time was fixed, with increasing melamine concentration, the fluorescence intensity also displayed a tendency to increase, indicating the signal was melamine concentration-dependent. Figure 3.41B plotted the fluorescence intensity at 30 min as a function of melamine concentration. A good sigmoidal fitting ($R^2 = 0.99$, $m = 3$, $n = 7$) was obtained between the fluorescence (Fl.) and melamine concentration ranging from 0.4 to 2 μM :

$$Fl. = 5143.2 + \frac{26143.2}{1 + \left(\frac{C_{\text{melamine}}/\mu\text{M}}{1.18}\right)^{-7.5}}$$

The LOD defined at 10% of the maximum response^{84, 143} was estimated to be 0.88 μM (0.11 mg/L; ppm). Without any further optimization, the obtained LOD is lower than that of colorimetric assays based on aggregation of unmodified AuNPs (from 0.15 to 2.5 ppm),¹⁶⁷ demonstrating the high sensitivity using catalytic amplification.

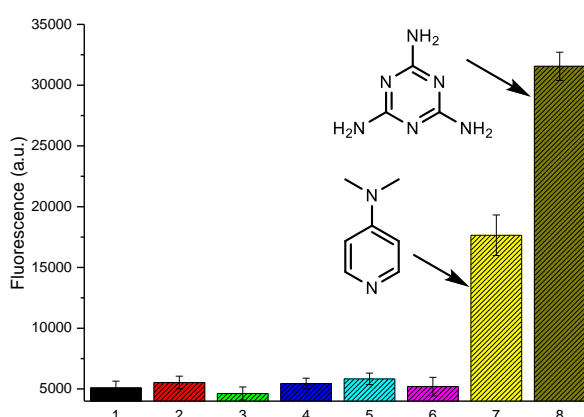


Figure 3.42 Specificity of the proposed method towards melamine. (1) blank, (2) ammonia, (3) ethanolamine, (4) glycine, (5) tryptophane, (6) 4-nitroaniline, (7) DMAP and (8) melamine. The concentration of melamine was 0.25 mg/mL (2 μM) while that of the other amino compounds was 5 mg/mL.

To investigate the specificity of the developed assay, the effects of potentially interfering amino compounds, such as ammonia, ethanolamine, glycine, tryptophane, 4-nitroaniline and DMAP were tested. As shown in Figure 3.42, the fluorescence was very strong in the presence of melamine, while other interfering components had little effect compared with the blank, except DMAP. This is because DMAP contains two electron-rich nitrogen atoms, which can serve as linker to induce the aggregation of AuNPs (Figure 3.43), resulting in relatively high fluorescence after catalysis. In contrast, 4-nitroaniline which also has two nitrogen atoms cannot cause the aggregation of AuNPs since the nitro group is electron-withdrawing.

3 Results and Discussion

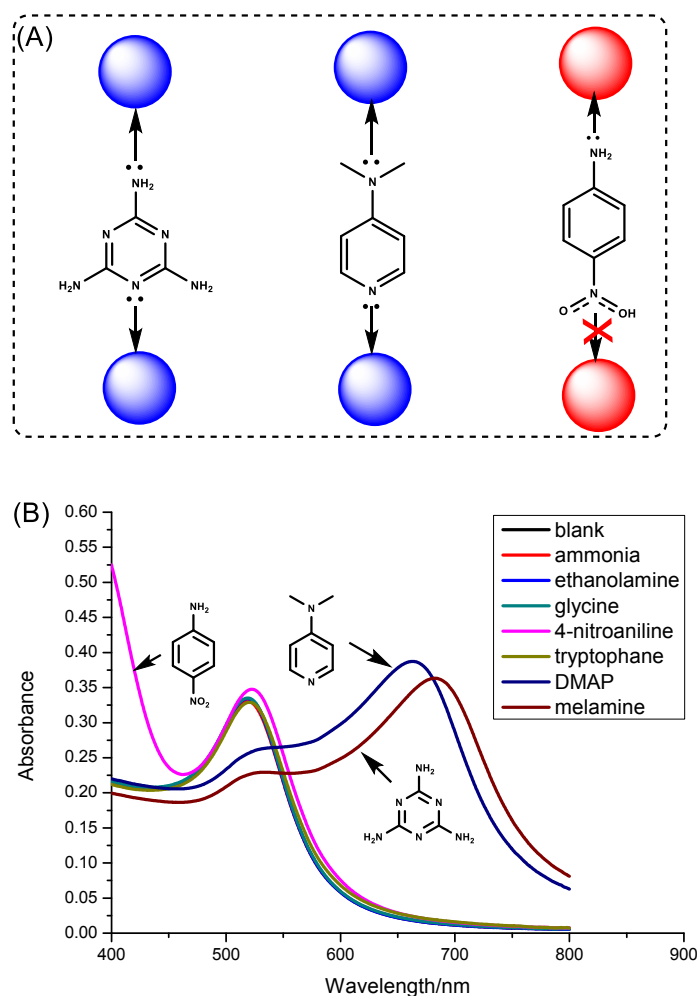


Figure 3.43 (A) Schematic illustration of the interactions between AuNPs and amino compounds. (B) Absorption spectra of AuNPs in the presence of different amino compounds. [Au] = 9.46 mg/L.

In order to validate the practicability of the developed method, milk samples spiked with different concentration of melamine were analyzed. As is known, milk is a complex matrix containing proteins, sugars, lipids and salts, which may interfere with the detection. Thus, it is critical to extract melamine while removing interferences from milk. Trichloroacetic acid and acetonitrile were used to precipitate proteins. In addition, lipids and other organic substances were removed by chloroform. After sample cleanup, the extracts were detected according to the procedure described in the experimental section. As shown in Figure 3.44, the catalytic reaction proceeded slower at higher concentrations of melamine in milk. The fluorescence at 30 min was linear to logarithmic concentration of melamine from 3 to 100 mg/L ($F_i = 12038.2 + 10069.4 \times \log C_{[\text{melamine}]}$, $m = 3$, $n = 6$)

with a correlation coefficient of 0.99, demonstrating the proposed approach could be utilized for the detection of melamine in milk.

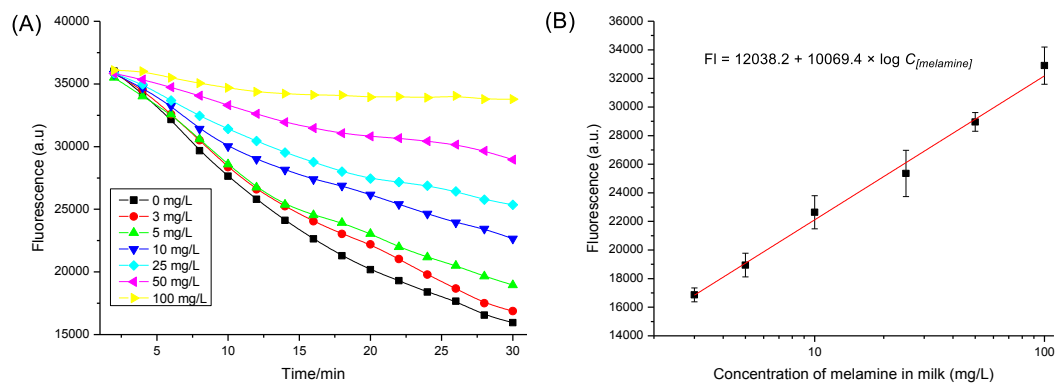


Figure 3.44 Kinetic-based fluorescent assay for melamine in milk ($\lambda_{ex}/\lambda_{em} = 485/528$ nm). (A) Time-dependent fluorescence changes, which correspond to different concentrations of melamine. (B) The dependence of fluorescence intensity at 30 min on melamine concentration in milk.

Combining the high-affinity binding between AuNPs and melamine with signal amplification procedure based on AuNP-catalyzed uranine reduction, the developed assay is simple and sensitive. The aggregation event is converted into fluorescence signal, which could be expanded to other aggregation-based assays using AuNPs.

3.3.5 Detection of AFB1

Further, we demonstrated that the catalytic reaction could be utilized for signal amplification in immunoassay. Figure 3.45 shows the principle of the method. Specifically, AFB1-BSA- Fe_3O_4 competed with target AFB1 for binding with the AuNP-labeled antibodies. The amount of Ab-AuNPs bound onto MBs decreased with increasing AFB1 concentration because of competitive inhibition. After magnetic separation of the formed particle assemblies (i.e. *anti*-AFB1-AuNP-AFB1-BSA- Fe_3O_4), the supernatant containing unbound AuNPs was utilized to promote the reduction of uranine, thereby producing a fluorescence change. The final fluorescence intensity, which depends on the concentration of Ab-AuNPs in the supernatant, is inversely proportional to the concentration of AFB1 in the sample.

3 Results and Discussion

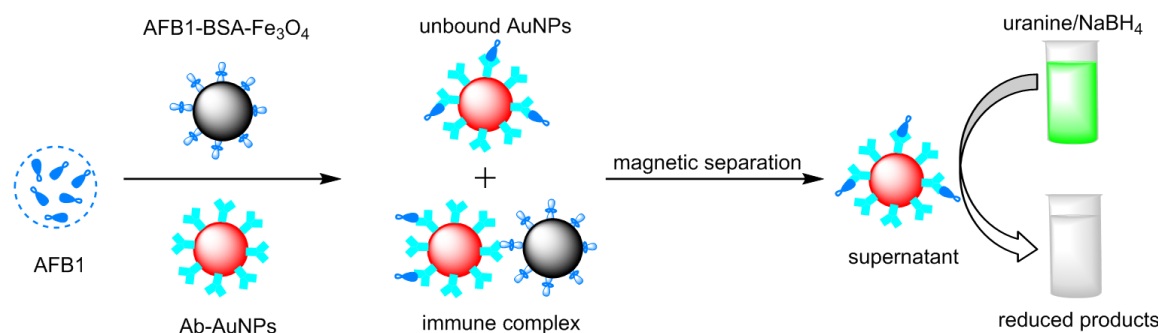


Figure 3.45 Schematic illustration of the fluorescent detection of AFB1 using AuNP-catalyzed uranine reduction.

It should be noted that the AuNPs become very stable after being coated by proteins, which is ascribed to steric repulsion between proteins on different AuNPs. As shown in Figure 3.46, the absorbance of Ab-AuNPs kept almost unchanged after the addition of melamine, indicating even melamine was not able to induce the aggregation of immunogold nanoparticles.

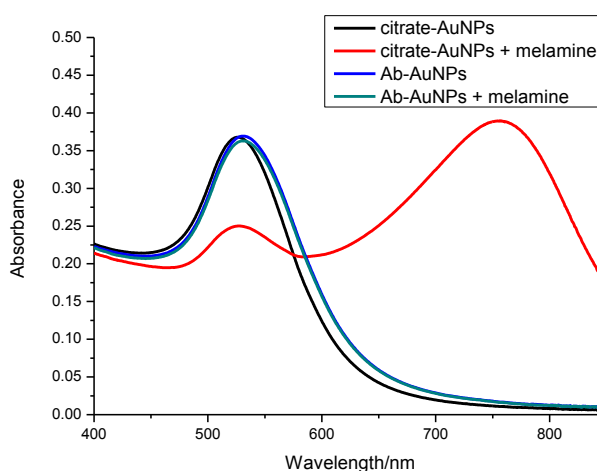


Figure 3.46 Absorption spectra of citrate-AuNPs and Ab-AuNPs in the absence/presence of 2 μM melamine. $[\text{Au}] = 9.46 \text{ mg/L}$.

Ruling out the possible interference from melamine, we tested AFB1 samples in PBS following the procedures described in the experimental section. Figure 3.47A shows the time-dependent fluorescence change of uranine catalyzed by unbound immunogold nanoparticles in the supernatant. The fluorescence decreased with increasing reaction

time, which demonstrates the AuNPs kept catalytic activity even after being coated by proteins. The catalytic reaction proceeded faster at higher concentration of AFB1, which reached balance after about 10 min. A good liner relationship was obtained between the fluorescence (Fl.) at 10 min and logarithmic concentration of AFB1 from 0.02 to 1 ng/mL (Figure 3.47B). The regression equation could be fitted to $Fl. = 2459.2 - 7294.1 \times \log C_{[AFB1]}$ (ng/mL, $R^2 = 0.99$, $m = 3$, $n = 6$). The LOD defined at 10% of maximum response inhibition^{84, 143} was 17.1 pg/mL, which was obviously lower than that of magnetic bead-based immunoassay using fluorescent nanoparticles (0.1 ng/mL).³³ Furthermore, the half maximal inhibitory concentration (IC_{50}) was 104 pg/mL, which was much lower than that of method 2 using gold staining for signal amplification (465 pg/mL), indicating the high sensitivity of the developed fluorescent immunoassay.

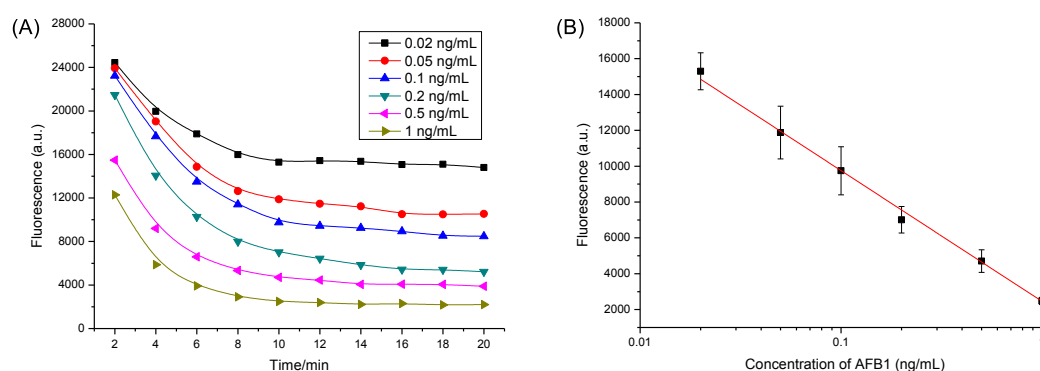


Figure 3.47 Kinetic-based fluorescent assay for AFB1 based on AuNPs catalysis ($\lambda_{ex}/\lambda_{em} = 485/528$ nm). (A) Time-dependent fluorescence change, which corresponds to different concentrations of AFB1. (B) The relationship between fluorescence intensity and AFB1 concentration.

To evaluate the specificity of the established immunoassay, control experiments were conducted by selecting OTA, T-2 toxin and FB1 as the interfering mycotoxins. As seen in Figure 3.48, a significant decrease in fluorescence was only observed in the presence of target AFB1, while the presence of other toxins caused very small fluorescence change. Thus, the selectivity of the proposed method was acceptable.

3 Results and Discussion

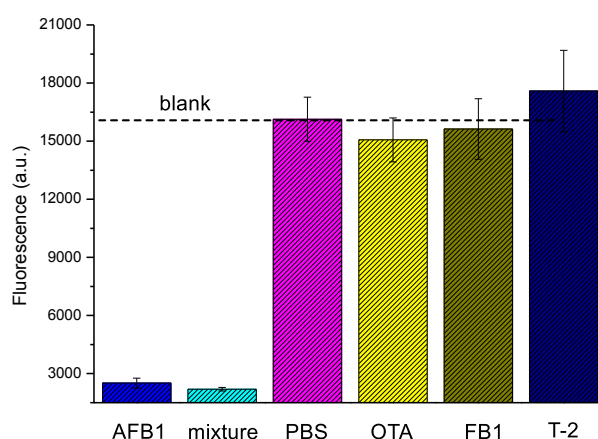


Figure 3.48 Specificity of the proposed method towards AFB1. AFB1 (1 ng/mL), OTA (20 ng/mL), FB1 (20 ng/mL), T-2 toxin (20 ng/mL), and their mixture with AFB1 (20 ng/mL of FB1, T-2 and OTA, and 1 ng/mL of AFB1).

To further evaluate the feasibility of applying the fluorescent immunoassay in complex matrices, AFB1 standards prepared in aflatoxin-free maize extract were analyzed. As seen in Figure 3.49, the signal response decreased obviously in maize extract compared with that in PBS under the same conditions, which was the result of matrix effect. The complicated food matrix could block binding sites of antibodies, resulting in higher concentration of immunogold nanoparticles in the supernatant after magnetic separation. So we diluted the supernatant with PBS (1:1, v/v) and then used the diluted solution for signal amplification. As indicated in Figure 3.50, larger signal change was achieved. A linear dependence existed between fluorescence at 20 min and AFB1 level in the dynamic range from 0.05 to 1 ng/mL ($F_l = 2350.9 - 10524.1 \times \log C_{[AFB1]}$, $R^2 = 0.98$, $m = 6$, $n = 5$). Then maize powders artificially spiked with AFB1 were analyzed and AFB1 levels were determined from the calibration curve. As listed in Table 3.4, acceptable recoveries were obtained in the range of 84.7% to 119.4%, demonstrating that the established method could be applied for AFB1 determination in real agricultural products.

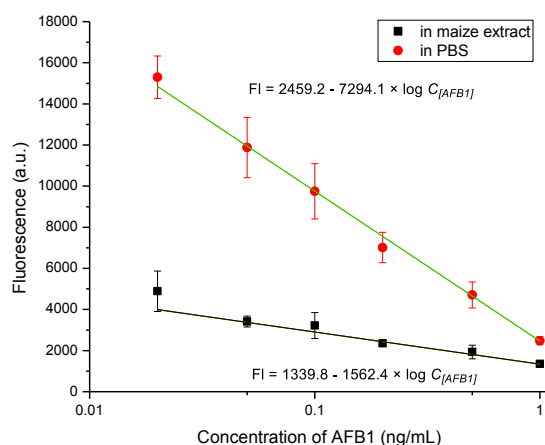


Figure 3.49 Dose-response curves of fluorescent immunoassays for the detection of AFB1 in maize extract and PBS under the same conditions ($m = 3$, $n = 6$).

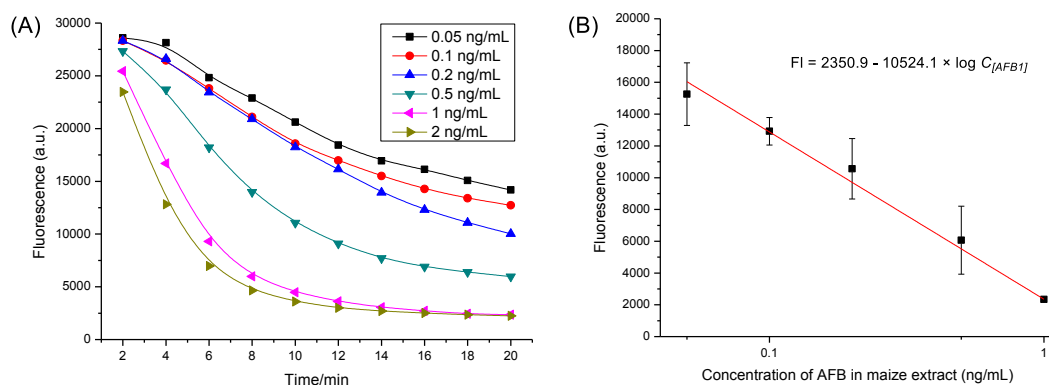


Figure 3.50 Kinetic-based fluorescent assay for AFB1 in maize extract ($\lambda_{ex}/\lambda_{em} = 485/528$ nm). (A) Time-dependent fluorescence changes, which correspond to different concentrations of AFB1. (B) The dependence of fluorescence intensity at 20 min on AFB1 concentration in maize extract ($m = 6$, $n = 5$).

Table 3.4 The detected results of AFB1 in maize samples and recoveries ($n = 3$).

In Spiked Sample ($\mu\text{g}/\text{kg}$)	After Dilution (ng/L)	Detected Concentration (ng/L)	Recovery (%)
8	0.10	0.104	104.0 ± 22.0
40	0.50	0.597	119.4 ± 16.8
80	1.00	0.847	84.7 ± 10.3

3.3.6 Summary

AuNPs can catalyze the reduction of uranine in the presence of NaBH_4 , which was monitored by fluorescence and UV-vis absorption spectroscopy. AuNPs may act as an electron relay system where electron transfer takes place between uranine and BH_4^- through the AuNP. NaBH_4 not only served as reducing reagent, but also controlled the solution pH. Kinetic studies demonstrated that the concentration, size and dispersion state of AuNPs greatly affect the reaction rate. Further, multifunctional detection using this catalyzed fluorescence assay was achieved. In detail, a label-free fluorescent assay for melamine and a magnetic bead-based fluorescent immunoassay for AFB1 were established using the catalytic reaction for signal amplification. Satisfactory results were obtained for the detection of melamine in milk and AFB1 in maize. The proposed methods are rapid, sensitive and cost-effective, which offer great promise for the detection of other analytes.

3.4 Comparison between three methods

Section 3.1 described a colorimetric immunoassay for AFB1 using AFB1-BSA- Fe_3O_4 and Ab-AuNPs (method 1). Because AuNPs have high molar extinction coefficient, the signal was directly read out by a UV-vis spectrophotometer. Under optimal conditions, AFB1 levels within the ng/L range in PBS and maize sample extract could be detected. Although the detection was simple and time-saving, the signal change was relatively low. So we tried to enhance the signal intensity using gold staining (Section 3.2, method 2). After gold enlargement, the absorbance of immunogold increased significantly. So, higher sensitivity was obtained for the detection of AFB1. In addition, AuNPs were employed as artificial enzyme and a fluorescent immunoassay was developed for AFB1 (Section 3.3, method 3). The corresponding experimental results of the three methods were summarized in Table 3.5.

Table 3.5 Summary of experimental results for the analysis of AFB1.

Method	Detection Range (ng/L)	LOD (ng/L)	IC ₅₀ (ng/L)	Analysis Time
1	20 - 800	12 ^[1]	436	40 min
2	10 - 1000	7 ^[1]	465	~ 1 h
3	20 - 1000	17 ^[2]	104	~ 1 h

1: calculated based on three times of signal-to-noise ratio;

2: calculated based on 10% of the response inhibition.

Because color development and signal amplification steps are eliminated, method 1 is simplest and only 40 min is needed. But the detection range is more narrow (20-800 ng/L) with a LOD of 12 ng/L. After signal amplification using homogeneous gold staining, the LOD is pushed down to 7 ng/L with a broader detection range of 10-1000 ng/L. Since gold enlargement takes about 20 min, a bit longer analysis time is required. The detection range and assay time of method 3 are comparable with that of method 2. It is noteworthy that the IC₅₀ of method 3 is much lower than that of method 1 and 2, indicating the fluorescent immunoassay is the most sensitive. This is because one AuNP can catalyze the reduction of millions of uranine molecules, the signal is significantly amplified. Furthermore, fluorometry is generally more sensitive than absorbance measurements.

3 Results and Discussion

4 Summary and Outlook

4 Summary and Outlook

4.1 Research summary

In this thesis, different methods have been established for the detection of AFB1 in real agriculture products. In the first section, a magnetic bead-based colorimetric immunoassay was developed utilizing AuNPs as signal probe. Because AuNPs have extremely high molar extinction coefficient, the signal was directly read out by a UV-vis spectrophotometer. AuNPs of different size were tested and 34.8-nm AuNPs gave the largest signal change. The detection was also affected by ionic strength, pH value and incubation time. 50 mM phosphate buffer with pH 7.4 was used for the preparation AFB1 standards and 30 min incubation was selected for the immunoreaction. Under optimal conditions, AFB1 levels within 20-800 ng/L could be detected. The LOD was 12 ng/L and the total assay time was ~ 40 min. Compared with conventional ELISA, the proposed method was simple and fast because tedious washing and color development steps were eliminated. But the absorbance change was relatively small due to the lack of signal amplification.

In the second section, homogeneous gold staining was investigated in-depth. The immunogold nanoparticles could be utilized as seeds for the catalytic deposition of gold atoms in aqueous HAuCl_4 solution using AA as reducing reagent and CTAB as stabilizing surfactant. UV-vis spectroscopy and RLS technique were used to monitor the gold enlargement process. The absorbance and RLS intensity increased significantly after gold enhancement. In addition, the reaction could be effectively stopped by sodium thiosulfate, making the gold staining more controllable and convenient. The controlled homogenous gold enlargement was then utilized for signal amplification in competitive immunoassay for the detection of AFB1. After gold staining, the signal change was enhanced obviously. The LOD was pushed down to 7 ng/L and a broader detection range (10-1000) ng/L was achieved. Satisfactory recoveries in the range of 90.7% to 115.1% were obtained for the analysis of AFB1 in maize samples.

4 Summary and Outlook

In the third section, AuNPs were employed as catalyst to promote the reduction of uranine, which was quantitatively measured by fluorescence and UV-vis spectroscopy. During the reaction, AuNPs may act as an electron relay system by receiving and transferring the electrons to uranine molecules. When uranine molecules were reduced, their absorption and fluorescence intensity decreased greatly. NaBH₄ acted as reducing reagent, as well as controlled the pH value of reaction mixture. Kinetic studies demonstrated that smaller AuNPs showed higher catalytic activity and CTAB coating could accelerate the reaction. When AuNPs aggregated, their catalytic activity decreased correspondingly, and thereby a label-free fluorescence assay was established for the detection of melamine. Melamine levels in milk from 3 to 100 mg/L could be detected using the proposed method. In addition, the catalytic reaction was used for signal amplification and a fluorescence immunoassay was developed for AFB1. The dynamic range was 20-1000 ng/L with a LOD of 17 ng/L. The recoveries for spiked maize samples ranged from 84.7 to 119.4%.

4.2 Outlook

The use of magnetic particles as solid carrier reduces the incubation time, and facilitates the rapid separation of immune complexes. Thus, the assays are very fast and can be completed within 1h. But usually the same batch of AFB1-BSA-Fe₃O₄ has to be utilized for all the measurements, including the establishment of calibration curves and the analysis of real samples. Otherwise new calibration curves have to be made. This is because the batch-to-batch reproducibility of magnetic particles is not that good. In addition, the samples have to be separated one by one with magnet. Thus, only limited samples can be analyzed at one time, which may not be suitable for high-throughput screening of AFB1 in agricultural products.

As an alternative, the well established microtiter plate format could be utilized. AFB1-BSA conjugates are immobilized on microtiter plate and then a direct competitive assay format can be used for the detection of AFB1 (Figure 4.1A). A large number of samples

can be analyzed simultaneously in a 96-well or 384-well plate. Furthermore, because the difference between wells of microtiter plate is very small, good reproducibility is anticipated.

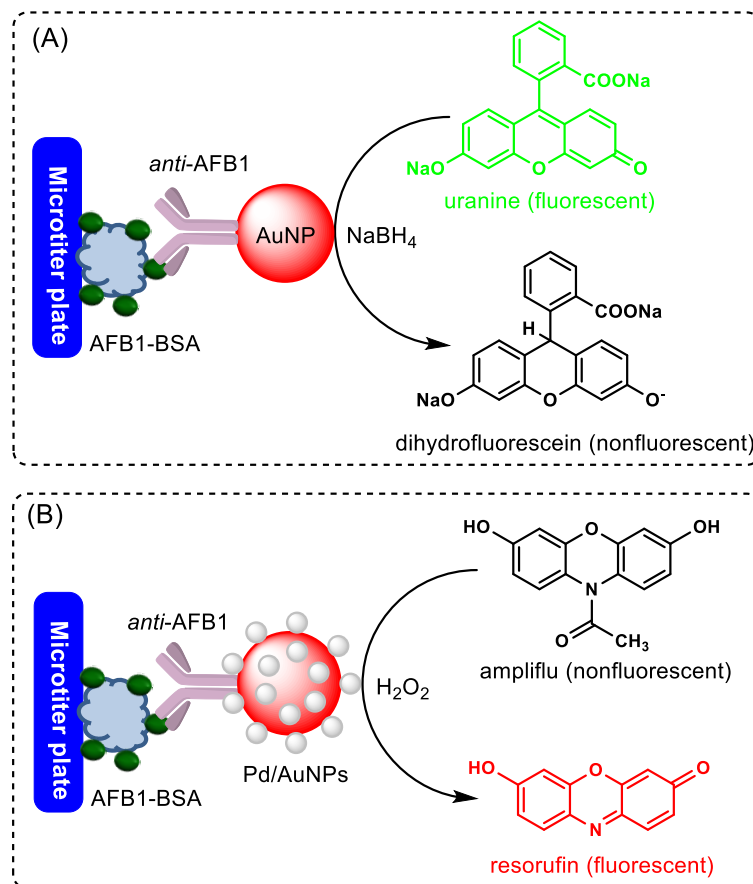


Figure 4.1 Schematic illustration of fluorescence immunoassays for AFB1 using microtiter plate as solid carrier and nanoparticles as enzyme mimics. (A) Fluorescence turn-off mode based on AuNP-catalyzed uranine reduction by NaBH₄. (B) Fluorescence turn-on mode based on Pd/AuNP-catalyzed Ampliflu Red oxidation by H₂O₂.

Recently, several types of nanomaterials such as Fe₃O₄ NPs, Pd/Au bimetallic NPs, graphene oxide and sheet-like FeS nanostructures have been demonstrated to possess special catalytic activity, which could be utilized as artificial enzyme for signal amplification.¹⁵⁰ These enzyme mimics are generally more stable and cost-effective than natural enzymes. In addition, compared with enzyme-conjugated antibody frequently utilized in conventional ELISA, the preparation and purification of nanoparticle-labeled antibody are much simpler and easier. Figure 4.1B shows a competitive immunoassay for

4 Summary and Outlook

AFB1 using Pd/AuNPs as artificial enzyme. Pd/AuNPs exhibit strong peroxidase-like activity,¹⁷² which can catalyze the oxidation of Ampliflu Red, producing a strong fluorescence signal. Since the fluorescence generated could be accumulated, the detection limit is expected to be further improved compared with the 'turn-off' mode based on AuNP-catalyzed uranine reduction. Beside Pd/AuNPs, other nanomaterials could be also employed as enzyme mimics in immunoassays. Further, the proposed system could be utilized for the detection of other mycotoxins and organic pollutants.

5 Abbreviations

5 Abbreviations

AA	Ascorbic acid
AF	Aflatoxin
AFB1	Aflatoxin B1
ALP	Alkaline phosphatase
AP	4-Aminophenol
APTES	3-Aminopropyltriethoxysilane
a.u.	Arbitrary unit
AuNPs	Gold nanoparticles
AUR	Amplex UltraRed
BSA	Albumin from bovine serum
Con A	Concanavalin A
CTAB	Cetyltrimethylammonium bromide
CVs	Variation coefficients
DAB	3, 3'-Diaminobenzidine
DLS	Dynamic light scattering
DMAP	4-Dimethylaminopyridine
DNA	Deoxyribonucleic acid
ELISA	Enzyme-linked immunosorbent assay
FB1	Fumonisin B1
FITC	Fluorescein 5(6)-isothiocyanate
FRET	Förster resonance energy transfer
GCE	Glassy carbon electrode
HPLC	High-performance liquid chromatography
HRP	Horseradish peroxidase
IgM	Immunoglobulin M
ITO	Indium tin oxide
IWC	Institute of Hydrochemistry
LC-MS	Liquid chromatography coupled to mass spectrometry
LOD	Limit of detection
MMSN	Magnetic mesoporous silica nanoparticles
MSN	Mesoporous silica nanocontainers
NPs	Nanoparticles

5 Abbreviations

OPD	<i>o</i> -Phenylenediamine
OTA	Ochratoxin A
PBS	Phosphate buffered solution
PEG	Polyethylene glycol
PEI	Polyethylenimine
pI	Isoelectric point
PMMA	Polymethylmethacrylate
QDs	Quantum dots
QI	<i>p</i> -Quinone imine
RLS	Resonance light scattering
RNA	Ribonucleic acid
SADC	Sodium acetate dicarboxylate
SDS	Sodium dodecyl sulfate
SERS	Surface-enhanced Raman scattering
SPR	Surface plasmon resonance
TMB	3,3,5,5-Tetramethylbenzidine
TRITC	Tetramethylrhodamine-5-isothiocyanate
Tween-20	Polyoxyethylene (20) sorbitan monolaurate
UV	Ultra violet
Vis	Visible

6 References

6 References

1. Wacoo, A. P.; Wendi, D.; Vuzi, P. C.; Hawumba, J. F., Methods for Detection of Aflatoxins in Agricultural Food Crops. *J. Appl. Chem.* **2014**, *2014*, article ID: 706291.
2. Aflatoxins: Occurrence and Health Risks. <http://www.ansci.cornell.edu/plants/toxicagents/aflatoxin/aflatoxin.html>.
3. Li, P.; Zhang, Q.; Zhang, W., Immunoassays for Aflatoxins. *TrAC-Trend. Anal. Chem.* **2009**, *28*, 1115-1126.
4. Kensler, T. W.; Roebuck, B. D.; Wogan, G. N.; Groopman, J. D., Aflatoxin: A 50-Year Odyssey of Mechanistic and Translational Toxicology. *Toxicol. Sci.* **2011**, *120*, 28-48.
5. Li, P.; Zhang, Q.; Zhang, D.; Guan, D.; Liu, D. X.; Fang, S.; Wang, X.; Zhang, W., Aflatoxin Measurement and Analysis. In *Aflatoxins-Detection, Measurement and Control*, INTECH Open Access Publisher: 2011.
6. Aflatoxin Mycotoxins. <http://blackmold.awardspace.com/aflatoxinmycotoxins.html>.
7. Levy, D. D.; Groopman, J. D.; Lim, S. E.; Seidman, M. M.; Kraemer, K. H., Sequence Specificity of Aflatoxin B1-Induced Mutations in a Plasmid Replicated in Xeroderma Pigmentosum and DNA Repair Proficient Human Cells. *Cancer Res.* **1992**, *52*, 5668-5673.
8. Bbosa, G. S.; Kitya, D.; Odda, J.; Ogwal-Okeng, J., Aflatoxins Metabolism, Effects on Epigenetic Mechanisms and Their Role in Carcinogenesis. *Health* **2013**, *5*, 14-34.
9. Oswald, S. Entwicklung einer immunologischen Multianalytmethode zur Detektion von Mykotoxinen in Getreide. Dissertation. Technical University of Munich, 2013.
10. Lin, L.; Zhang, J.; Wang, P.; Wang, Y.; Chen, J., Thin-Layer Chromatography of Mycotoxins and Comparison with Other Chromatographic Methods. *J. Chromatogr. A* **1998**, *815*, 3-20.
11. Reddy, T.; Viswanathan, L.; Venkatasubramanian, T., Thin-Layer Chromatography of Aflatoxins. *Anal. Biochem.* **1970**, *38*, 568-571.
12. Stroka, J.; Van Otterdijk, R.; Anklam, E., Immunoaffinity Column Clean-up Prior to Thin-Layer Chromatography for the Determination of Aflatoxins in Various Food Matrices. *J. Chromatogr. A* **2000**, *904*, 251-256.
13. Jaimez, J.; Fente, C.; Vazquez, B.; Franco, C.; Cepeda, A.; Mahuzier, G.; Prognon, P., Application of the Assay of Aflatoxins by Liquid Chromatography with Fluorescence Detection in Food Analysis. *J. Chromatogr. A* **2000**, *882*, 1-10.
14. Herzallah, S. M., Determination of Aflatoxins in Eggs, Milk, Meat and Meat Products Using HPLC Fluorescent and UV Detectors. *Food Chem.* **2009**, *114*, 1141-1146.
15. Palmisano, F.; Zambonin, P. G.; Visconti, A.; Bottalico, A., Profiling of Alternaria Mycotoxins in Foodstuffs by High-Performance Liquid Chromatography with Diode-Array Ultraviolet Detection. *J. Chromatogr. A* **1989**, *465*, 305-313.
16. Scott, P. M.; Trucksess, M. W., Application of Immunoaffinity Columns to Mycotoxin Analysis. *J. AOAC. Int.* **1996**, *80*, 941-949.
17. Senyuva, H. Z.; Gilbert, J., Immunoaffinity Column Clean-up Techniques in Food Analysis: A Review. *J. Chromatogr. B* **2010**, *878*, 115-132.
18. Komarova, N., Determination of Aflatoxin M1 in Milk Using Solid-Phase Extraction and High-Performance Liquid Chromatography with Fluorescence Detection. *J. Anal. Chem.* **2000**, *55*, 929-932.
19. Kussak, A.; Andersson, B.; Andersson, K., Automated Sample Clean-up with Solid-Phase Extraction for the Determination of Aflatoxins in Urine by Liquid Chromatography. *J. Chromatogr. B* **1993**, *616*, 235-241.

20. Zheng, M. Z.; Richard, J. L.; Binder, J., A Review of Rapid Methods for the Analysis of Mycotoxins. *Mycopathologia* **2006**, *161*, 261-273.
21. Joshua, H., Determination of Aflatoxins by Reversed-Phase High-Performance Liquid Chromatography with Post-Column in-Line Photochemical Derivatization and Fluorescence Detection. *J. Chromatogr. A* **1993**, *654*, 247-254.
22. Kok, W. T., Derivatization Reactions for the Determination of Aflatoxins by Liquid Chromatography with Fluorescence Detection. *J. Chromatogr. B* **1994**, *659*, 127-137.
23. Francis Jr, O.; Kirschenheuter, G.; Ware, G.; Carman, A.; Kuan, S., Beta-Cyclodextrin Post-Column Fluorescence Enhancement of Aflatoxins for Reverse-Phase Liquid Chromatographic Determination in Corn. *J. Assoc. Off. Anal. Chem.* **1987**, *71*, 725-728.
24. Cavaliere, C.; Foglia, P.; Pastorini, E.; Samperi, R.; Laganà, A., Liquid Chromatography/Tandem Mass Spectrometric Confirmatory Method for Determining Aflatoxin M1 in Cow Milk: Comparison between Electrospray and Atmospheric Pressure Photoionization Sources. *J. Chromatogr. A* **2006**, *1101*, 69-78.
25. Cavaliere, C.; Foglia, P.; Guarino, C.; Nazzari, M.; Samperi, R.; Laganà, A., Determination of Aflatoxins in Olive Oil by Liquid Chromatography–Tandem Mass Spectrometry. *Anal. Chim. Acta* **2007**, *596*, 141-148.
26. Bacaloni, A.; Cavaliere, C.; Cucci, F.; Foglia, P.; Samperi, R.; Laganà, A., Determination of Aflatoxins in Hazelnuts by Various Sample Preparation Methods and Liquid Chromatography–Tandem Mass Spectrometry. *J. Chromatogr. A* **2008**, *1179*, 182-189.
27. Kim, S.-H.; Cha, S.-H.; Karyn, B.; Park, S.-W.; Son, S.-W.; Kang, H.-G., Production of Group Specific Monoclonal Antibody to Aflatoxins and Its Application to Enzyme-Linked Immunosorbent Assay. *Toxicol. Res.* **2011**, *27*, 125.
28. Cervino, C.; Weber, E.; Knopp, D.; Niessner, R., Comparison of Hybridoma Screening Methods for the Efficient Detection of High-Affinity Hapten-Specific Monoclonal Antibodies. *J. Immunol. Methods.* **2008**, *329*, 184-193.
29. Zhang, D.; Li, P.; Zhang, Q.; Zhang, W.; Huang, Y.; Ding, X.; Jiang, J., Production of Ultrasensitive Generic Monoclonal Antibodies against Major Aflatoxins Using a Modified Two-Step Screening Procedure. *Anal. Chim. Acta* **2009**, *636*, 63-69.
30. Korde, A.; Pandey, U.; Banerjee, S.; Sarma, H.; Hajare, S.; Venkatesh, M.; Sharma, A.; Pillai, M., Development of a Radioimmunoassay Procedure for Aflatoxin B1 Measurement. *J. Agric. Food Chem.* **2003**, *51*, 843-846.
31. Li, D.; Ying, Y.; Wu, J.; Niessner, R.; Knopp, D., Comparison of Monomeric and Polymeric Horseradish Peroxidase as Labels in Competitive ELISA for Small Molecule Detection. *Microchim. Acta* **2013**, *180*, 711-717.
32. Soares, R.; Novo, P.; Azevedo, A.; Fernandes, P.; Chu, V.; Conde, J.; Aires-Barros, M., Aqueous Two-Phase Systems for Enhancing Immunoassay Sensitivity: Simultaneous Concentration of Mycotoxins and Neutralization of Matrix Interference. *J. Chromatogr. A* **2014**, *1361*, 67-76.
33. Tang, D.; Yu, Y.; Niessner, R.; Miró, M.; Knopp, D., Magnetic Bead-Based Fluorescence Immunoassay for Aflatoxin B1 in Food Using Biofunctionalized Rhodamine B-Doped Silica Nanoparticles. *Analyst.* **2010**, *135*, 2661-2667.
34. Zekavati, R.; Safi, S.; Hashemi, S. J.; Rahmani-Cherati, T.; Tabatabaei, M.; Mohsenifar, A.; Bayat, M., Highly Sensitive FRET-Based Fluorescence Immunoassay for Aflatoxin B1 Using Cadmium Telluride Quantum Dots. *Microchim. Acta* **2013**, *180*, 1217-1223.

35. Ko, S.; Kim, C.; Kwon, D. In *Detection of Aflatoxin B1 by SPR Biosensor Using Fusion Proteins as a Linker*, Proceedings of the 2010 NSTI Nanotechnology Conference and Expo, 2010.
36. Paniel, N.; Radoi, A.; Marty, J.-L., Development of an Electrochemical Biosensor for the Detection of Aflatoxin M1 in Milk. *Sensors* **2010**, *10*, 9439-9448.
37. Langone, J. J.; Van Vunakis, H., Aflatoxin B; Specific Antibodies and Their Use in Radioimmunoassay. *J. Natl. Cancer Inst.* **1976**, *56*, 591-595.
38. Qian, G. S.; Yasei, P.; Yang, G. C., Rapid Extraction and Detection of Aflatoxin M1 in Cow's Milk by High-Performance Liquid Chromatography and Radioimmunoassay. *Anal. Chem.* **1984**, *56*, 2079-2080.
39. Technical Guide for ELISA. <http://www.kpl.com/docs/techdocs/KPL%20ELISA%20Technical%20Guide.pdf>.
40. Kawamura, O.; Nagayama, S.; Sato, S.; Ohtani, K.; Ueno, I.; Ueno, Y., A Monoclonal Antibody-Based Enzyme-Linked Immunosorbent Assay of Aflatoxin B1 in Peanut Products. *Mycotoxin Res.* **1988**, *4*, 75-88.
41. Thirumala-Devi, K.; Mayo, M.; Hall, A.; Craufurd, P.; Wheeler, T.; Waliyar, F.; Subrahmanyam, A.; Reddy, D., Development and Application of an Indirect Competitive Enzyme-Linked Immunoassay for Aflatoxin M1 in Milk and Milk-Based Confectionary. *J. Agric. Food Chem.* **2002**, *50*, 933-937.
42. Pestka, J.; Gaur, P.; Chu, F. S., Quantitation of Aflatoxin B1 and Aflatoxin B1 Antibody by an Enzyme-Linked Immunosorbent Microassay. *Appl. Environ. Microb.* **1980**, *40*, 1027-1031.
43. Stroka, J.; Anklam, E., New Strategies for the Screening and Determination of Aflatoxins and the Detection of Aflatoxin-Producing Moulds in Food and Feed. *TrAC-Trend. Anal. Chem.* **2002**, *21*, 90-95.
44. Huybrechts, B., Evaluation of Immunoassay Kits for Aflatoxin Determination in Corn & Rice. *National Reference Laboratory on Mycotoxins* **2011**.
45. Dzantiev, B. B.; Byzova, N. A.; Urusov, A. E.; Zherdev, A. V., Immunochromatographic Methods in Food Analysis. *TrAC-Trend. Anal. Chem.* **2014**, *55*, 81-93.
46. Anfossi, L.; Baggiani, C.; Giovannoli, C.; Giraudi, G., *Lateral Flow Immunoassays for Aflatoxins B and G and for Aflatoxin M1*. INTECH Open Access Publisher: 2013.
47. Moon, J.; Kim, G.; Lee, S., A Gold Nanoparticle and Aflatoxin B1-BSA Conjugates Based Lateral Flow Assay Method for the Analysis of Aflatoxin B1. *Materials* **2012**, *5*, 634-643.
48. Lee, S.; Kim, G.; Moon, J., Performance Improvement of the One-Dot Lateral Flow Immunoassay for Aflatoxin B1 by Using a Smartphone-Based Reading System. *Sensors* **2013**, *13*, 5109-5116.
49. Pal, A.; Dhar, T. K., An Analytical Device for On-Site Immunoassay. Demonstration of Its Applicability in Semiquantitative Detection of Aflatoxin B1 in a Batch of Samples with Ultrahigh Sensitivity. *Anal. Chem.* **2004**, *76*, 98-104.
50. Shim, W.-B.; Kim, M. J.; Mun, H.; Kim, M.-G., An Aptamer-Based Dipstick Assay for the Rapid and Simple Detection of Aflatoxin B1. *Biosens. Bioelectron.* **2014**, *62*, 288-294.
51. Ren, M.; Xu, H.; Huang, X.; Kuang, M.; Xiong, Y.; Xu, H.; Xu, Y.; Chen, H.; Wang, A., Immunochromatographic Assay for Ultrasensitive Detection of Aflatoxin B1 in Maize by Highly Luminescent Quantum Dot Beads. *ACS Appl. Mater. Interfaces* **2014**, *6*, 14215-14222.

52. Mosiello, L.; Lamberti, I., *Biosensors for Aflatoxins Detection*. INTECH Open Access Publisher: 2011.
53. Tan, Y.; Chu, X.; Shen, G.-L.; Yu, R.-Q., A Signal-Amplified Electrochemical Immunosensor for Aflatoxin B1 Determination in Rice. *Anal. Biochem.* **2009**, *387*, 82-86.
54. Parker, C. O.; Tothill, I. E., Development of an Electrochemical Immunosensor for Aflatoxin M1 in Milk with Focus on Matrix Interference. *Biosens. Bioelectron.* **2009**, *24*, 2452-2457.
55. Masoomi, L.; Sadeghi, O.; Banitaba, M. H.; Shahrjerdi, A.; Davarani, S. S. H., A Non-Enzymatic Nanomagnetic Electro-Immunosensor for Determination of Aflatoxin B1 as a Model Antigen. *Sens. Actuator. B-Chem.* **2013**, *177*, 1122-1127.
56. Liu, Y.; Qin, Z.; Wu, X.; Jiang, H., Immune-Biosensor for Aflatoxin B1 Based Bio-Electrocatalytic Reaction on Micro-Comb Electrode. *Biochem. Eng. J.* **2006**, *32*, 211-217.
57. Sun, A.-L.; Qi, Q.-A.; Dong, Z.-L.; Liang, K. Z., An Electrochemical Enzyme Immunoassay for Aflatoxin B1 Based on Bio-Electrocatalytic Reaction with Room-Temperature Ionic Liquid and Nanoparticle-Modified Electrodes. *Sens. Instrum. Food Qual. Saf.* **2008**, *2*, 43-50.
58. Daly, S. J.; Keating, G. J.; Dillon, P. P.; Manning, B. M.; O'Kennedy, R.; Lee, H. A.; Morgan, M. R., Development of Surface Plasmon Resonance-Based Immunoassay for Aflatoxin B1. *J. Agric. Food Chem.* **2000**, *48* (11), 5097-5104.
59. van der Gaag, B.; Spath, S.; Dietrich, H.; Stigter, E.; Boonzaaijer, G.; van Osenbruggen, T.; Koopal, K., Biosensors and Multiple Mycotoxin Analysis. *Food Control* **2003**, *14*, 251-254.
60. Oswald, S.; Karsunke, X.; Dietrich, R.; Märtlbauer, E.; Niessner, R.; Knopp, D., Automated Regenerable Microarray-Based Immunoassay for Rapid Parallel Quantification of Mycotoxins in Cereals. *Anal. Bioanal. Chem.* **2013**, *405*, 6405-6415.
61. Colombo, M.; Carregal-Romero, S.; Casula, M. F.; Gutiérrez, L.; Morales, M. P.; Böhm, I. B.; Heverhagen, J. T.; Prospero, D.; Parak, W. J., Biological Applications of Magnetic Nanoparticles. *Chem. Soc. Rev.* **2012**, *41*, 4306-4334.
62. Saha, K.; Agasti, S. S.; Kim, C.; Li, X.; Rotello, V. M., Gold Nanoparticles in Chemical and Biological Sensing. *Chem. Rev.* **2012**, *112*, 2739-2779.
63. Sapsford, K. E.; Algar, W. R.; Berti, L.; Gemmill, K. B.; Casey, B. J.; Oh, E.; Stewart, M. H.; Medintz, I. L., Functionalizing Nanoparticles with Biological Molecules: Developing Chemistries That Facilitate Nanotechnology. *Chem. Rev.* **2013**, *113*, 1904-2074.
64. Fan, A.; Lau, C.; Lu, J., Magnetic Bead-Based Chemiluminescent Metal Immunoassay with a Colloidal Gold Label. *Anal. Chem.* **2005**, *77*, 3238-3242.
65. Zhou, Y.; Zhang, Y.; Lau, C.; Lu, J., Sequential Determination of Two Proteins by Temperature-Triggered Homogeneous Chemiluminescent Immunoassay. *Anal. Chem.* **2006**, *78*, 5920-5924.
66. Xu, C.; Xu, K.; Gu, H.; Zhong, X.; Guo, Z.; Zheng, R.; Zhang, X.; Xu, B., Nitrotri-acetic Acid-Modified Magnetic Nanoparticles as a General Agent to Bind Histidine-Tagged Proteins. *J. Am. Chem. Soc.* **2004**, *126*, 3392-3393.
67. Dyal, A.; Loos, K.; Noto, M.; Chang, S. W.; Spagnoli, C.; Shafi, K. V.; Ulman, A.; Cowman, M.; Gross, R. A., Activity of *Candida rugosa* Lipase Immobilized on Fe₂O₃ Magnetic Nanoparticles. *J. Am. Chem. Soc.* **2003**, *125*, 1684-1685.
68. Pan, Y.; Guo, M.; Nie, Z.; Huang, Y.; Pan, C.; Zeng, K.; Zhang, Y.; Yao, S., Selective Collection and Detection of Leukemia Cells on a Magnet-Quartz Crystal Microbalance System Using Aptamer-Conjugated Magnetic Beads. *Biosens. Bioelectron.* **2010**, *25*, 1609-1614.

69. Wang, J.; Xu, D.; Polsky, R., Magnetically-Induced Solid-State Electrochemical Detection of DNA Hybridization. *J. Am. Chem. Soc.* **2002**, *124*, 4208-4209.
70. Zhu, X.; Han, K.; Li, G., Magnetic Nanoparticles Applied in Electrochemical Detection of Controllable DNA Hybridization. *Anal. Chem.* **2006**, *78*, 2447-2449.
71. Son, S. J.; Reichel, J.; He, B.; Schuchman, M.; Lee, S. B., Magnetic Nanotubes for Magnetic-Field-Assisted Bioseparation, Biointeraction, and Drug Delivery. *J. Am. Chem. Soc.* **2005**, *127*, 7316-7317.
72. Beveridge, J. S.; Stephens, J. R.; Williams, M. E., The Use of Magnetic Nanoparticles in Analytical Chemistry. *Ann. Rev. Anal. Chem.* **2011**, *4*, 251-273.
73. Reddy, L. H.; Arias, J. L.; Nicolas, J.; Couvreur, P., Magnetic Nanoparticles: Design and Characterization, Toxicity and Biocompatibility, Pharmaceutical and Biomedical Applications. *Chem. Rev.* **2012**, *112*, 5818-5878.
74. Yamaura, M.; Camilo, R.; Sampaio, L.; Macedo, M.; Nakamura, M.; Toma, H., Preparation and Characterization of (3-Aminopropyl) Triethoxysilane-Coated Magnetite Nanoparticles. *J. Magn. Magn. Mater.* **2004**, *279*, 210-217.
75. Lu, A. H.; Salabas, E. e. L.; Schüth, F., Magnetic Nanoparticles: Synthesis, Protection, Functionalization, and Application. *Angew. Chem. Int. Ed.* **2007**, *46*, 1222-1244.
76. Sun, S.; Zeng, H.; Robinson, D. B.; Raoux, S.; Rice, P. M.; Wang, S. X.; Li, G., Monodisperse MFe_2O_4 (M= Fe, Co, Mn) Nanoparticles. *J. Am. Chem. Soc.* **2004**, *126*, 273-279.
77. Hyeon, T.; Lee, S. S.; Park, J.; Chung, Y.; Na, H. B., Synthesis of Highly Crystalline and Monodisperse Maghemite Nanocrystallites without a Size-Selection Process. *J. Am. Chem. Soc.* **2001**, *123*, 12798-12801.
78. Park, J.; An, K.; Hwang, Y.; Park, J.-G.; Noh, H.-J.; Kim, J.-Y.; Park, J.-H.; Hwang, N.-M.; Hyeon, T., Ultra-Large-Scale Syntheses of Monodisperse Nanocrystals. *Nature Mater.* **2004**, *3*, 891-895.
79. Park, J.; Lee, E.; Hwang, N. M.; Kang, M.; Kim, S. C.; Hwang, Y.; Park, J. G.; Noh, H. J.; Kim, J. Y.; Park, J. H., One-Nanometer-Scale Size-Controlled Synthesis of Monodisperse Magnetic Iron Oxide Nanoparticles. *Angew. Chem. Int. Ed.* **2005**, *117*, 2932-2937.
80. Wang, X.; Zhuang, J.; Peng, Q.; Li, Y., A General Strategy for Nanocrystal Synthesis. *Nature* **2005**, *437*, 121-124.
81. Deng, H.; Li, X.; Peng, Q.; Wang, X.; Chen, J.; Li, Y., Monodisperse Magnetic Single-Crystal Ferrite Microspheres. *Angew. Chem. Int. Ed.* **2005**, *117*, 2842-2845.
82. Laurent, S.; Forge, D.; Port, M.; Roch, A.; Robic, C.; Vander Elst, L.; Muller, R. N., Magnetic Iron Oxide Nanoparticles: Synthesis, Stabilization, Vectorization, Physicochemical Characterizations, and Biological Applications. *Chem. Rev.* **2008**, *108*, 2064-2110.
83. Mulens, V.; Morales, M. d. P.; Barber, D. F., Development of Magnetic Nanoparticles for Cancer Gene Therapy: A Comprehensive Review. *ISRN Nanomater.* **2013**, *2013*, 1-14.
84. Tudorache, M.; Bala, C., Sensitive Aflatoxin B1 Determination Using a Magnetic Particles-Based Enzyme-Linked Immunosorbent Assay. *Sensors* **2008**, *8*, 7571-7580.
85. Liu, M.; Jia, C.; Huang, Y.; Lou, X.; Yao, S.; Jin, Q.; Zhao, J.; Xiang, J., Highly Sensitive Protein Detection Using Enzyme-Labeled Gold Nanoparticle Probes. *Analyst.* **2010**, *135*, 327-331.
86. Li, J.; Li, W.; Qiang, W.; Wang, X.; Li, H.; Xu, D., A Non-Aggregation Colorimetric Assay for Thrombin Based on Catalytic Properties of Silver Nanoparticles. *Anal. Chim. Acta* **2014**, *807*, 120-125.

6 References

87. Yu, H.-W.; Jang, A.; Kim, L. H.; Kim, S.-J.; Kim, I. S., Bead-Based Competitive Fluorescence Immunoassay for Sensitive and Rapid Diagnosis of Cyanotoxin Risk in Drinking Water. *Environ. Sci. Technol.* **2011**, *45*, 7804-7811.
88. Hu, P.; Huang, C. Z.; Li, Y. F.; Ling, J.; Liu, Y. L.; Fei, L. R.; Xie, J. P., Magnetic Particle-Based Sandwich Sensor with DNA-Modified Carbon Nanotubes as Recognition Elements for Detection of DNA Hybridization. *Anal. Chem.* **2008**, *80*, 1819-1823.
89. Zhao, Q.; Lu, X.; Yuan, C.-G.; Li, X.-F.; Le, X. C., Aptamer-Linked Assay for Thrombin Using Gold Nanoparticle Amplification and Inductively Coupled Plasma–Mass Spectrometry Detection. *Anal. Chem.* **2009**, *81*, 7484-7489.
90. Fan, A.; Cai, S.; Cao, Z.; Lau, C.; Lu, J., Hydroxylamine-Amplified Gold Nanoparticles for the Homogeneous Detection of Sequence-Specific DNA. *Analyst.* **2010**, *135*, 1400-1405.
91. Wu, S.; Duan, N.; Zhu, C.; Ma, X.; Wang, M.; Wang, Z., Magnetic Nanobead-Based Immunoassay for the Simultaneous Detection of Aflatoxin B1 and Ochratoxin A Using Upconversion Nanoparticles as Multicolor Labels. *Biosens. Bioelectron.* **2011**, *30*, 35-42.
92. Nie, L.-b.; Wang, X.-l.; Li, S.; Chen, H., Amplification of Fluorescence Detection of DNA Based on Magnetic Separation. *Anal. Sci.* **2009**, *25*, 1327-1332.
93. Gao, L.; Zhuang, J.; Nie, L.; Zhang, J.; Zhang, Y.; Gu, N.; Wang, T.; Feng, J.; Yang, D.; Perrett, S., Intrinsic Peroxidase-Like Activity of Ferromagnetic Nanoparticles. *Nature Nanotech.* **2007**, *2*, 577-583.
94. Wei, H.; Wang, E., Fe₃O₄ Magnetic Nanoparticles as Peroxidase Mimetics and Their Applications in H₂O₂ and Glucose Detection. *Anal. Chem.* **2008**, *80*, 2250-2254.
95. Woo, M.-A.; Kim, M. I.; Jung, J. H.; Park, K. S.; Seo, T. S.; Park, H. G., A Novel Colorimetric Immunoassay Utilizing the Peroxidase Mimicking Activity of Magnetic Nanoparticles. *Int. J. Mol. Sci.* **2013**, *14*, 9999-10014.
96. Yang, M.; Guan, Y.; Yang, Y.; Xia, T.; Xiong, W.; Wang, N.; Guo, C., Peroxidase-Like Activity of Amino-Functionalized Magnetic Nanoparticles and Their Applications in Immunoassay. *J. Colloid Interf. Sci.* **2013**, *405*, 291-295.
97. Tong, S.; Ren, B.; Zheng, Z.; Shen, H.; Bao, G., Tiny Grains Give Huge Gains: Nanocrystal-Based Signal Amplification for Biomolecule Detection. *ACS Nano* **2013**, *7*, 5142-5150.
98. Chen, Y.; Xianyu, Y.; Wang, Y.; Zhang, X.; Cha, R.; Sun, J.; Jiang, X., One-Step Detection of Pathogens and Viruses: Combining Magnetic Relaxation Switching and Magnetic Separation. *ACS Nano* **2015**, *9*, 3184-3191.
99. Jans, H.; Huo, Q., Gold Nanoparticle-Enabled Biological and Chemical Detection and Analysis. *Chem. Soc. Rev.* **2012**, *41*, 2849-2866.
100. Dykman, L.; Khlebtsov, N., Gold Nanoparticles in Biomedical Applications: Recent Advances and Perspectives. *Chem. Soc. Rev.* **2012**, *41*, 2256-2282.
101. Sun, J.; Xianyu, Y.; Jiang, X., Point-of-Care Biochemical Assays Using Gold Nanoparticle-Implemented Microfluidics. *Chem. Soc. Rev.* **2014**, *43*, 6239-6253.
102. Turkevich, J.; Stevenson, P. C.; Hillier, J., A Study of the Nucleation and Growth Processes in the Synthesis of Colloidal Gold. *Discuss. Faraday Soc.* **1951**, *11*, 55-75.
103. Frens, G., Controlled Nucleation for the Regulation of the Particle Size in Monodisperse Gold Suspensions. *Nature-Phys. Sci.* **1973**, *241*, 20-22.
104. Ji, X.; Song, X.; Li, J.; Bai, Y.; Yang, W.; Peng, X., Size Control of Gold Nanocrystals in Citrate Reduction: The Third Role of Citrate. *J. Am. Chem. Soc.* **2007**, *129*, 13939-13948.
105. Liu, X. Nanoparticles and Surface-Enhanced Optical Effects for Chemical and Biological Sensing. Dissertation. Technical University of Munich, 2012.

106. Brown, K. R.; Natan, M. J., Hydroxylamine Seeding of Colloidal Au Nanoparticles in Solution and on Surfaces. *Langmuir*. **1998**, *14*, 726-728.
107. Bastús, N. G.; Comenge, J.; Puntès, V., Kinetically Controlled Seeded Growth Synthesis of Citrate-Stabilized Gold Nanoparticles of up to 200 nm: Size Focusing Versus Ostwald Ripening. *Langmuir*. **2011**, *27*, 11098-11105.
108. Ziegler, C.; Eychmüller, A., Seeded Growth Synthesis of Uniform Gold Nanoparticles with Diameters of 15-300 nm. *J. Phys. Chem. C* **2011**, *115*, 4502-4506.
109. Huang, X.; El-Sayed, M. A., Gold Nanoparticles: Optical Properties and Implementations in Cancer Diagnosis and Photothermal Therapy. *J. Adv. Res.* **2010**, *1*, 13-28.
110. Gold Nanoparticles: Properties and Applications. <http://www.sigmaaldrich.com/china-mainland/zh/materials-science/nanomaterials/gold-nanoparticles.html>.
111. Liu, D.; Wang, S.; Swierczewska, M.; Huang, X.; Bhirde, A. A.; Sun, J.; Wang, Z.; Yang, M.; Jiang, X.; Chen, X., Highly Robust, Recyclable Displacement Assay for Mercuric Ions in Aqueous Solutions and Living Cells. *ACS Nano* **2012**, *6*, 10999-11008.
112. Liu, D.; Huang, X.; Wang, Z.; Jin, A.; Sun, X.; Zhu, L.; Wang, F.; Ma, Y.; Niu, G.; Hight Walker, A. R., Gold Nanoparticle-Based Activatable Probe for Sensing Ultralow Levels of Prostate-Specific Antigen. *ACS Nano* **2013**, *7*, 5568-5576.
113. Tang, D.; Liu, B.; Niessner, R.; Li, P.; Knopp, D., Target-Induced Displacement Reaction Accompanying Cargo Release from Magnetic Mesoporous Silica Nanocontainers for Fluorescence Immunoassay. *Anal. Chem.* **2013**, *85*, 10589-10596.
114. Nash, M. A.; Waitumbi, J. N.; Hoffman, A. S.; Yager, P.; Stayton, P. S., Multiplexed Enrichment and Detection of Malarial Biomarkers Using a Stimuli-Responsive Iron Oxide and Gold Nanoparticle Reagent System. *ACS Nano* **2012**, *6*, 6776-6785.
115. Valentini, P.; Fiammengo, R.; Sabella, S.; Gariboldi, M.; Maiorano, G.; Cingolani, R.; Pompa, P. P., Gold-Nanoparticle-Based Colorimetric Discrimination of Cancer-Related Point Mutations with Picomolar Sensitivity. *ACS Nano* **2013**, *7*, 5530-5538.
116. Kato, D.; Oishi, M., Ultrasensitive Detection of DNA and RNA Based on Enzyme-Free Click Chemical Ligation Chain Reaction on Dispersed Gold Nanoparticles. *ACS Nano* **2014**, *8*, 9988-9997.
117. Gao, Z.; Xu, M.; Hou, L.; Chen, G.; Tang, D., Magnetic Bead-Based Reverse Colorimetric Immunoassay Strategy for Sensing Biomolecules. *Anal. Chem.* **2013**, *85*, 6945-6952.
118. Zhou, W.-H.; Zhu, C.-L.; Lu, C.-H.; Guo, X.; Chen, F.; Yang, H.-H.; Wang, X., Amplified Detection of Protein Cancer Biomarkers Using DNAzyme Functionalized Nanoprobes. *Chem. Commun.* **2009**, 6845-6847.
119. Ambrosi, A.; Castañeda, M. T.; Killard, A. J.; Smyth, M. R.; Alegret, S.; Merkoçi, A., Double-Codified Gold Nanolabels for Enhanced Immunoanalysis. *Anal. Chem.* **2007**, *79*, 5232-5240.
120. Li, Y.; Zhou, Y.; Meng, X.; Zhang, Y.; Liu, J.; Zhang, Y.; Wang, N.; Hu, P.; Lu, S.; Ren, H., Enzyme-Antibody Dual Labeled Gold Nanoparticles Probe for Ultrasensitive Detection of k-Casein in Bovine Milk Samples. *Biosens. Bioelectron.* **2014**, *61*, 241-244.
121. Nam, J.-M.; Jang, K.-J.; Groves, J. T., Detection of Proteins Using a Colorimetric Bio-Barcode Assay. *Nat. Protoc.* **2007**, *2*, 1438-1444.
122. Vilela, D.; González, M. C.; Escarpa, A., Sensing Colorimetric Approaches Based on Gold and Silver Nanoparticles Aggregation: Chemical Creativity Behind the Assay. A Review. *Anal. Chim. Acta* **2012**, *751*, 24-43.
123. Xianyu, Y.; Wang, Z.; Jiang, X., A Plasmonic Nanosensor for Immunoassay via Enzyme-Triggered Click Chemistry. *ACS Nano* **2014**, *8*, 12741-12747.

6 References

124. Qu, W.; Liu, Y.; Liu, D.; Wang, Z.; Jiang, X., Copper-Mediated Amplification Allows Readout of Immunoassays by the Naked Eye. *Angew. Chem. Int. Ed.* **2011**, *123*, 3504-3507.
125. Chen, G.; Song, F.; Xiong, X.; Peng, X., Fluorescent Nanosensors Based on Fluorescence Resonance Energy Transfer (FRET). *Ind. Eng. Chem. Res.* **2013**, *52*, 11228-11245.
126. Chen, J.; Huang, Y.; Zhao, S.; Lu, X.; Tian, J., Gold Nanoparticles-Based Fluorescence Resonance Energy Transfer for Competitive Immunoassay of Biomolecules. *Analyst.* **2012**, *137*, 5885-5890.
127. Liu, R.; Zhang, Y.; Zhang, S.; Qiu, W.; Gao, Y., Silver Enhancement of Gold Nanoparticles for Biosensing: From Qualitative to Quantitative. *Appl. Spectrosc. Rev.* **2014**, *49*, 121-138.
128. Zhou, C.-H.; Zhao, J.-Y.; Pang, D.-W.; Zhang, Z.-L., Enzyme-Induced Metallization as a Signal Amplification Strategy for Highly Sensitive Colorimetric Detection of Avian Influenza Virus Particles. *Anal. Chem.* **2014**, *86*, 2752-2759.
129. Kim, D.; Daniel, W. L.; Mirkin, C. A., Microarray-Based Multiplexed Scanometric Immunoassay for Protein Cancer Markers Using Gold Nanoparticle Probes. *Anal. Chem.* **2009**, *81*, 9183-9187.
130. Pavlov, V.; Xiao, Y.; Shlyahovsky, B.; Willner, I., Aptamer-Functionalized Au Nanoparticles for the Amplified Optical Detection of Thrombin. *J. Am. Chem. Soc.* **2004**, *126*, 11768-11769.
131. Fan, A.; Lau, C.; Lu, J., Hydroxylamine-Amplified Gold Nanoparticles for the Naked Eye and Chemiluminescent Detection of Sequence-Specific DNA with Notable Potential for Single-Nucleotide Polymorphism Discrimination. *Analyst.* **2009**, *134*, 497-503.
132. Lin, Y.; Ren, J.; Qu, X., Nano-Gold as Artificial Enzymes: Hidden Talents. *Adv. Mater.* **2014**, *26*, 4200-4217.
133. Wang, C.-I.; Chen, W.-T.; Chang, H.-T., Enzyme Mimics of Au/Ag Nanoparticles for Fluorescent Detection of Acetylcholine. *Anal. Chem.* **2012**, *84*, 9706-9712.
134. Wang, C.-I.; Huang, C.-C.; Lin, Y.-W.; Chen, W.-T.; Chang, H.-T., Catalytic Gold Nanoparticles for Fluorescent Detection of Mercury (II) and Lead (II) Ions. *Anal. Chim. Acta* **2012**, *745*, 124-130.
135. Wu, Y.-S.; Huang, F.-F.; Lin, Y.-W., Fluorescent Detection of Lead in Environmental Water and Urine Samples Using Enzyme Mimics of Catechin-Synthesized Au Nanoparticles. *ACS Appl. Mat. Interfaces* **2013**, *5*, 1503-1509.
136. Das, J.; Aziz, M. A.; Yang, H., A Nanocatalyst-Based Assay for Proteins: DNA-Free Ultrasensitive Electrochemical Detection Using Catalytic Reduction of p-Nitrophenol by Gold-Nanoparticle Labels. *J. Am. Chem. Soc.* **2006**, *128*, 16022-16023.
137. Que, X.; Tang, D.; Xia, B.; Lu, M.; Tang, D., Gold Nanocatalyst-Based Immunosensing Strategy Accompanying Catalytic Reduction of 4-Nitrophenol for Sensitive Monitoring of Chloramphenicol Residue. *Anal. Chim. Acta* **2014**, *830*, 42-48.
138. Chang, C.-C.; Chen, C.-P.; Lee, C.-H.; Chen, C.-Y.; Lin, C.-W., Colorimetric Detection of Human Chorionic Gonadotropin Using Catalytic Gold Nanoparticles and a Peptide Aptamer. *Chem. Commun.* **2014**, *50*, 14443-14446.
139. Li, W.; Li, J.; Qiang, W.; Xu, J.; Xu, D., Enzyme-Free Colorimetric Bioassay Based on Gold Nanoparticle-Catalyzed Dye Decolorization. *Analyst.* **2013**, *138*, 760-766.
140. Li, W.; Qiang, W.; Li, J.; Li, H.; Dong, Y.; Zhao, Y.; Xu, D., Nanoparticle-Catalyzed Reductive Bleaching for Fabricating Turn-off and Enzyme-Free Amplified Colorimetric Bioassays. *Biosens. Bioelectron.* **2014**, *51*, 219-224.

141. Xu, X.; Liu, X.; Li, Y.; Ying, Y., A Simple and Rapid Optical Biosensor for Detection of Aflatoxin B1 Based on Competitive Dispersion of Gold Nanorods. *Biosens. Bioelectron.* **2013**, *47*, 361-367.
142. Xu, W.; Xiong, Y.; Lai, W.; Xu, Y.; Li, C.; Xie, M., A Homogeneous Immunosensor for AFB1 Detection Based on FRET between Different-Sized Quantum Dots. *Biosens. Bioelectron.* **2014**, *56*, 144-150.
143. Zhang, Z.; Lin, M.; Zhang, S.; Vardhanabhuti, B., Detection of Aflatoxin M1 in Milk by Dynamic Light Scattering Coupled with Superparamagnetic Beads and Gold Nanoprobes. *J. Agric. Food Chem.* **2013**, *61*, 4520-4525.
144. Ko, J.; Lee, C.; Choo, J., Highly Sensitive SERS-Based Immunoassay of Aflatoxin B1 Using Silica-Encapsulated Hollow Gold Nanoparticles. *J. Hazard. Mater.* **2015**, *285*, 11-17.
145. Tang, D.; Zhong, Z.; Niessner, R.; Knopp, D., Multifunctional Magnetic Bead-Based Electrochemical Immunoassay for the Detection of Aflatoxin B1 in Food. *Analyst.* **2009**, *134*, 1554-1560.
146. Lin, Y.; Zhou, Q.; Lin, Y.; Tang, D.; Niessner, R.; Knopp, D., Enzymatic Hydrolysate-Induced Displacement Reaction with Multifunctional Silica Beads Doped with Horseradish Peroxidase-Thionine Conjugate for Ultrasensitive Electrochemical Immunoassay. *Anal. Chem.* **2015**, *87*, 8531-8540.
147. Abhijith, K.; Ragavan, K.; Thakur, M., Gold Nanoparticles Enhanced Chemiluminescence—a Novel Approach for Sensitive Determination of Aflatoxin-B1. *Anal. Methods* **2013**, *5*, 4838-4845.
148. Tang, D.; Lin, Y.; Zhou, Q.; Lin, Y.; Li, P.; Niessner, R.; Knopp, D., Low-Cost and Highly Sensitive Immunosensing Platform for Aflatoxins Using One-Step Competitive Displacement Reaction Mode and Portable Glucometer-Based Detection. *Anal. Chem.* **2014**, *86*, 11451-11458.
149. Cui, X.; Liu, M.; Li, B., Homogeneous Fluorescence-Based Immunoassay via Inner Filter Effect of Gold Nanoparticles on Fluorescence of CdTe Quantum Dots. *Analyst.* **2012**, *137*, 3293-3299.
150. Wang, Z.; Zheng, S.; Cai, J.; Wang, P.; Feng, J.; Yang, X.; Zhang, L.; Ji, M.; Wu, F.; He, N., Fluorescent Artificial Enzyme-Linked Immunoassay System Based on Pd/C Nanocatalyst and Fluorescent Chemodosimeter. *Anal. Chem.* **2013**, *85*, 11602-11609.
151. Lu, Y.; Huang, X.; Ren, J., Sandwich Immunoassay for Alpha-Fetoprotein in Human Sera Using Gold Nanoparticle and Magnetic Bead Labels Along with Resonance Rayleigh Scattering Readout. *Microchim. Acta* **2013**, *180*, 635-642.
152. Tang, J.; Tang, D.; Niessner, R.; Chen, G.; Knopp, D., Magneto-Controlled Graphene Immunosensing Platform for Simultaneous Multiplexed Electrochemical Immunoassay Using Distinguishable Signal Tags. *Anal. Chem.* **2011**, *83*, 5407-5414.
153. Cao, X.; Ye, Y.; Liu, S., Gold Nanoparticle-Based Signal Amplification for Biosensing. *Anal. Biochem.* **2011**, *417*, 1-16.
154. Liu, Y.; Wu, Z.; Zhou, G.; He, Z.; Zhou, X.; Shen, A.; Hu, J., Simple, Rapid, Homogeneous Oligonucleotides Colorimetric Detection Based on Non-Aggregated Gold Nanoparticles. *Chem. Commun.* **2012**, *48*, 3164-3166.
155. Jans, H.; Jans, K.; Demeyer, P.-J.; Knez, K.; Stakenborg, T.; Maes, G.; Lagae, L., A Simple Double-Bead Sandwich Assay for Protein Detection in Serum Using UV-Vis Spectroscopy. *Talanta* **2011**, *83*, 1580-1585.
156. Haiss, W.; Thanh, N. T.; Aveyard, J.; Fernig, D. G., Determination of Size and Concentration of Gold Nanoparticles from UV-Vis Spectra. *Anal. Chem.* **2007**, *79*, 4215-4221.

6 References

157. Li, X.; Li, P.; Zhang, Q.; Li, Y.; Zhang, W.; Ding, X., Molecular Characterization of Monoclonal Antibodies against Aflatoxins: A Possible Explanation for the Highest Sensitivity. *Anal. Chem.* **2012**, *84*, 5229-5235.
158. Zhan, Z.; Cao, C.; Sim, S. J., Quantitative Detection of DNA by Autocatalytic Enlargement of Hybridized Gold Nanoprobes. *Biosens. Bioelectron.* **2010**, *26*, 511-516.
159. Gold Enhancement. <http://www.nanoprobes.com/products/GoldEnhance.html>.
160. Ma, Z.; Sui, S. F., Naked - Eye Sensitive Detection of Immunoglobulin G by Enlargement of Au Nanoparticles in Vitro. *Angew. Chem. Int. Ed.* **2002**, *41*, 2176-2179.
161. Cao, C.; Li, X.; Lee, J.; Sim, S. J., Homogenous Growth of Gold Nanocrystals for Quantification of PSA Protein Biomarker. *Biosens. Bioelectron.* **2009**, *24*, 1292-1297.
162. Khan, Z.; Singh, T.; Hussain, J. I.; Hashmi, A. A., Au (III)-CTAB Reduction by Ascorbic Acid: Preparation and Characterization of Gold Nanoparticles. *Colloid. Surface B* **2013**, *104*, 11-17.
163. AL-Thabaiti, S. A.; Hussain, J. I.; Hashmi, A. A.; Khan, Z., Au (III)-Surfactant Complex-Assisted Anisotropic Growth of Advanced Platonic Au-Nanoparticles. *Can. Chem. Trans.* **2013**, *1*, 238-252.
164. Wu, W. B.; Zhan, L.; Wang, J.; Huang, C. Z., A Plasmon Resonance Light Scattering Assay of Glucose Based on the Formation of Gold Nanoparticles. *Anal. Methods* **2014**, *6*, 3779-3783.
165. An Introduction to Fluorescence Measurements. <http://www.turnerdesigns.com/t2/doc/appnotes/998-0050.pdf>.
166. Shahzad, A.; Köhler, G.; Knapp, M.; Gaubitzer, E.; Puchinger, M.; Edetsberger, M., Emerging Applications of Fluorescence Spectroscopy in Medical Microbiology Field. *J. Transl. Med.* **2009**, *7*, 99-104.
167. Li, Y.; Xu, J.; Sun, C., Chemical Sensors and Biosensors for the Detection of Melamine. *RSC Adv.* **2015**, *5*, 1125-1147.
168. Chi, H.; Liu, B.; Guan, G.; Zhang, Z.; Han, M.-Y., A Simple, Reliable and Sensitive Colorimetric Visualization of Melamine in Milk by Unmodified Gold Nanoparticles. *Analyst.* **2010**, *135*, 1070-1075.
169. Weber, G.; Teale, F., Fluorescence Excitation Spectrum of Organic Compounds in Solution. Part 1. Systems with Quantum Yield Independent of the Exciting Wavelength. *Trans. Faraday Soc.* **1958**, *54*, 640-648.
170. Jiang, Z.-J.; Liu, C.-Y.; Sun, L.-W., Catalytic Properties of Silver Nanoparticles Supported on Silica Spheres. *J. Phys. Chem. B.* **2005**, *109*, 1730-1735.
171. Martin, M. M.; Lindqvist, L., The pH Dependence of Fluorescein Fluorescence. *J. Lumin.* **1975**, *10*, 381-390.
172. Gao, Z.; Hou, L.; Xu, M.; Tang, D., Enhanced Colorimetric Immunoassay Accompanying with Enzyme Cascade Amplification Strategy for Ultrasensitive Detection of Low-Abundance Protein. *Sci. Rep.* **2014**, *4*, article number: 3966.